**TITLE**

# Mfn2 ubiquitination by PINK1/parkin gates the p97-dependent release of ER from mitochondria to drive mitophagy

**AUTHORS/AFFILIATIONS**

Gian-Luca McLelland[1,2,*], Thomas Goiran[1,2], Wei Yi[1,2], Geneviève Dorval[1,2,3], Carol X. Chen[1,2,3], Nadine D. Lauinger[1,2,3], Andrea I. Krahn[1,2], Sepideh Valimehr[4], Aleksandar Rakovic[5], Isabelle Rouiller[4], Thomas M. Durcan[1,2,3], Jean-François Trempe[6] and Edward A. Fon[1,2,3]

[1]McGill Parkinson Program, [2]Neurodegenerative Diseases Group and [3]iPSC-CRISPR Platform, Montreal Neurological Institute, McGill University, Montreal, Quebec, Canada

[4]Department of Anatomy & Cell Biology, McGill University, Montreal, Quebec, Canada

[5]Institute of Neurogenetics, University of Lübeck, Lübeck, Germany

[6]Department of Pharmacology & Therapeutics, McGill University, Montreal, Quebec, Canada

[*]current address: Netherlands Cancer Institute, Amsterdam, the Netherlands

**CORRESPONDING AUTHOR INFORMATION**

Edward A. Fon

Montreal Neurological Institute

3801 University Street, Montreal, Quebec, Canada H3A 2B4

phone: (514) 398-8398; e-mail: ted.fon@mcgill.ca

**ABSTRACT**

Despite their importance as signaling hubs, the function of mitochondria-ER contact sites in mitochondrial quality control pathways remains unexplored. Here we describe a mechanism by which Mfn2, a mitochondria-ER tether, gates the autophagic turnover of mitochondria by PINK1 and parkin. Mitochondria-ER appositions are destroyed during mitophagy, and reducing mitochondria-ER contacts increases the rate of mitochondrial degradation. Mechanistically, parkin/PINK1 catalyze a rapid burst of Mfn2 phosphoubiquitination to trigger p97-dependent disassembly of Mfn2 complexes from the outer mitochondrial membrane, dissociating mitochondria from the ER. We additionally demonstrate that a major portion of the facilitatory effect of p97 on mitophagy is epistatic to Mfn2 and promotes the availability of other parkin substrates such as VDAC1. Finally, we reconstitute the action of these factors on Mfn2 and VDAC1 ubiquitination in a cell-free assay. We show that mitochondria-ER tethering suppresses mitophagy and describe a parkin-/PINK1-dependent mechanism that regulates the destruction of mitochondria-ER contact sites.

39 **INTRODUCTION**

40 Loss of *PRKN* or *PINK1* results in an early-onset form of hereditary Parkinson's
41 disease (PD), a neurological disorder that is linked to mitochondrial dysfunction (Kitada
42 et al., 1998; Ryan et al., 2015; Valente et al., 2004). Accordingly, parkin and PINK1
43 promote mitochondrial health through several mitochondrial quality control mechanisms;
44 the turnover of outer mitochondrial membrane (OMM) proteins by the proteasome, the
45 generation of mitochondrial-derived vesicles, and whole-organellar degradation by
46 mitophagy, a form of selective autophagy (Sugiura et al., 2014; Yamano et al., 2016).
47 During mitophagy, PINK1, a mitochondrial kinase, builds up on the surface of damaged
48 mitochondria where it activates parkin directly via phosphorylation and allosterically
49 through the generation of phosphoubiquitin (pUb) (Kane et al., 2014; Kazlauskaite et al.,
50 2014; Kondapalli et al., 2012; Koyano et al., 2014; Shiba-Fukushima et al., 2012).
51 Parkin, an E3 ubiquitin (Ub) ligase, mediates the ubiquitination of resident OMM
52 proteins, recruiting Ub-binding autophagic machinery through a feed-forward mechanism
53 to ultimately degrade the organelle via the lysosome (Heo et al., 2015; Lazarou et al.,
54 2015; Ordureau et al., 2015; Ordureau et al., 2014).

55 Contact sites between mitochondria and the endoplasmic reticulum (ER) act as
56 crucial signaling hubs in the context of non-selective, starvation-induced autophagy,
57 where they serve as the site of autophagosome formation (Hamasaki et al., 2013; Kishi-
58 Itakura et al., 2014). Indeed, autophagosome biogenesis is impaired in cells with
59 defective mitochondria-ER tethering (Hamasaki et al., 2013), as lipid transfer between
60 organelles may be important for their formation (Hailey et al., 2010; Klecker et al.,
61 2014). As steady-state mitophagy in yeast requires mitochondria-ER contacts (Bockler

62 and Westermann, 2014), it has been assumed that parkin-dependent mitophagy follows a
63 similar mechanism (Yoshii and Mizushima, 2015). However, this model directly conflicts
64 with the observation that mitofusin-2 (Mfn2) – a mitochondria-ER tether required for
65 starvation-induced autophagosome formation in mammals (de Brito and Scorrano, 2008;
66 Hamasaki et al., 2013; Naon et al., 2016) – is ubiquitinated by parkin and rapidly turned
67 over by the proteasome (Tanaka et al., 2010). Thus, how mitophagy is regulated by
68 contacts between mitochondria and the ER (if at all), and the location from which the
69 mitophagic membrane originates, remain open questions in the field.
70

71 **RESULTS**

72 *Parkin and PINK1 destroy mitochondria-ER contact during mitophagy*

73 We hypothesized that PINK1 and parkin may regulate contact between both
74 organelles during mitophagy, based on studies demonstrating high levels of parkin
75 ubiquitination activity on Mfn2 in both cells and *in organello* ubiquitination assays
76 (Tanaka et al., 2010; Tang et al., 2017). To first determine whether parkin destroys the
77 OMM-ER interface of depolarized mitochondria, we analyzed contacts between the two
78 organelles by electron microscopy (EM) (Csordas et al., 2006). We quantified ER tubules
79 within 100 nm of the OMM, as this distance is enough to capture tubules closely
80 associated with the OMM (Fig. 1A, left panel and inset). To induce PINK1-/parkin-
81 mediated mitophagy, we treated U2OS cells stably-expressing GFP-parkin (U2OS:GFP-
82 parkin) and control U2OS:GFP cells with CCCP for four hours, and observed by EM a
83 decrease the total length of ER-OMM contact in both cell lines, although this decrease
84 was greater in magnitude in cells expressing GFP-parkin (Fig. 1A, quantified in 1B).

85 However, when CCCP-induced, parkin-independent mitochondrial fragmentation was
86 taken into account (Fig. 1C), parkin had a specific effect on reducing the percentage of
87 the OMM that remained in contact with the ER in depolarized cells (Fig. 1D), as well as
88 the percentage of total mitochondria that were still connected to the ER (Fig. 1E). This
89 effect was robust, as repeating our quantification using a variety of interorganellar
90 tethering lengths – ER-OMM distances of 100 nm, 50 nm and 25 nm (Fig. 1–figure
91 supplement 1A and B) – pointed us to the same conclusion; parkin disrupts mitochondria-
92 ER contact upon activation of mitophagy. Indeed, this effect was indiscriminate in that it
93 was not selective for one subset of ER-OMM distances (Fig. 1–figure supplement 1C).
94 Moreover, the subsets of remaining contacts observed after the ~75% reduction in CCCP-
95 treated, GFP-parkin-expressing cells (Fig. 1D and Fig. 1–figure supplement 1C) were
96 biased towards longer interorganellar distances (Fig. 1–figure supplement 1D), consistent
97 with parkin driving the OMM and ER apart. Given that the mitochondria observed in our
98 EM analyses were still intact organelles and not yet engulfed by the isolation membrane
99 (IM) of the autophagosome (Fig. 1A, right panel), we concluded that parkin ablates
100 contact between mitochondria and the ER as an early step during depolarization-induced
101 mitophagy in cells.

102 We next took a closer look at how this process of contact site removal may occur
103 (for the remainder of our study, we used the <100 nm interorganellar distance to quantify
104 ER-OMM contacts). Parkin has been reported, through its ability to ubiquitinate OMM
105 proteins and target them for proteasomal degradation, to eventually mediate the rupture
106 the OMM prior to or during engulfment by the autophagosome (Yoshii et al., 2011).
107 Indeed, we observed rare (likely transient) mitochondrial structures where we believed

108 OMM rupture to be occurring at the time of fixation (Fig. 1F, the blue arrowheads
109 indicate the limits of OMM rupture, where the organelle is being wrapped by the IM
110 [indicated by the broken green line]). Concordantly, ER contacts with the still-intact
111 OMM were observed (Fig. 1F, red arrowheads), leading us to postulate that the removal
112 of OMM-ER contacts may precede OMM rupture. To this end, we quantified ER-OMM
113 contacts in CCCP-treated cells that were co-incubated with the proteasome inhibitor
114 MG132, which stabilizes the unmodified band of OMM parkin substrates, including
115 Mfn2, and prevents rupture of the OMM (Chan et al., 2011; Rakovic et al., 2011; Yoshii
116 et al., 2011) (Fig. 1G, GFP-parkin$^{C431S}$, which cannot ligate Ub (Trempe et al., 2013), is
117 used as a negative control). MG132 co-incubation rescued ER-OMM contact in
118 U2OS:GFP-parkin cells treated with CCCP (Fig. 1H, I and J). As expected, we also
119 prevented OMM-ER disruption in cells depleted of PINK1 (Fig. 1H, I and J).

120 Finally, we replicated our U2OS cell data in induced pluriopotent stem cell
121 (iPSC) -derived dopaminergic (iDA) neurons isolated from either control individuals or a
122 patient carrying compound heterozygous deletions in the *PRKN* gene (*PRKN*$^{del}$; see
123 *Materials and Methods*). iDA neuronal cultures express endogenous parkin at a level
124 comparable to that in the cytosolic fraction from mouse brain (Fig. 1K), as well as the
125 catecholinergic marker tyrosine hydroxylase (TH) (Fig. 1L). Full-length parkin was
126 undetectable in *PRKN*$^{del}$ cells (Fig. 1K), as expected given the genetic background of this
127 line (Grunewald et al., 2010). Upon treatment of these neurons with CCCP for only one
128 hour, we observed Mfn2 ubiquitination in both control lines but not in the parkin deletion
129 line (Fig. 1M). When we analyzed mitochondria-ER appositions in these cells, we again
130 observed a CCCP-dependent decrease in the amount of <100 nm ER-OMM appositions

131 in both control lines (Fig. 1N and O). However, this decrease was absent in the parkin
132 deletion line (Fig. 1N and O), supporting our previous overexpression data in U2OS cells
133 (Fig. 1A to E). Thus, PINK1 and parkin function to destroy contacts between the ER and
134 mitochondria during mitophagy, likely through parkin-mediated OMM protein
135 ubiquitination and turnover, as this process can be prevented by inhibiting proteasomal
136 degradation. Moreover, this is a relevant biological process in human dopamine neurons,
137 where it is regulated by endogenous parkin.
138
139 *Phosphoubiquitination of Mfn2 by the PINK1/parkin system disrupts its antagonistic*
140 *effect on mitophagy*
141 Our EM data demonstrated that ER-mitochondria uncoupling occurs as an early
142 step in the mitophagy pathway, prior to autophagosomal engulfment of the organelle
143 (Fig. 1F), and we sought to understand the underlying mechanism of this phenomenon.
144 Mfn2 is both a mitochondria-ER tether and parkin ubiquitination substrate (de Brito and
145 Scorrano, 2008; Sarraf et al., 2013; Tanaka et al., 2010), and thus the modulation of
146 interorganellar contact by PINK1/parkin may occur through their effect on Mfn2. We
147 began by examining the ubiquitination (via the disappearance of the unmodified band) of
148 various parkin substrates (Khan et al., 2016; Sarraf et al., 2013) during a CCCP time
149 course in U2OS:GFP-parkin cells, using the A320R mutant – which fails to bind pUb
150 and initiate mitophagy (Wauer et al., 2015a; Yamano et al., 2015) – as a negative control.
151 Turnover of both Mfn1 and Mfn2 occurred early (almost complete disappearance by two
152 hours) compared to other OMM proteins (Fig. 2A). Upon higher exposure (Fig. 2B) of
153 these immunoblots (from Fig. 2A), we observed a rapid "burst" of Mfn2 ubiquitination

154 that occurred between 30 and 60 minutes CCCP. When compared to TOM20, a protein
155 that is not promptly ubiquitinated by parkin (Sarraf et al., 2013), the rapidity of this Ub
156 burst on Mfn2 was emphasized as TOM20 ubiquitination occurs gradually over a period
157 of hours, rather than rapidly over a period of minutes (Fig. 2B). Thus, ubiquitination of
158 the mitofusins is one of the very first steps after the induction of mitophagy.

159 Mechanistically, this Ub burst would require local activation of parkin by PINK1
160 in the vicinity of Mfn2, which could be achieved by PINK1-catalyzed phosphorylation of
161 the resulting Ub chains – events that would dually serve to activate parkin and tether it in
162 place (Okatsu et al., 2015). To test this, we first immunoprecipitated WT or A320R GFP-
163 parkin from cells treated with CCCP over time. We observed robust
164 coimmunoprecipitation of ubiquitinated Mfn1 and Mfn2 with GFP-parkin$^{WT}$ at one hour
165 CCCP (corresponding to the Ub burst observed in Fig. 2B), with no apparent binding at
166 four hours (Fig. 2C), likely due to turnover of the Mfns by the proteasome at this time
167 (Fig. 1G, 2B and (Tanaka et al., 2010)). When we analyzed other parkin substrates that
168 are ubiquitinated less rapidly than the Mfns (Fig. 2A), we observed binding to WT parkin
169 only at four hours of CCCP treatment in the case of ubiquitinated Miro1, and binding of
170 mono-ubiquitinated HK1 at one hour CCCP, which was further shifted at four hours,
171 indicative of processivity of HK1 ubiquitination (Fig. 2C). None of these ubiquitinated
172 species coimmunoprecipitated with GFP-parkin$^{A320R}$ (Fig. 2C). To confirm that GFP-
173 parkin was indeed binding ubiquitinated Mfn2, we treated GFP-parkin
174 immunoprecipitates from CCCP-treated cells with Usp2 deubiquitinase (see schematic in
175 Fig. 2D), which is active on both phosphorylated and unphosphorylated Ub chains
176 (Wauer et al., 2015b), and observed the release of Mfn2 from the parkin-bound bead

177 fraction into the supernatant after separation by centrifugation (Fig. 2E). These results
178 strongly suggested that, early on in the mitophagy pathway, parkin was binding
179 ubiquitinated Mfn2, likely through interactions with pUb moieties.

180 We next confirmed the phosphoubiquitination of Mfn2 during mitochondrial
181 depolarization. When we immunoprecipitated Mfn2 from U2OS:GFP-parkin$^{WT}$ cells that
182 were treated with CCCP for one hour, we detected Ub-modified species by immunoblot
183 (Fig. 2E). This was concomitant with a decrease in overall Mfn2 levels (Fig. 2F), owing
184 to its proteasomal turnover (Fig. 1G). Liquid-chromatography coupled to mass
185 spectrometry (LC/MS) confirmed that the Mfn2 immunoprecipitation contained pS65 Ub
186 selectively in the CCCP-treated condition (Fig. 2G), despite lower Mfn2 levels (Fig. 2A,
187 2F and Fig. 2–figure supplement 1). We then confirmed that both pS65 and
188 unphosphorylated Ub were covalently attached to Mfn2 by its precipitation under
189 denaturing conditions and detecting pS65 Ub and total Ub by immunoblot (Fig. 2H).
190 Finally, profiting from the nanomolar affinity of the parkin R0RBR module for pS65 Ub
191 (Sauve et al., 2015), we used GST-R0RBR to pull down phosphoubiquitinated species
192 from CCCP-treated U2OS:GFP-parkin$^{WT}$ cell lysates. We again used the A320R mutant
193 – which abolishes the parkin-pUb interaction (Fig. 2I) (Wauer et al., 2015a; Yamano et
194 al., 2015) – as a negative control. In a CCCP-dependent manner, pS65 Ub, Ub and
195 (shifted) Mfn2 could be detected in GST-R0RBR$^{WT}$ pulldowns (Fig. 2J). Strikingly, we
196 did not observe any of these factors in pulldowns using GST-R0RBR$^{A320R}$ (Fig. 2J).
197 Mfn2 is therefore phosphoubiquitinated and, taken together with our previous data, a
198 burst of phosphoubiquitination – parkin-mediated ubiquitination coupled to PINK1-

199 catalyzed phosphorylation – occurs on Mfn2 at an early time point in the mitophagy
200 pathway.

201 Our observations so far demonstrated that mitochondria are separated from the
202 ER during mitophagy, and that the OMM-ER tether Mfn2 is rapidly degraded at the onset
203 of the pathway. We thus hypothesized that Mfn2 may antagonize mitophagy through its
204 ability to tether mitochondria and the ER, necessitating its destruction. To test this, we
205 silenced Mfn2 (siMfn2) in U2OS:GFP-parkin$^{WT}$ cells, as well as Mfn1 – which promotes
206 mitochondrial fusion without any apparent role in interorganellar tethering (de Brito and
207 Scorrano, 2008) – to control for phenomena resulting from fusion defects. We confirmed
208 Mfn1 and Mfn2 depletion by immunoblot (Fig. 3A), and observed mitochondrial
209 fragmentation in both siMfn1 and siMfn2 cells (Fig. 3B and Fig. 3–figure supplement 1A
210 and B) with an ER-OMM apposition defect unique to the siMfn2 condition (Fig. 3–figure
211 supplement 1A, C and D), as expected. Next, we investigated the kinetics of parkin
212 recruitment to depolarized mitochondria in these cells (in our analyses, a cell is
213 considered to have recruited parkin if the parkin signal covers the mitochondrial
214 reticulum in its entirety). Moreover, we took advantage of delayed pathway kinetics of
215 respiring cells by culturing cells in growth medium containing galactose as a carbon
216 source (rather than glucose). This forces ATP generation through the electron transport
217 chain and mitigates parkin-dependent mitophagy (Lee et al., 2015; McCoy et al., 2014);
218 mitochondrial translocation of parkin, and the buildup of Ub, p62 and LC3 on
219 mitochondria are all slowed in galactose-grown cells (Fig. 3–figure supplement 2).
220 Remarkably, we observed faster mitochondrial recruitment in siMfn2 (but not siMfn1)
221 cells, under both bioenergetic conditions (Fig. 3C and D). A significant difference was

222 visible within one hour of CCCP treatment in glucose-cultured cells, and was exacerbated
223 in their galactose-grown counterparts, owing to their slower kinetics in the control
224 siRNA-transfected condition (Fig. 3E). Strikingly, Mfn2 silencing increased recruitment
225 in galactose-grown cells to levels seen in glucose-maintained cells transfected with
226 control siRNA (Fig. 3E). Silencing Mfn1 and Mfn2 simultaneously (Fig. 3–figure
227 supplement 3A) did not further enhance the kinetics of parkin recruitment beyond single,
228 Mfn2-depleted cells (Fig. 3–figure supplement 3B-D), implying that this phenotype was
229 Mfn2-specific and unrelated to a loss of mitochondrial fusion.

230 We next determined whether, more generally, this increase in recruitment kinetics
231 could be induced by disrupting mitochondria-ER contacts via other means than removing
232 Mfn2. To test this, we silenced two other genes that have been shown to promote
233 mitochondria-ER association; PACS2 and Stx17 (Fig. 3–figure supplement 3E) (Arasaki
234 et al., 2015; Simmen et al., 2005). Unlike Mfn2 knockdown, we did not observe
235 mitochondrial fragmentation in either PACS2- or Stx17-silenced cells (Fig. 3–figure
236 supplement 3F). When we tested parkin recruitment in these cells, we saw that, similarly
237 to Mfn2 knockdown, silencing of either PACS2 (siPACS2) or Stx17 (siStx17) increased
238 the translocation of parkin to mitochondria (Fig. 3–figure supplement 3G and H). Again,
239 the increase was most pronounced in galactose-cultured cells that were treated with
240 CCCP for one hour, where parkin was recruited to near-glucose levels in Mfn2-, PACS2-
241 and Stx17-silenced cells despite remaining predominantly cytosolic in cells transfected
242 with control siRNA at this time point (Fig. 3–figure supplement 3G and I). Thus,
243 disruption of mitochondrion-ER tethering increases the kinetics of parkin translocation to
244 depolarized mitochondria.

245 We next directly tested the effect of Mfn2 depletion on mitochondrial turnover
246 using quantitative, ratiometric measurements of mitochondrially-targeted mKeima
247 (mtKeima), a protein that shifts its fluorescence excitation when acidified by the
248 lysosome (Katayama et al., 2011). We transfected U2OS cells stably-expressing
249 mtKeima (U2OS:mtKeima), grown on either glucose or galactose, with siRNA targeting
250 Mfn1 or Mfn2, followed by wild-type (WT) GFP-parkin, using the ligase-dead C431S
251 mutant as a negative control. Next, we treated these cells with CCCP (or DMSO) for four
252 hours and then determined the ratio of acidified mtKeima per cell by FACS (see
253 *Materials and Methods*) as a quantitative indicator of mitophagy (Katayama et al., 2011;
254 Tang et al., 2017). As expected, in the glycolytic, CCCP-treated condition, a higher
255 proportion of control siRNA-transfected cells had an increased ratio of acidified
256 mtKeima compared with DMSO-treated counterparts (as these cells were undergoing
257 mitophagy) and this population shift was similarly replicated in siMfn1 cells (Fig. 3F and
258 G). However, in Mfn2-depleted cells, we observed a ~2-fold increase in the proportion of
259 cells undergoing mitophagy (Fig. 3F and G). In respiring conditions, we did not observe a
260 shift at all in either control siRNA-transfected or Mfn1-depleted cells but observed a
261 level of mitophagy in siMfn2 cells similar to control cells cultured in glucose medium
262 (Fig. 3F and G). These data demonstrate that, in Mfn2-depleted cells, depolarization-
263 induced mitophagy is enhanced, in line with our parkin recruitment experiments (Fig. 3A
264 to E), and demonstrate that Mfn2 represses mitophagy at the level of pathway initiation.
265 To ensure that we were observing on-target effects from depletion of our siRNA
266 targets, we replicated our recruitment data in Mfn2 knock-out (KO) U2OS cells that were
267 generated using the CRISPR-Cas9 system (see *Materials and Methods*). Genetic

268 disruption was confirmed by sequencing in two clones (A4 and A5) in which a premature
269 stop codon was introduced via a single base-pair frame shift following the codon
270 corresponding to leucine-29 in the human Mfn2 gene (Fig. 3–figure supplement 4A). We
271 validated these KO cells by immunoblot, along with a clone that underwent the complete
272 procedure and selection but in which Mfn2 knock out failed (B4) as a further negative
273 control; importantly, Mfn1 levels remained similar across all lines, and the core subunits
274 of the mitochondrial $Ca^{2+}$ uniporter remained unperturbed (Fig. 3–figure supplement 4B,
275 compensation in the latter has been reported in MEFs isolated from $Mfn2^{-/-}$ mice (Filadi
276 et al., 2015)). Accordingly, Mfn2 KO cells had mitochondrial reticula that were similarly
277 polarized but fragmented compared to WT U2OS cells (Fig. 3–figure supplement 4C and
278 D). Corroborating our earlier data in siMfn2 cells, Mfn2 KO cells (grown on glucose)
279 transiently transfected with GFP-parkin displayed increased recruitment kinetics (Fig. 3–
280 figure supplement 4E and F) and increased mitophagy (Fig. 3–figure supplement 4G and
281 H). Finally, we ensured that parkin translocation in Mfn2 KO cells (Fig. 3–figure
282 supplement 5A to C) and U2OS:GFP-parkin cells depleted of Mfn2 (Fig. 3–figure
283 supplement 5D) remained PINK1-dependent. Moreover, cells expressing GFP-
284 $parkin^{A320R}$ (Fig. 3–figure supplement 5E) failed to translocate under conditions of Mfn2-
285 depletion (Fig. 3–figure supplement 5F and G). This indicates a clear requirement for
286 PINK1 and Ub phosphorylation for parkin translocation in Mfn2-depleted cells,
287 demonstrating that Mfn2 reduction increases on-pathway mitophagy kinetics. Taken
288 together, our data not only show that mitochondria-ER contact is dispensable for
289 mitophagy, but that this type of organellar coupling in fact antagonizes the pathway.

290 We next sought to demonstrate that the antagonistic effect of mitochondria-ER
291 tethering on mitophagy was functioning directly through the degradation of Mfn2.
292 Conceivably, we could manipulate the pathway by preventing ER-OMM dissociation
293 through the blockage of Mfn2 turnover, which is mediated by proteasomal degradation
294 coupled to parkin ubiquitination (Tanaka et al., 2010; Ziviani et al., 2010). This
295 hypothesis is supported by our EM data demonstrating that MG132 blocks mitochondria-
296 ER uncoupling during mitophagy (Fig. 1H to J). To achieve this, we created Mfn2 KO
297 cells stably-expressing YFP-parkin (Mfn2 KO:YFP-parkin) and re-expressed ectopic
298 Mfn2, which was able to rescue mitochondrial morphology from a fragmented reticulum
299 to a collection of tubules (Fig. 4A; CFP is used to identify cells expressing untagged
300 Mfn2). We could additionally rescue morphology by overexpression of Mfn1 (Fig. 4A), a
301 phenomenon that has been described previously (Chen et al., 2003). Turning to
302 recruitment assays – in which we observed faster GFP-parkin recruitment in Mfn2 KO
303 cells (Fig. 3–figure supplement 4E and F) – we observed that ectopic expression of Mfn2,
304 but not Mfn1, was able to suppress the recruitment of YFP-parkin to depolarized
305 mitochondria (Fig. 4B and C). This is in line with our previous data showing that the
306 antagonistic effect of Mfn2 on mitophagy occurs through its ability to tether
307 mitochondria to the ER (Fig. 3–figure supplement 3H to J) and not its effect on
308 mitochondrial fusion (Fig. 3–figure supplement 3A to D). Immunoblot analysis of Mfn2
309 KO:YFP-parkin$^{WT}$ cells ectopically expressing Mfn2 revealed that it was expressed at
310 near-endogenous levels in the parental U2OS line and degraded rapidly upon CCCP
311 treatment compared to the control Mfn2 KO:YFP-parkin$^{C431S}$ cell line (Fig. 4D). Mfn2 is
312 ubiquitinated by parkin on at least ten lysine residues, although several sites are clustered

313 in the heptad repeat (HR) domains (Sarraf et al., 2013). Additionally, Mfn2 itself has
314 been reported to be directly phosphorylated by PINK1 on T111 and S442, and that these
315 phosphorylation events are critical for the interaction of parkin with Mfn2 and parkin
316 recruitment in cardiomyocytes (Chen and Dorn, 2013). Focusing on these putative
317 phosphorylation sites and the clustered ubiquitination sites in the HR1 and HR2 domains,
318 phylogenic analysis of their conservation demonstrated that only T111 in the GTPase
319 domain and K737 in the HR2 domain were completely conserved from human Mfn2 to
320 the sole *Drosophila* mitofusin, MARF (Fig. 4–figure supplement 1A and B; both the
321 traditional and single-pass Mfn2 topologies (Mattie et al., 2017) are depicted in Fig. 4–
322 figure supplement 1B). However, in the case of the sites of ubiquitination, at least two
323 HR1 sites and three HR2 sites were conserved as lysines down through *Xenopus* Mfn2,
324 while MARF retained one site each in HR1 and HR2 (Fig. 4–figure supplement 1A). We
325 thus posited that mutation of several lysine residues would likely be required to reduce
326 Mfn2 ubiquitination. While mutation of all major sites of Mfn2 ubiquitination almost
327 completely abolishes its modification by parkin (Heo et al., 2015), we found that
328 mutation of K406, K416 and K420 in the HR1 domain ($Mfn2^{HR1}$) reduced its CCCP-
329 induced ubiquitination by ~75%, as measured by the disappearance of the unmodified
330 band by immunoblot (Fig. 4E and F; here Mfn2 levels are normalized to the untreated
331 condition for each construct). This effect was greater than what we observed with the
332 single mutant, $Mfn2^{K406R}$ (K416 and K420 appear dispensable in this assay), and
333 mutation of all four sites in HR2 ($Mfn2^{HR2}$) or the double T111A/S442A phosphomutant
334 ($Mfn2^{TS/AA}$) failed to significantly reduce Mfn2 modification (Fig. 4E and F). We thus
335 considered $Mfn2^{HR1}$ as a "hypomorph" with respect to parkin ubiquitination compared to

336 WT, HR2 and TS/AA constructs, despite similar expression patterns with the latter two
337 (Fig. 4G). Introduction of either Mfn2$^{HR1}$, Mfn2$^{HR2}$ or Mfn2$^{T111A/S442A}$ into Mfn2
338 KO:YFP-parkin cells rescued morphology in a similar manner to WT Mfn2 (Fig. 4H),
339 demonstrating these mutations did not disrupt mitochondrial fusion. We also monitored
340 the ability of these Mfn2 mutants to form high molecular weight (HMW) complexes
341 (Karbowski et al., 2006) that function in mitochondria-ER tethering (de Brito and
342 Scorrano, 2008). By blue native polyacrylamide gel electrophoresis (BN-PAGE), we
343 observed that all three mutants (HR1, HR2 and T11A/S442A) formed HMW complexes
344 similar to WT in solubilized mitochondria (Fig. 4I). When we assayed mitophagy in
345 Mfn2 KO:YFP-parkin$^{WT}$ cells, we found that only rescue of Mfn2 with Mfn2$^{HR1}$ – the
346 ubiquitination of which is compromised (Fig. 4E and F) – blocked the turnover of
347 mitochondria (Fig. 4J and K). Thus, ubiquitination of the Mfn2 HR1 domain by parkin is
348 required for efficient mitophagy and, taken together with our previous mitophagic data in
349 Mfn2-depleted cells, demonstrates that parkin and PINK1 directly counter Mfn2-
350 mediated mitochondria-ER tethering through Mfn2 turnover to promote mitophagy.
351
352 *Mfn2 complexes are extraced by p97 to drive mitochondria and the ER apart*
353 We next investigated exactly how parkin and PINK1 act on Mfn2-mediated
354 OMM-ER tethering. Examining HMW complexes by BN-PAGE in untreated
355 U2OS:GFP-parkin$^{WT}$ cells (expressing endogenous Mfn2), we observed a bimodal
356 distribution of Mfn2 into two complexes, weighing approximately ~250 kDa and ~500
357 kDa (Fig. 5A, leftmost lane, similar to what was seen in Fig. 4I). By contrast, Mfn1 –
358 which, in our assays, appears dispensable for mitochondria-ER tethering as assayed by

359 EM (Fig. 3–figure supplement 1) and its effect on parkin recruitment (Fig. 3C to E) –
360 only formed a ~250 kDa HMW complex (Fig. 5A). We thus considered the ~500 kDa
361 complex containing solely Mfn2 as a dimer of the ~250 kDa Mfn2-containing
362 subcomplex that potentially bridges the ER and OMM. We then monitored the stability of
363 Mfn2- (and Mfn1-) containing HMW complexes during mitophagy. Upon CCCP
364 treatment, we observed a rapid loss Mfn2- (and Mfn1-) containing complexes (Fig. 5A),
365 concomitant with its phosphoubiquitination (Fig. 2) and dependent upon parkin ligase
366 activity (Fig. 5B and C). While treatment of mitochondrial lysates with Usp2
367 deubiquitinase slightly increased levels of the unmodified Mfn1 or Mfn2 band in
368 mitochondria isolated from CCCP-treated cells (Fig. 5D; the densitometry measurements
369 correspond to the shorter exposures of Mfn1 and Mfn2), this was not to levels seen in
370 mitochondria from untreated cells. This result indicated that the disappearance of HMW
371 Mfn complexes are predominantly due to their extraction from the OMM (and not a high
372 level of modification by Ub). This process is thought to be mediated by the AAA-ATPase
373 p97/VCP (Tanaka et al., 2010) and, accordingly, when we treated U2OS:GFP-parkin$^{WT}$
374 cells with CCCP in the presence of the non-competitive p97 inhibitor NMS-873
375 (Magnaghi et al., 2013), extraction of HMW complexes containing either Mfn1 or Mfn2
376 was accordingly repressed (Fig. 5E). Indeed, both ~250 kDa (containing Mfn1 and/or
377 Mfn2) and ~500 kDa (Mfn2 only) complexes were stabilized in the presence of NMS-
378 873 (Fig. 5E), with smearing occurring due to Mfn ubiquitination (see Fig. 2), indicating
379 that parkin-mediated ubiquitination itself was not sufficient to drive apart the ~500 kDa
380 Mfn2-containing interorganellar bridge. Analysis of OMM-ER appositions in these cells
381 revealed that p97 inhibition prevented the dissociation of mitochondria from the ER (Fig.

382 5F to H). Thus, p97-dependent extraction of Mfn2 HMW complexes from the OMM
383 separates mitochondria from the ER during mitophagy.

384 We then addressed the relationship between parkin-dependent Mfn2
385 ubiquitination and p97 extraction more closely. Consistent with our HMW complex
386 extraction data (Fig. 5E), co-incubation of cells with CCCP and NMS-873 completely
387 blocked the mitochondrial translocation of p97 (Fig. 6A and B) which occurs during
388 mitophagy (Kimura et al., 2013; Tanaka et al., 2010). Accordingly, NMS-873 stabilized
389 ubiquitinated Mfn1 and Mfn2 conjugates induced by CCCP in whole-cell extracts (Fig.
390 6C) and, consistent with our BN-PAGE data (Fig. 5E), these ubiquitinated Mfn2 species
391 were present on mitochondria (Fig. 6D). We observed a similar effect when we silenced
392 p97 with siRNA (sip97); in p97-depleted cells treated with CCCP, we saw an increase in
393 ubiquitinated Mfn2 upon depolarization (Fig. 6E). Additionally, basal levels of Mfn2
394 increased upon prolonged p97 depletion (Fig. 6E), consistent with the possible
395 involvement of p97 in steady-state Mfn2 turnover (Zhang et al., 2017). In Mfn2
396 KO:YFP-parkin$^{WT}$ cells rescued with WT Mfn2, CCCP induced Mfn2 turnover and,
397 when cells were co-incubated with NMS-873, we observed a stabilization of
398 ubiquitinated Mfn2 (Fig. 6F) similar to WT U2OS cells expressing GFP-parkin (Fig. 6C).
399 When we expressed Mfn2$^{HR1}$ in Mfn2 KO:YFP-parkin$^{WT}$ cells, we observed a severe
400 reduction in NMS-873-dependent stabilization of CCCP-induced Mfn2-Ub conjugates
401 (Fig. 6F). We confirmed this reduction in ubiquitination by immunoprecipiting Mfn2
402 from reconstituted cells treated with CCCP and NMS-873 under denaturing conditions
403 and immunoblotting for Ub (Fig. 6G). This supports our mutagenesis data showing a
404 reduction of Mfn2$^{HR1}$ turnover (Fig. 4E and F) and is mechanistically consistent with

405 ubiquitination of lysines in the Mfn2 HR1 domain being recognized by p97 and signaling
406 for extraction of the protein.

407 While we posited that Mfn2 may be acting as a p97 receptor during mitophagy,
408 we observed robust p97 recruitment in depolarized Mfn2 KO:YFP-parkin$^{WT}$ cells (Fig.
409 6H and I). Moreover, p97 recruitment was similar in cells expressing either Mfn2$^{WT}$ or
410 Mfn2$^{HR1}$ (Fig. 6H and I). p97 recruitment levels in both Mfn2 rescue conditions were
411 lower than in cells transfected with empty vector (Fig. 6H and I) likely owing to the
412 delayed parkin recruitment kinetics in Mfn2-expressing cells (Fig. 4B and C). Thus,
413 ubiquitinated Mfn2 is not the sole p97-binding protein on the OMM. We next tested if
414 pUb moieties conjugated to Mfn2 play a role in p97 binding. As we detected pUb
415 conjugated to immunoprecipitated Mfn2 from cells treated with CCCP (Fig. 2G and H),
416 we co-treated cells with CCCP and NMS-873 and observed that the interaction between
417 parkin and ubiquitinated Mfn2 – which is normally transient owing to Mfn2 turnover –
418 was stabilized (Fig. 6J and K). Finally, we probed for the existence of a pUb-p97
419 interaction by performing a GST pull-down using either S65-phosphorylated or
420 unphosphorylated 4xUb chains from mouse brain lysate (see Fig. 6 –figure supplement
421 1A for experimental schematic) and identified interactors by LC/MS. Using nearly fully-
422 phosphorylated chains (Fig. 6 –figure supplement 1B), we consistently observed the
423 presence of p97, as well as its cofactors p47 and UBXN1, in 4xUb pull-downs, and these
424 proteins were almost totally absent in parallel 4xpUb pull-downs (Fig. 6 –figure
425 supplement 1C and Supplementary File 1). Thus, while p97 mediates the turnover of
426 ubiquitinated Mfn2, this likely does not involve interactions between the p97 complex
427 and pUb.

428 The herein-described role of p97 in separating mitochondria from the ER is
429 critical; parkin-mediated ubiquitination on its own appears to be insufficient to drive the
430 disassembly of Mfn2 HMW complexes (Fig. 5E) or to dissociate the ER from the OMM
431 (Fig. 5F and G) in the absence of p97 activity. To clarify the role of p97 in mitophagy,
432 we investigated the potentially epistatic relationship between p97 and Mfn2. We first
433 measured mitophagy in U2OS:mtKeima cells expressing GFP-parkin$^{WT}$, comparing the
434 effect of p97 inhibition in cells depleted of Mfn2 to control cells. In control siRNA-
435 transfected cells, inhibition of p97 by NMS-873 abolished the CCCP-dependent, ~3-fold
436 increase in cells with acidified mtKeima (Fig. 7A and B, red and orange bars in Fig. 7B).
437 When cells were depleted of Mfn2 (siMfn2), p97 inhibition reduced the rate of mtKeima
438 acidification (Fig. 7A and B, dark and light blue bars), but mitophagy was still
439 permissive. Indeed, the number of cells with acidified mtKeima in siMfn2 cells treated
440 with NMS-873 was still ~5-fold greater than their DMSO treated counterparts (Fig. 7B,
441 light blue bar), which was more of an increase that was observed for control cells with
442 active p97 (Fig. 7B, red bar). Thus, in the absence of Mfn2, inhibition of p97 fails to
443 suppress mitophagy, demonstrating that a significant component of the role of p97 in
444 mitophagy functions through Mfn2. As p97 extracts Mfn2-containing interorganellar
445 bridges to uncouple mitochondria from the ER (Fig. 5), we reasoned that Mfn2-mediated
446 mitochondria-ER tethering may restrict the parkin-mediated ubiquitination of specific
447 OMM substrates. Thus, we analyzed a sample of parkin substrates by immunoblot in
448 CCCP-treated cells depleted of Mfn2 compared to control, in the presence or absence of
449 NMS-873 (Fig. 7C). We observed that the parkin-dependent ubiquitination of VDAC1 –
450 which has been reported to form a complex with pUb and parkin that is stable over a

451 period of hours (Callegari et al., 2016) – was sensitive to p97 inhibition in control cells,
452 but not cells depleted of Mfn2 (Fig. 7C to E). Indeed, the half-time of VDAC1
453 modification during mitophagy increased two-fold in the presence of NMS-873
454 specifically in control cells compared to cells transfected with siMfn2 (Fig. 7F). We
455 observed a similar effect pertaining to the difference in CCCP-dependent VDAC1
456 modification between cells treated with NMS-873 *versus* control across all cells depleted
457 of promoters of mitochondria-ER tethering (Mfn2, PACS2 and Stx17) (Fig. 7G and H).
458 Notably, cells depleted of Mfn1 were comparable to control siRNA-transfected cells in
459 this regard (Fig. 7G and H). Thus, p97 relieves Mfn2-dependent inhibition of the
460 ubiquitination of VDAC1 (and likely other OMM substrates). In this manner, Mfn2 gates
461 the availability of the stable parkin receptor VDAC1 (Callegari et al., 2016), and
462 mechanistically reconciles our data concerning the destruction of ER-OMM contacts
463 during mitophagy, Mfn2-dependent mitophagy inhibition, and p97-mediated facilitation
464 of ER-OMM uncoupling.
465
466 *Cell-free reconstitution of mitochondria-ER uncoupling by PINK1/parkin/p97*
467 Cell-free reconstitution assays have proven useful in interrogating the activation
468 of parkin-dependent ubiquitination by both PINK1 (Lazarou et al., 2013) and designer
469 mutations in parkin itself (Tang et al., 2017). We thus sought to recapitulate our findings
470 in cells concerning Mfn2 and VDAC1 ubiquitination in a cell free assay (see diagram in
471 Fig. 8A). We first isolated mitochondria from HeLa cells – which lack endogenous
472 parkin (Denison et al., 2003) – that were either depolarized with CCCP for four hours
473 ("mito$^{CCCP}$") or treated with DMSO as a control ("mito$^{DMSO}$"). Accordingly, we observed

474 PINK1 stabilization in the CCCP-treated condition only (Fig. 8B). We were then able to
475 reconstitute parkin-dependent ubiquitination of Mfn2 on the OMM of these isolated
476 mitochondria by adding the E1, E2 and E3 (parkin) components of this pathway, as well
477 as Ub and other factors, as previously described (Tang et al., 2017), in a time-,
478 depolarization- and ligase-dependent manner (Fig. 8C). Using depolarized mitochondria
479 isolated from cells depleted of PINK1 (Fig. 8D), Mfn2 ubiquitination was almost
480 completely abolished (Fig. 8E), demonstrating an as-expected requirement for PINK1 in
481 parkin-dependent ubiquitination.

482 Although we observed robust Mfn2 (and Mfn1) ubiquitination in reactions with
483 depolarized mitochondria and WT parkin, we observed very little to no ubiquitination of
484 other OMM substrates, such as VDAC1, HK1 or TOM20 (Fig. 8F, compare with Fig. 2A
485 and B). Based on our data in cells, we reckoned that a dearth of p97 in this *in organello*
486 system may prohibit modification of parkin substrates downstream of Mfn2. We first
487 addressed this by isolating cytosol ("S200k") from mouse brain – which was devoid of
488 mitochondrial, ER and endosomal markers (Fig. 8G) – to use as a source of cytosolic p97
489 ATPase (Otter-Nilsson et al., 1999). As parkin itself is cytosolic (Fig. 8G), we initially
490 proceeded to co-incubuate *in organello* ubiquitination reactions with cytosol from
491 parkin$^{+/+}$ ("WT cytosol") and parkin$^{-/-}$ ("KO cytosol") mouse brain in the absence of
492 recombinant ligase, and observed that cytosolic, mouse parkin was able to catalyze Mfn2
493 ubiquitination in a depolarization-dependent manner, albeit not to the extent of 100 nM
494 recombinant GST-parkin (Fig. 8H; here the GST tag was not cleaved in order to visualize
495 the different forms of parkin by immunoblot). Based on this result, we proceeded to co-
496 incubate isolated mitochondria with KO cytosol and recombinant parkin. Under these

497 conditions, we observed robust ubiquitination of both Mfn2 and VDAC1 compared to
498 reactions lacking KO cytosol (Fig. 8I). This result indicated a potential role for p97
499 (which was present in the cytosol, Fig. 8H and I) in this process and, remarkably, in
500 cytosol-containing reactions, VDAC1 ubiquitination displayed sensitivity to NMS-873
501 (Fig. 8J and K). Importantly, NMS-873 had no effect on ubiquitination in the absence of
502 cytosol (Fig. 8–figure supplement 1), indicating that the small amount of p97 present in
503 reactions lacking cytosol was either negligible or already engaged with other substrates.
504 To ensure that p97 was truly stimulating VDAC1 ubiquitination, we added recombinant
505 p97 hexamer to our reactions (Fig. 8L). The addition of recombinant hexamer, in a
506 parkin-dependent manner, stimulated both Mfn2 and VDAC1 ubiquitination (Fig. 8M).
507 This was, however, not to the extent seen with cytosol (which is p97-dependent, Fig. 8J
508 and K), as other cytosolic factors, notably p97 cofactors and E4 ligases, are also likely
509 involved.

510 Finally, we tested whether retrotranslocation of Mfn2 by recombinant p97 was
511 occurring in our *in organello* reactions. By fractionating samples post-reaction into
512 mitochondria (pellet) and soluble factors (supernatant), we observed a small amount of
513 Mfn2 appear in the supernatant only when recombinant p97 was added to the
514 ubiquitination reaction (Fig. 8N; samples were solubilized with TX-100 as a positive
515 control). A longer exposure revealed that retrotranslocated Mfn2 was indeed
516 ubiquitinated (box in Fig. 8N). Taken together, our *in organello* ubiquitination data show
517 that, in a cell-free assay, we can reconstitute PINK1/parkin-dependent, p97-stimulated
518 Mfn2 and VDAC1 ubiquitination, and Mfn2 retrotranslocation. These results are in line
519 with our experiments in cells which demonstrate that PINK1, parkin and p97 collaborate

520 to uncouple OMM-ER contacts via Mfn2 ubiquitination and degradation during
521 mitophagy, which in turn allows ubiquitination and degradation of additional parkin
522 substrates such as VDAC1.
523

524 **DISCUSSION**

525 Here, we have described a reciprocal relationship between mitochondria-ER
526 tethering and mitophagy. Contacts between both organelles are destroyed during
527 mitophagy, in both heterologous cell cultures and dopaminergic neurons, and we
528 demonstrate a requirement for parkin, PINK1, p97 and proteasomal activity in this
529 process. Complementarily, mitochondria-ER contacts themselves are negative regulators
530 of mitophagy, as their reduction facilitates parkin substrate ubiquitination, its
531 translocation to mitochondria and mitochondrial turnover. We identify the known
532 mitochondria-ER tether Mfn2 as a factor that is rapidly phosphoubiquitinated upon the
533 induction of mitophagy, and show that Mfn2-containing HMW complexes are extracted
534 from the OMM by p97 in a manner requiring parkin-dependent ubiquitination in the
535 Mfn2 HR1 domain. Both reduction of Mfn2 ubiquitination and p97 inhibition repress
536 mitophagy, and we reconstitute the main concepts of this PINK1/parkin/p97 enzymatic
537 system in a cell-free system. Overall, we identify a regulatory role for Mfn2-mediated
538 mitochondria-ER coupling within the parkin/PINK1 pathway, which is counteracted by
539 the ubiquitination of Mfn2 by parkin and its p97-dependent proteasomal turnover.

540 We propose a model in which the PINK1/parkin/p97 axis acts rapidly on Mfn2
541 HMW complexes to separate mitochondria from the ER in order to facilitate mitophagy,
542 potentially by making more substrates available to the parkin/PINK1 system (Fig. 9).

543 Emerging from this model is the intriguing possibility that mitochondria-ER contacts are
544 initial sites of PINK1/parkin activity and Ub phosphorylation, and would thus be critical
545 loci of mitophagic regulation by deubiquitinating enzymes and as-yet unidentified
546 ubiquitin phosphatases. A recent cryoelectron tomographical study on the ancestral yeast
547 mitofusin Fzo1p demonstrated the existence of a ring-like structure formed by Fzo1p
548 during the docking stage of mitochondrial fusion (Brandt et al., 2016). Mfn2 bridges
549 between mitochondria and the ER may therefore form a similar type of ring, potentially
550 restricting the availability of non-mitofusin OMM substrates such as VDAC1 (Fig. 7C to
551 H, and Fig. 8I to M) to parkin and/or PINK1. With respect to the latter case, PINK1 has
552 recently been shown to localize to the mitochondria-associated membrane of the ER
553 (MAM) upon depolarization (Gelmetti et al., 2017), and a physical interaction between
554 VDACs on the OMM and $IP_3$ receptors on the ER places this parkin substrate at contacts
555 between both organelles (Szabadkai et al., 2006). The existence of a ~500 kDa Mfn2-
556 containing interorganellar bridge is supported by our BN-PAGE data (Fig. 5A)
557 demonstrating that Mfn2 uniquely exists in a homotypic dimer of ~250 kDa subunits, as
558 it has been demonstrated that ~500 kDa mitofusin complexes form from subcomplexes
559 on adjacent membranes (Ishihara et al., 2004). Our observation of a steady-state ~500
560 kDa complex containing Mfn2 but not Mfn1 correlates with the reduced activity of the
561 Mfn2 GTPase domain in comparison to Mfn1 (Ishihara et al., 2004), supports a distinct
562 role for Mfn2 in OMM-ER tethering (Fig. 3–figure supplement 1 and (de Brito and
563 Scorrano, 2008)), and fits a model in which Mfns tether membranes in the GTP-bound
564 state (Brandt et al., 2016; Ishihara et al., 2004; Qi et al., 2016). Here, we show that the
565 stability of these complexes can be negatively regulated by parkin-mediated Mfn2

566 ubiquitination crucially coupled to p97-dependent retrotranslocation. Intriguingly, we
567 observed both ubiquitinated and unmodified forms of retrotranslocated Mfn2 upon p97
568 addition (Fig. 8N). This may hint that, while the hexamer engages directly with Mfn2 at
569 the high concentrations used in our assay, Ub-binding cofactors may localize the hexamer
570 to ubiquitinated Mfn2 at physiological levels of p97. Indeed, in ER-associated
571 degradation, p97 recognizes both Ub-dependent and intrinsic signals (Ye et al., 2003).
572 The above findings, taken together with another study demonstrating that MITOL-
573 mediated Mfn2 ubiquitination (on different lysine residues) can positively regulate
574 complex formation and mitochondria-ER tethering (Sugiura et al., 2013), emphasize
575 Mfn2 ubiquitination as an important regulator of mitochondria-ER contact.

576 Robust parkin activation during mitophagy occurs through a feed-forward
577 mechanism (Ordureau et al., 2014). PINK1-phosphorylated Ub serves to both activate
578 and anchor parkin to the OMM, where it can ligate more Ub moieties that are
579 subsequently phosphorylated (Okatsu et al., 2015; Ordureau et al., 2014). Here, our data
580 hint at a hierarchy of parkin substrates. The Mfns undergo a burst of
581 phosphoubiquitination at the onset of mitophagy, driven by localized parkin activation –
582 potentially due to their proximity to PINK1 (Chen and Dorn, 2013). Indeed, our GFP-
583 parkin immunoprecipitation (Fig. 2C), OMM substrate turnover kinetics (Fig. 2A), and
584 reconstitution assays (Fig. 8F) clearly show a preference for the Mfns above other parkin
585 substrates such as HK1 and Miro1. The Mfns are then rapidly extracted from the OMM
586 by p97 (Fig. 5A and E, Fig. 8N) in a step that coincides temporally with parkin
587 translocation to mitochondria. It is therefore unlikely that Mfn1 or Mfn2 act as a parkin
588 receptor in this paradigm – as others have suggested (Chen and Dorn, 2013) – for this

589 reason, especially when our recruitment data in Mfn2-deficient cells (Fig. 3C to E and
590 Fig. 3–figure supplement 4) are taken into account. Indeed, we demonstrate that Mfn2
591 acts as a stable parkin tether only under conditions where retrotranslocation by p97 is
592 inhibited (Fig. 6J and K). Our data support a role for the involvement of VDAC1 in a
593 stable complex that tethers parkin to the OMM (Callegari et al., 2016); as β-barrel
594 channels fully integrated into the membrane, VDACs may not be amenable to p97-
595 dependent retrotranslocation. Mfn2 may act as a parkin receptor in cardiomyocytes (Chen
596 and Dorn, 2013), where parkin-dependent clearance of mitochondria by autophagy plays
597 a role in metabolic development (Gong et al., 2015) rather than quality control, and thus
598 may occur by a distinct mechanism; the phosphomutant $Mfn2^{T111A/S442A}$ or Mfn2 deletion
599 blocks parkin-mediated mitophagy in the heart but not in cell lines (Fig. 4J and K, Fig. 3–
600 figure supplement 4, and (Narendra et al., 2008)). Conceivably, phosphorylation of Mfn2
601 on T111 and S442 by a cardiac-specific S/T kinase (or cardiac PINK1, as has been
602 proposed (Chen and Dorn, 2013)) may facilitate mitophagy in the heart by uncoupling
603 mitochondria from the sarcoplasmic reticulum.

604 Our study describes an antagonistic, reciprocal relationship between mitophagy
605 and interorganellar tethering between mitochondria and the ER. This highlights a
606 fundamental difference between mitophagy and the more canonical starvation-induced
607 autophagy pathway, the latter of which requires mitochondria-ER contact sites for
608 autophagosome formation (Hamasaki et al., 2013). While mitophagy functions as a
609 quality control mechanism (Ryan et al., 2015), starvation-induced autophagy is a
610 metabolic response, and thus its initiation at contact sites between mitochondria and the
611 ER may serve to decode the metabolic needs of the cell. Mechanistically, both

612 mitochondria (Hailey et al., 2010) and the ER (Hayashi-Nishino et al., 2009) have been
613 reported to function as autophagosomal membrane sources during starvation, and
614 mitochondrial damage may preclude the former from participating in this process during
615 mitophagy. Accordingly, the SNARE Stx17, which governs autophagosome-lysosome
616 fusion during starvation (Itakura et al., 2012b), is dispensable for mitophagy (McLelland
617 et al., 2016; Nguyen et al., 2016). Indeed, Stx17 appears to suppress mitophagy (Fig. 3–
618 figure supplement 3G to I) through its role in supporting mitochondria-ER contact
619 (Arasaki et al., 2015). While mitophagy does indeed share morphological and several
620 mechanistic similarities with canonical macroautophagy – including the recruitment of
621 ULK1 complexes and ATG9A vesicles to depolarized mitochondria (Itakura et al.,
622 2012a; Lazarou et al., 2015) – molecular dissection of mitophagosome formation and
623 fusion requires further study.

624 Finally, our data posit the possibility of steady-state regulation of mitochondria-
625 ER contact by PINK1/parkin, separately from mitophagy. In flies, phenotypes of *PINK1*
626 and *PRKN* mutants are duplicated by overexpression of the sole *Drosophila* mitofusin
627 MARF, and suppressed by p97 overexpression (Yun et al., 2014; Zhang et al., 2017).
628 Thus, PINK1/parkin/p97 counteract MARF *in vivo* through its ubiquitination and
629 turnover (Wang et al., 2016; Zhang et al., 2017; Ziviani et al., 2010). Indeed, a proposed
630 mechanism of cell death due to deletion of *PINK1* is the sensitization of mitochondria to
631 $Ca^{2+}$ overload (Akundi et al., 2011; Gandhi et al., 2009; Kostic et al., 2015), the root
632 cause of which may be dysregulation of mitochondria-ER contact. Accordingly, deletion
633 of the mitochondrial $Ca^{2+}$ uniporter protects dopaminergic neurons from cell death in
634 *PINK1*-deficient zebrafish (Soman et al., 2017). While we did not observe any steady-

635 state differences in the extent of mitochondria-ER coupling in either parkin
636 overexpression (Fig. 1A to E) or loss-of-function (Fig. 1N and O) systems, others have
637 observed an increased degree of contact and metabolite transfer in both fibroblasts from
638 *PRKN* and *PINK1* patients, as well as brains from *PINK1* and *PRKN* mutant flies
639 (Celardo et al., 2016; Gautier et al., 2016). Conversely, we (Fig. 1H to J) and others
640 (Gelmetti et al., 2017) measured a destabilization of mitochondria-ER tethering when
641 PINK1 was transiently depleted. While differences between studies can be attributed to
642 cell type and culture conditions, how mitochondria-ER contact is quantified is certainly a
643 determinant; whereas we quantified ER tubules within 25 to 100 nm of the OMM (Fig. 1
644 and Fig. 1–figure supplement 1), Gautier *et al*. extended this distance to 500 nm, and this
645 may effectively account for observed differences. For this study, our <100 nm criterion
646 was sufficient to capture ER tubules directly opposite the OMM (see OMM extension
647 outlines in Fig. 1O and the comparison of ER-OMM distances in Fig. 1–figure
648 supplement 1). Future work will aim to a) address when and where PINK1/parkin act to
649 regulate the OMM-ER interface via Mfn2, b) solve precisely how Mfn2 is recognized and
650 retrotranslocated by p97, and c) understand how dysregulation of mitochondria-ER
651 contact during mitophagy and in other PINK1/parkin-related paradigms may contribute to
652 disease pathology. The work described here lays the foundation for these future studies,
653 identifying a molecular mechanism for contact site destabilization through the
654 ubiquitination of Mfn2 tethering complexes by the PINK1/parkin system and their
655 extraction and destruction via p97 and the proteasome.

656 **MATERIALS AND METHODS**

657 *Key resources table*

| **Reagent type (species) or resource** | **Designation** | **Source or reference** | **Identifiers** | **Additional information** |
|---|---|---|---|---|
| cell line (Homo sapiens) | U2OS | PMID 24446486 | | |
| cell line (Hs) | U2OS:GFP | PMID 24446486 | | |
| cell line (Hs) | U2OS:GFP-parkin WT | PMID 24446486 | | |
| cell line (Hs) | U2OS:GFP-parkin A320R | PMID 28276439 | | |
| cell line (Hs) | Mfn2 KO | this paper | | see Plasmids and transfection |
| cell line (Hs) | Mfn2 KO:YFP-parkin WT | this paper | | see Plasmids and transfection |
| cell line (Hs) | Mfn2 KO:YFP-parkin C431S | this paper | | see Plasmids and transfection |
| cell line (Hs) | HeLa | PMID 24446486 | | |
| cell line (Hs) | control-1 | NIH | NCRM-1 | |
| cell line (Hs) | control-2 | PMID 27641647 | | |
| cell line (Hs) | *PRKN*(del) | PMID 20885945 | | |
| transfected construct (Hs) | HA-Ub | PMID 25216678 | | |
| transfected construct (Hs) | DsRed2-LC3 | PMID 18596167 | | |
| transfected construct (Hs) | Mfn1-HA | PMID 15878861 | | |
| transfected construct (Hs) | Mfn2 WT | PMID 15878861 | | |
| transfected construct (Hs) | Mfn2 K406R | this paper | | see Plasmids and transfection |
| transfected construct (Hs) | Mfn2 K416R | this paper | | see Plasmids and transfection |
| transfected construct (Hs) | Mfn2 K420R | this paper | | see Plasmids and transfection |
| transfected construct (Hs) | Mfn2 HR1 | this paper | | see Plasmids and transfection |
| transfected construct (Hs) | Mfn2 HR2 | this paper | | see Plasmids and transfection |

| | | | | |
|---|---|---|---|---|
| transfected construct (Hs) | Mfn2 TS/AA | this paper | | see Plasmids and transfection |
| transfected construct (Hs) | GFP-parkin WT | PMID 24446486 | | |
| biological sample (Mus musculus) | parkin WT brain cytosol | this paper | | see In organello ubiquitination assays |
| biological sample (Mm) | parkin KO brain cytosol | this paper | | see In organello ubiquitination assays |
| antibody | anti-actin | Millipore | MAB1501 | |
| antibody | anti-B-III-tubulin | Sigma | T8660 | |
| antibody | anti-MAVS | Enzo | ALX-210-929-C100 | |
| antibody | anti-cytochrome c | BD | 556432 | |
| antibody | anti-GFP | Abcam | ab6673 | IP |
| antibody | anti-GFP | Invitrogen | A6455 | WB |
| antibody | anti-Grp78 | Santa Cruz | sc-376768 | |
| antibody | anti-HA | Abcam | ab9134 | |
| antibody | anti-HK1 | Cell Signaling | 2024S | |
| antibody | anti-Mfn1 | Santa Cruz | sc-50330 | |
| antibody | anti-Mfn2 | Sigma | M6319 | WB in Fig. 3-S2D |
| antibody | anti-Mfn2 | Cell Signaling | 9482 | all other assays (IF, WB, IP) |
| antibody | anti-CIV-COXI | Abcam | ab14705 | |
| antibody | anti-p62 | Progen | GP62-C | |
| antibody | anti-PDH E1a | Abcam | ab110330 | |
| antibody | anti-PDH E2/E3bp | Abcam | ab110333 | |
| antibody | anti-PDI | Abcam | ab2792 | |
| antibody | anti-PINK1 | Cell Signaling | 6946 | |
| antibody | anti-pS65 Ub | Millipore | ABS1513-I | |
| antibody | anti-Rab11A | Cell Signaling | 2413 | |
| antibody | anti-Miro1 | Sigma | HPA010687 | |
| antibody | anti-CII-SDHA | Abcam | ab14715 | |
| antibody | anti-Stx17 | ProteinTech | 17815-1-AP | |
| antibody | anti-TH | Pel-Freez | P40101-150 | |
| antibody | anti-TIM23 | BD | 611222 | |
| antibody | anti-TOM20 | Santa Cruz | sc-11414 | |
| antibody | anti-TOM70 | Santa Cruz | sc-390545 | |
| antibody | anti-Ub [FK2] | Enzo | BML-PW8810 | IF |
| antibody | anti-Ub [P4D1] | Santa Cruz | sc-8017 | WB |

| | | | | |
|---|---|---|---|---|
| antibody | anti-CIII-core2 | Abcam | ab14745 | |
| antibody | anti-CIII-Rieske | Abcam | ab14746 | |
| antibody | anti-p97 | Abcam | ab11433 | |
| antibody | anti-VDAC1 | Abcam | ab14734 | |
| recombinant protein (Rattus norvegicus) | GST-R0RBR WT | PMID 23661642 | | |
| recombinant protein (Rn) | GST-R0RBR A320R | this paper | | see Plasmids and transfection |
| recombinant protein (Rn) | GST-parkin WT | PMID 28276439 | | |
| recombinant protein (Rn) | GST-parkin C431A | PMID 28276439 | | |
| recombinant protein (Hs) | UbcH7 | PMID 28276439 | | |
| recombinant protein (Hs) | UBE1 | BostonBiochem | E-305 | |
| recombinant protein (Hs) | Ubiquitin | BostonBiochem | U-100H | |
| recombinant protein (Hs) | Usp2 catalytic domain | BostonBiochem | E-504 | |
| recombinant protein (Tribolium castaneum) | *Tc*PINK1 | PMID 24784582 | | |
| recombinant protein (Hs) | GST-4xUb G76V | PMID 23670163 | | |
| recombinant protein (Mm) | His-p97 | PMID 19506019 | | |
| commercial assay or kit | QuikChange II site-directed mutagenesis kit | Agilent | 200523 | |
| commercial assay or kit | BCA protein assay | ThermoFisher | 23227 | |
| chemical compound, drug | CCCP | Sigma | C2759 | |
| chemical compound, drug | MG132 | Sigma | M8699 | |
| chemical compound, drug | Hoechst 33342 | ThermoFisher | H3570 | |
| chemical compound, | NMS-873 | ApexBio | B2168 | |

| | | | | |
|---|---|---|---|---|
| drug | | | | |
| software, algorithm | BioTools | Bruker | | |
| software, algorithm | MASCOT | Matrix Science | | |
| software, algorithm | Data Analysis | Bruker | | |
| software, algorithm | ImagJ | NIH | | |
| software, algorithm | PyMOL | Schrodinger | | |
| software, algorithm | Excel | Microsoft | | |
| software, algorithm | Prism | GraphPad | | |

658

659 *Antibodies and other reagents*

660 Antibodies used in this study include anti-actin (Millipore, MAB1501), anti-β-III tubulin
661 (Sigma-Aldrich, T8660), anti-Cardif (referred to herein as MAVS, Enzo Life Sciences,
662 ALX-210-929-C100), anti-cytochrome c (BD Biosciences, 556432), anti-GFP (ab6673,
663 Abcam), anti-GFP (A6455, Invitrogen), anti-Grp78 (Santa Cruz, sc-376768), anti-HA
664 (Abcam, ab9134), anti-HK1 (Cell Signaling Technology, 2024S), anti-Mfn1 (Santa Cruz,
665 sc-50330), anti-Mfn2 (Sigma-Aldrich, M6319), anti-Mfn2 (Cell Signaling, 9482), anti-
666 MTCO1 (herein referred to as CIV-COXI, ab14705), anti-p62 (Progen, GP62-C), anti-
667 PDH E1a (Abcam, ab110330), anti-PDH E2/E3bp (Abcam, ab110333), anti-PDI
668 (Abcam, ab2792), anti-PINK1 (Cell Signaling, 6946), anti-pS65 ubiquitin (Millipore,
669 ABS1513-I), anti-Rab11A (Cell Signaling, 2413), anti-Rhot1 (referred to herein as
670 Miro1, Sigma-Aldrich, HPA010687), anti-SDHA (referred to herein as CII-SDHA,
671 Abcam, ab14715), anti-Stx17 (ProteinTech, 17815-1-AP), anti-TH (Pel-Freez, P40101-
672 150), anti-TIM23 (BD, 611222), anti-TOM20 (Santa Cruz, sc-11414), anti-TOM70
673 (Santa Cruz, sc-390545), anti-ubiquitin [FK2] (Enzo Life Sciences, BML-PW8810), anti-

674 ubiquitin [P4DI] (Santa Cruz, sc-8017), anti-UQCRC2 (referred to herein as CIII-core2,
675 Abcam, ab14745), anti-UQCRFS1 (referred to herein as CIII-Rieske, Abcam, ab14746),
676 anti-VCP (referred to herein as p97, Abcam, ab11433) and anti-VDAC1 (Abcam,
677 ab14734). Halt phosphatase inhibitor cocktail was purchased from Thermo Fisher
678 Scientific, and NMS-873 was purchased from ApexBio. Unless otherwise specified, all
679 other reagents were purchased from Sigma-Aldrich.
680
681 *Cell culture and iPS cell differentiation*
682 U2OS and HeLa cells were purchased from ATCC, tested negative during routine tests
683 for mycoplasma contamination, and were maintained in DMEM supplemented with L-
684 glutamine, penicillin/streptomycin, and 10% FBS in the presence of either 25 mM
685 glucose or 10 mM galactose (Wisent, Saint-Bruno, QC). Glucose-maintained cells were
686 cultured in galactose-containing medium for at least seven days before use in
687 experiments. The parkin mutant iPSC line (*PRKN*$^{del}$) was initially isolated from a patient
688 carrying compound heterozygous deletions (delEx7/c.1072delT) in the *PRKN* gene
689 (Grunewald et al., 2010). Control lines used in this study were NCRM1 (NIH, Bethesda,
690 MD) and L2131 (Chung et al., 2016). Differentiation of iPSCs into dopaminergic neurons
691 was based on a protocol by Xi and colleagues (Xi et al., 2012). iPSCs were initially
692 grown in non-coated flasks for one week in DMEM/F12 supplemented with N2 and B27,
693 in the presence of 10 μM SB431542, 200 ng/ml noggin, 1 μM CHIR99021, 200 ng/ml
694 Shh and 100 ng/ml FGF-8. Embryoid bodies were transferred to polyornithine- and
695 laminin-coated flasks to form rosettes, grown in the presence and then absence of the
696 above-indicated differentiation factors for one week each. Neural progenitors were then

697 cultured in 50% DMEM/F12 and 50% Neurobasal medium, supplemented with N2 and
698 B27, in the presence of 1 μg/ml laminin, 500 μM db-cAMP, 20 ng/ml BDNF, 20 ng/ml
699 GDNF, 200 μM ascorbic acid, 50 μM valproic, 100 nM Compound A and 1 ng/ml TGF-β.
700 Progenitors were then grown in 25% DMEM/F12 and 75% Neurobasal medium,
701 supplemented as above, for three days, and final differentiation into dopaminergic
702 neurons occurred over four weeks in Neurobasal medium (supplemented as above).
703
704 *Plasmids and transfection*
705 Cells were transfected with siRNA or DNA using jetPRIME transfection reagent
706 (Polyplus Sciences) according to the manufacturer's instructions. Cells were typically
707 analyzed three or one days after siRNA or DNA transfection, respectively. The codon-
708 optimized GST-R0RBR (Trempe et al., 2013), DsRed-LC3 (Boland et al., 2008), HA-Ub
709 (Durcan et al., 2014), His-p97 (Halawani et al., 2009) and Mfn2 (Neuspiel et al., 2005)
710 plasmids have been described previously. Mfn mutants were generated using the
711 QuikChange II site-directed mutagenesis kit (Agilent Technologies) according to the
712 manufacturer's instructions and confirmed by sequencing. While duplexed
713 oligonucleotides were used in the mutagenesis reactions, only forward primers are listed
714 below. $Mfn2^{HR1}$ was created by sequential reactions with 5'-
715 CTGAAATTTATTGACAGACAGCTGGAGCTCTTG-3' and 5'-
716 CTTGGCTCAAGACTATAGGCTGCGAATTAAGCAG-3' to create $Mfn2^{K406R/K416R}$,
717 then with 5'-CTATAGGCTGCGAATTAGGCAGATTACGGAGGAAG-3' to make
718 $Mfn2^{HR1}$, as this last primer contains the K416R substitution already present. Likewise,
719 $Mfn2^{HR2}$ was created by sequential reactions with 5'-

720 CCGCCATGAACAAGAGAATTGAGGTTCTTG-3', 5'-
721 CTCACTTCAGAGCAGAGCAAAGCTGCTC-3' and 5'-
722 CTGCTCAGGAATAGAGCCGGTTGGTTG-3' to make Mfn2$^{K720R/K730R/K737R}$, and then
723 with 5'-GCCGCCATGAACAGGAGAATTGAGGTTC-3' to make the final K719R
724 mutation. Mfn2$^{T111A/S442A}$ was created using 5'-
725 CAATGGGAAGAGCGCCGTGATCAATGC-3' and 5'-
726 GAGGAGATCAGGCGCCTCGCAGTACTGGTGGACGATTAC-3'. U2OS:GFP,
727 U2OS:GFP-parkin$^{WT}$, U2OS:GFP-parkin$^{C431S}$ and U2OS:mtKeima stable cell lines have
728 been described previously (Tang et al., 2017), and the Mfn2 KO:YFP-parkin$^{WT}$ and Mfn2
729 KO:YFP-parkin$^{C431S}$ lines were created in the same manner using YFP-parkin constructs
730 generated in that study. To create the initial Mfn2 KO U2OS cell lines, the human *MFN2*
731 gene was disrupted in exon 3 using the following guide RNA: 5'-
732 CACUUAAGCACUUUGUCACU-3'. To create the GST-4xUb$^{G76V}$ construct, the 4xUb
733 fragments from pCMV-TOM70-2xFLAG-4xUb (Zheng and Hunter, 2013) were
734 subcloned by digestion with BamHI and XhoI and ligation into pGEX6P1. This Ub chain
735 is composed of four tandem copies of ubiquitin G76V, which mimic a linear Ub chain but
736 cannot be cleaved in the cell by the Ub processing machinery.
737
738 *RNA interference*
739 siRNA targeting p97, PINK1 and Stx17 have been previously described (McLelland et
740 al., 2016; McLelland et al., 2014). Non-targeting siRNA oligonucleiotides, as well as
741 siRNA targeting Mfn1 (5'-GAUACUAGCUACUGUGAAAdTdT-3') (Zhao et al., 2013),
742 Mfn2 (5'-GGAAGAGCACCGUGAUCAAdTdT-3') (Zhao et al., 2013) and PACS2 (5'-

743 AACACGCCCGUGCCCAUGAACdTdT-3') (Simmen et al., 2005) were purchased
744 from Thermo Fisher Scientific.
745
746 *Cell lysis and immunoblotting*
747 Cells were lysed in lysis buffer (20 mM Tris pH 7.5, 150 mM NaCl, 1 mM EDTA, 1 mM
748 EGTA, 1% NP-40 substitute, 1% sodium deoxycholate, protease inhibitor cocktail
749 [aprotinin, leupeptin and benzamidine], and phosphatase inhibitor cocktail) on ice.
750 Lysates were cleared by centrifugation, protein was quantified by BCA assay
751 (Pierce/Thermo Scientific), separated by SDS-PAGE over Tris-glycine gels and
752 transferred to nitrocellulose membrane. Primary antibodies were diluted in 3% BSA in
753 PBS-Tween and incubations performed overnight at 4°C. The following day, membranes
754 were washed and incubated in HRP-conjugated secondary antibodies (Jackson
755 ImmunoResearch Laboratories), diluted in 5% milk in PBS-Tween, at room temperature
756 for one hour. Protein bands were detected using Western Lightning ECL and Plus-ECL
757 kits (PerkinElmer), according to the manufacturer's instructions.
758
759 *Immunoprecipitation*
760 Cells were lysed in HEPES-IP buffer (20 mM HEPES pH 7.2, 150 mM NaCl, 1% NP-40
761 substitute, 0.1% sodium deoxycholate, and protease/phosphatase inhibitor cocktails) and
762 protein content was quantified by BCA assay after clearing by centrifugation. For
763 immunoprecipitation under denaturing conditions, cells were alternatively lysed in 10
764 mM Tris pH 7.4, 1% SDS, 5 mM EDTA, 10 mM DTT and protease/phosphatase inhibitor
765 cocktails and incubated for 10 minutes at 90°C. Post-lysis, nine volumes of 10 mM Tris

766 pH 7.4, 150 mM NaCl, 1% Triton X-100, 1 mM EDTA, 1 mM EGTA and
767 protease/phosphatase inhibitor cocktails were added to the sample, and then protein was
768 quantified. Lysates were equilibrated to 1 to 2 mg/ml protein and immunocapture was
769 performed with the indicated antibody overnight at 4°C at a 1:10 to 1:100 dilution. The
770 following day, immunoprecipitation was performed with protein A- or protein G-
771 sepharose (GE Healthcare) for four hours at 4°C. Immunoprecipitates were washed five
772 times in buffer and eluted by incubating in SDS-PAGE sample buffer at 90°C.
773
774 *Mitochondrial isolation and BN-PAGE*
775 After treatment, U2OS cells were collected from 2 x 15-cm plates per condition in
776 isolation buffer (20 mM Hepes pH 7.4, 220 mM mannitol, 68 mM sucrose, 76 mM KCl,
777 4 mM KOAc, and 2 mM $MgCl_2$, supplemented with protease inhibitors benzamidine,
778 PMSF, aprotinin, and leupeptin) and passed through a 27.5-gauge syringe twenty times.
779 Cell lysates were centrifuged at 600 g for 10 minutes at 4°C. Supernatants were then
780 centrifuged at 10,000 g for 10 minutes at 4°C. The mitochondrial pellet was resuspended
781 in isolation buffer and centrifuged again at 12,000 g for 10 minutes at 4°C. Protein
782 content of mitochondria was determined by BCA assay, and equilibrated to 1 mg/ml prior
783 to lysis with 1% NP-40 substitute at 4°C for 30 minutes. Mitochondrial lysates were
784 clarified by centrifugation and added to sample buffer and Coomassie Blue G-250.
785 Solubilized complexes were separated over 4-16% and 3-12% Bis-Tris gels and
786 transferred to PVDF membrane using the NativePAGE Novex Bis-Tris gel system (Life
787 Technologies) according to the manufacturer's instruction prior to immunoblotting. In

788 addition, certain samples were incubated with 1 μM Usp2 (Boston Biochem) for 30
789 minutes at 37°C following NP-40 lysis, then separated by SDS-PAGE as above.
790
791 *In organello ubiquitination assays*
792 *In organello* ubiquitination was performed as previously described (Tang et al., 2017).
793 HeLa cells were depolarized with 20 μM CCCP (or DMSO control) for 4 hours, and then
794 mitochondria were isolated in isolation buffer as described in the previous section.
795 Isolated mitochondria were incubated (at a final concentration of 0.5 to 1.0 mg/ml) with
796 20 nM E1 Ub activating enzyme, 100 nM UbcH7, 5 μM Ub, 4 mM ATP, 5 mM $MgCl_2$,
797 50 μM TCEP and (unless otherwise indicated) 100 nM parkin at 37°C for the indicated
798 time (typically 30-60 minutes, vortexing at 15 minute intervals), then quenched in SDS-
799 PAGE sample buffer. E1 enzyme and Ub were purchased from Boston Biochem
800 (Cambridge, MA). In certain cases, reactions were co-incubated with 200 nM His-p97
801 hexamer or 2 mg/ml mouse brain cytosol. Purification of murine His-p97 has been
802 described previously (Halawani et al., 2009). Additionally, isolation of mouse brain
803 cytosol (200,000 g supernatant) was performed as previously described (McLelland et al.,
804 2016). SDS-PAGE sample buffer was then added to pellets and supernatants prior to
805 SDS-PAGE and immunoblot analysis.
806
807 *LC/MS on immunoprecipitated Mfn2*
808 Mfn2 was immunoprecipitated under denaturing conditions as described above.
809 Immunoprecipitates were washed twice in PBS, then twice more in 50 mM ammonium
810 acetate pH 7.0, and eluted twice in 50% acetic acid on ice for 10 minutes. Eluates were

811 pooled, cleared by centrifugation and dried by speedvac. Pellets were resuspended in 8 µl
812 6M urea, 50 mM TEAB pH 8.5, and diluted with 40 µl 50 mM TEAB pH 8.5. The
813 sample was reduced in 2 mM TCEP at 37°C for ten minutes, and then alkylated in 20
814 mM iodoacetamide for 30 minutes at room temperature in the dark. The 50 µl sample was
815 then digested with 0.2 µg of trypsin for two hours at 37°C, and then quenched in 0.5%
816 trifluoroacetic acid (TFA) and 5% acetonitrile. Digests were C18-purified using ZipTips
817 (Millipore), eluted in 0.1% TFA/80% acetonitrile, evaporated and resuspended in 0.1%
818 TFA/4% acetonitrile. Peptides were diluted in 0.1% TFA/4% acetonitrile, and eluted
819 from an Acclaim PepMap100 C18 column (75 µm × 25cm) with a 1h 5-40% gradient of
820 acetonitrile in 0.1% formic acid at 300 nL/min. The eluted peptides were analyzed with
821 an Impact II Q-TOF spectrometer equipped with a Captive Spray nano electrospray
822 source (Bruker). Data was acquired using data-dependent auto-MS/MS with a range 150-
823 2200 m/z range, a fixed cycle time of 3 sec, a dynamic exclusion of 1 min, m/z-
824 dependent isolation window (1.5-5 Th) and collision energy 25-75 eV (Beck et al., 2015).
825 MS/MS data were analyzed using MASCOT using a search procedure against the
826 SwissProt proteome database (taxonomy: mammalia). The search parameters included a
827 peptide tolerance of 15.0 ppm, an MS/MS tolerance of 0.05 Da, up to two $^{13}C$ atoms per
828 peptide, up to two missed trypsin cleavage sites, fixed carbamidomethyl and variable
829 methionine oxidation and Ser/Thr phosphorylation modifications. The significance
830 threshold was set to $p<0.05$. The MASCOT automatic peptide decoy search was
831 performed, and false discovery rates of 1.04% and 1.88% for the DMSO and CCCP-
832 treated samples were obtained, respectively. Only peptides with scores above 18.0 were
833 accepted. For ubiquitin analysis, only one peptide was identified with MASCOT; other

834 Ub peptides were identified by generating tryptic peptides with up to one missed
835 cleavage, and then matched to the LC-MS data with BioTools (Bruker). Peptides with
836 BioTools scores above 10 ($\Delta m/z < 10$ ppm for the parent ion and at least 7 MS/MS
837 fragments within less than 0.2 Da) were included in the analysis. Extracted ion
838 chromatograms were integrated using the Data Analysis software (Bruker).
839
840 *GST protein purification, in vitro phosphorylation and pulldown*
841 *Tribolium castaneum* PINK1 (*Tc*PINK1, amino acids 128–570), GST-4xUb$^{G76V}$ and
842 GST-R0RBR were expressed as GST fusion proteins in BL21 cells from pGEX6P1
843 vectors as described (Koyano et al., 2014; Trempe et al., 2013). Protein expression was
844 induced at 16°C for 16 hours with 100 µM IPTG. After harvesting, the *E. coli* pellet was
845 lysed by sonication in lysis buffer (TBS: 50 mM Tris-HCl pH 8.0, 300 mM NaCl, 1 mM
846 DTT, 0.5% Tween-20 and 5 mM $MgSO_4$), in the presence of lysozyme, DNase I and
847 EDTA-free protease inhibitors. The suspension was centrifuged and the supernatant was
848 applied to Glutathione Sepharose 4B beads (GE Healthcare). After 1 h of agitation at 4°C
849 the beads were washed with TBS and eluted with TBS containing 20 mM glutathione and
850 1% CHAPS. GST-*Tc*PINK1 was further cleaved in solution by incubation with GST-3C
851 protease for 12 h at 4°C before further purification by gel filtration (Superdex 75, GE
852 Life Sciences) in low salt buffer as a final step. GST-4xUb was purified via buffer
853 exchange to remove extra glutathione. GST-4xUb phosphorylation was performed in
854 phosphorylation buffer (50mM Tris-HCl pH 7.5, 100m M NaCl, 1 mM ATP, and 5 mM
855 $MgSO_4$) at 30°C for 90 min, at final concentrations of 0.1 mg/ml *Tc*PINK1 and 0.25
856 mg/ml GST-4xUb. After phosphorylation, the entire reaction was purified with

857 glutathione Sepharose 4B and washed with TBS briefly to remove extra *Tc*PINK1 and
858 ATP. A portion of the beads was boiled in SDS-PAGE sample buffer and separated by
859 Phos-tag gel to monitor the efficiency of phosphorylation. Whole mouse brain was
860 homogenized in 10 mM HEPES pH 7.4, 0.32 M sucrose supplemented with protease
861 inhibitors and phosphatase inhibitors (Roche). The homogenate was centrifuged for
862 10min at 1,000 g, and the supernatant was collected. After adding Trion X-100 to a final
863 concentration of 1%, the lysate was rocked at 4°C for 30 min, then centrifuged at 16,200
864 g for 30 min. The resulting supernatant was used as whole brain lysate for pull-downs.
865 Pull-downs were performed with 50 μg GST-4x(p)Ub bait and 4 mg lysate at 4°C,
866 incubated overnight in the presence of phosphatase inhibitors. After washing with TBS
867 for 5 times, reactions were resuspended in 50 μl of TBS with 2 μg GST-3C protease and
868 incubated at RT for 4 hours. After separating the beads by centrifugation, the supernatant
869 was prepared for MS sample preparation. The sample was evaporated and then
870 resuspended with 100 mM $NH_4HCO_3$ and 5 mM TCEP, then vortexed at 37°C for 30
871 min. 110 mM chloroacetamide in 100 mM $NH_4HCO_3$ was added to a final concentration
872 55 mM chloroacetamide. Samples were further vortexed for 30 min at 37°C. Trypsin was
873 added to reach an enzyme:protein ratio of 1/50, and digestion was performed overnight.
874 Samples were then dried in a Speed-Vac and reconstituted in 40 μl 0.2% formic acid.
875 Tryptic peptides were loaded on a C18 stem trap from New Objective and separated on a
876 home-made C18 column (15 cm x 150 μm id) at a flow rate of 600 nl/min with a gradient
877 of 5-30% B (A: 0.2% formic acid in water, B: 0.2% formic acid in acetonitrile). The
878 analytical column was coupled to a Q-Exactive Plus (Thermo Fisher Scientific).
879 Resolution was set at 70000 for the survey scan and 17500 for the tandem MS

880 acquisition. A maximum of 12 precursors were sequenced for each duty cycle. AGC
881 target values for MS and MS/MS scans were set to 3e6 (max fill time 50 ms) and 2e4
882 (max fill time 150 ms), respectively. The precursor isolation window was set to m/z 1.6
883 with a high energy dissociation normalized collision energy of 25. The dynamic
884 exclusion window was set to 30 s. Tandem mass spectra were searched against the
885 Uniprot human database with carbamidomethylation (C) as fixed modifications,
886 deamidation (NQ) and oxidation (M) as variable modifications. Tolerance was set at 10
887 ppm on precursor mass and 0.01 Da on the fragments. The raw data was searched against
888 the Universal Protein Resource (UniProt) (http://www.pir.uniprot.org/) database by using
889 Mascot (http://www.matrixscience.com). Scaffold was used to validate MS/MS based
890 peptide and protein identifications. Peptide identifications were accepted if they could be
891 established at greater than 95.0% probability as specified by the Peptide Prophet
892 algorithm. Protein identifications were accepted if they could be established at greater
893 than 99.0% probability and contained at least 2 identified peptides. For each group –
894 GST, GST-4xUb$^{G76V}$ and GST-4xpUb$^{G76V}$ – we performed 3 biological repeats. P-values
895 against the spectrum counts in GST-4xUb pulled-down samples and GST-4xpUb pulled-
896 down samples for each protein were obtained via Fisher's Exact Test built in the Scaffold
897 software. For final analysis of quantified proteins, values were transferred and analysed
898 in Microsoft Excel. The following cut-offs were applied: minimum number of two total
899 spectrum counts; ratio of spectrum counts in the GST pulled down control divided by the
900 total spectrum counts in all samples is lower than 30%. For the GST-R0RBR pulldown,
901 U2OS:GFP-parkin$^{WT}$ cells were treated with 20 μM CCCP for one hour (or left
902 untreated) prior to lysis in 20 mM HEPES pH 7.2, 150 mM NaCl, 1% NP-40 substitute,

903 0.2% sodium deoxycholate, and protease/phosphatase inhibitor cocktails and then
904 incubated overnight with 10 μg/ml GST-R0RBR WT or A320R on beads (or
905 unconjugated beads as an additional control). The following day, pulldowns were washed
906 five times in lysis buffer and eluted from beads by incubating in SDS-PAGE sample
907 buffer at 90°C.
908
909 *Transmission electron microscopy*
910 After treatment, cells grown in chamber slides were fixed in 2.5% glutaraldehyde in PBS
911 for one hour at room temperature, then stored at 4°C overnight before processing. Thin
912 sections on grids were observed in a Tecnai 12 BioTwin transmission electron
913 microscope (FEI) at 120 keV. Images were acquired with a charge coupled device camera
914 (AMT).
915
916 *Immunofluorescence and fluorescence microscopy*
917 Cells were grown on glass coverslips, treated then fixed in 6% formaldehyde in PBS for
918 15 minutes 37°C. Fixed cells were permeabilized in 0.25% Triton X-100 in PBS for 10
919 minutes, and blocked in 10% FBS in PBS. Primary antibodies were diluted in 5% FBS in
920 PBS, and incubations were performed for one hour at room temperature. Alexa Fluor-
921 conjugated secondary antibodies (Thermo Fisher Scientific) were performed in the same
922 manner. Cells were counterstained with Hoechst 33342 (Invitrogen) and mounted on
923 glass slides using Aqua Poly/Mount (Polysciences Inc.). Confocal slices (<1 micron-
924 thick) were acquired via a spinning disc confocal microscope (with Andor Yokogawa
925 system IX81, Olympus) through a 100X, 1.4 NA or 60X, 1.4 NA objective lens.

926 Widefield microscopy was performed using a Zeiss AxioObserver Z1 microscope
927 through a 63X, 1.4 NA objective lens.
928
929 *Fluorescence-activated cell sorting and mtKeima measurements*
930 Quantitative analysis of mitophagy was performed as described previously (Tang et al.,
931 2017). U2OS:mtKeima were first transfected with siRNA targeting Mfn1 or Mfn2. Two
932 days later, mtKeima was induced with 10 μM ponasterone A, and cells were transfected
933 with GFP-parkin WT or C431S for 12 to 18h. The next day (3 days post-siRNA
934 transfection), cells were treated with 20 μM CCCP (or DMSO) for four hours, trypsinized
935 and collected in PBS. Cell fluorescence was analyzed by an LSR Fortessa (BD
936 Bioscience) fluorescence-activated cell sorter, using excitation wavelengths of 405 nm
937 and 561 nm to detect Keima at pH 7.0 and 4.0, respectively, and 488 nm to detect GFP-
938 parkin. Cell fluorescence data were analyzed using FlowJo (Tree Star). For each
939 condition, $10^5$ cells, gated for GFP-parkin expression, were used for the analysis.
940
941 *Image and statistical analyses*
942 The numbers of cells quantified per experiment are explicitly indicated in the figure
943 legends. No statistical method was used to predetermine the experimental sample size.
944 Statistical tests and representations of the data were generated using Prism (GraphPad
945 Software, La Jolla, CA). Data are displayed as the mean ± standard error of the mean
946 (SEM). Statistical significance was determined by one- (Fig. 3-S1B, 3-S1C, 3-S1D, 4F,
947 4G, 4K, 8K) and two-way (Fig. 1B, 1C, 1D, 1E, 1I, 1J, 1N, 3E, 3G, 3-S2B, 3-S3D, 3-S3I,
948 3-S4F, 3-S4H, 3-S5C, 3-S5D, 3-S5G, 4C, 5G, 5H, 6I, 7B) ANOVAs followed by

949 Bonferroni post-hoc tests, or one-tailed t-test (Fig. 1-S1B, 6K and 7E). Differences were
950 considered significant if $p<.05$. The diagram of the crystal structure of the pUb-parkin
951 complex was created with PyMOL. Images were analyzed using ImageJ (NIH), and
952 analyses were performed blindly.
953

954 **CONTRIBUTION OF AUTHOURS**

955 GLM and EAF framed the question, with input from JFT. GLM, TG, and WY collected
956 and analyzed most of the data, which was interpreted with JFT and EAF. CXC and NDL
957 optimized the differentiation of dopaminergic neurons and provided cells for the
958 experiments at the end of in Figure 1, and GD created the Mfn2 KO cell lines, under the
959 supervision of TMD. SV, under the supervision of IR, expressed and purified p97 for use
960 in in organelle assays. AIK purified GST-R0RBR and helped perform the R0RBR
961 pulldown assay. JFT ran and analyzed the MS samples in Figure 2 and Figure 2-
962 supplement 1. AR provided the *PARKIN* mutant iPSC line. GLM wrote the manuscript,
963 which was edited by EAF, JFT and TMD.
964

965 **ACKNOWLEDGMENTS**

966 This work was supported by an operating grant from the Canadian Institutes for Health
967 Research (CIHR) to E.A.F. G.L.M. was supported by a Canada Graduate Scholarship
968 from the CIHR, and an award from the Montreal Neurological Institute and Desjardins
969 Foundation. We would like to thank Dr. Heidi McBride (McGill), Dr. Julien Prudent
970 (MRC, Cambridge, UK) and Dr. Atsushi Tanaka (Yamagata University, Yamagata,
971 Japan) for stimulating discussions concerning the data presented herein. We are grateful

972 to Dr. Matthew Tang for technical advice regarding mtKeima acquisition experiments,
973 stable cell line creation and cell sorting, Dr. Marta Vranas for technical help and advice
974 concerning the *in organello* ubiquitination assay, and Dr. Adele Tufford for discussions
975 regarding statistical analyses. We also thank Jeannie Mui and the Facility for Electron
976 Microscopy Research (McGill) for TEM sample processing and technical advice.
977 Proteomic analyses for the GST-Ub pulldown were performed by the Centre for
978 Advanced Proteomics Analyses at the *Institut de la Recherche en Immunologie et*
979 *Cancérologie* (Montreal, QC), a Node of the Canadian Genomic Innovation Network that
980 is supported by the Canadian Government through Genome Canada. The pCMV-
981 TOM70-2xFLAG-4xUb plasmid was a kind gift from Dr. Xinde Zheng (Salk Institute).
982 The antibodies against MCU, MICU1 and MICU2, as well as the Mfn2 and Mfn1-HA
983 plasmids, were kind gifts from Dr. Heidi McBride. All cell lines and reagents generated
984 by the Montreal Neurological Institute (MNI) IPSC/CRISPR Platform are available
985 without restriction upon request through the Platform under the Open Science Policy of
986 the MNI.
987

988 **COMPETING INTERESTS**

989 The authors declare no conflict of interest.

990 **REFERENCES**
991


992 Akundi, R.S., Z. Huang, J. Eason, J.D. Pandya, L. Zhi, W.A. Cass, P.G. Sullivan, and H.
993 Bueler. 2011. Increased mitochondrial calcium sensitivity and abnormal
994 expression of innate immunity genes precede dopaminergic defects in Pink1-
995 deficient mice. *PloS one*. 6:e16038.

996 Arasaki, K., H. Shimizu, H. Mogari, N. Nishida, N. Hirota, A. Furuno, Y. Kudo, M.
997 Baba, N. Baba, J. Cheng, T. Fujimoto, N. Ishihara, C. Ortiz-Sandoval, L.D.
998 Barlow, A. Raturi, N. Dohmae, Y. Wakana, H. Inoue, K. Tani, J.B. Dacks, T.
999 Simmen, and M. Tagaya. 2015. A role for the ancient SNARE syntaxin 17 in
1000 regulating mitochondrial division. *Developmental cell*. 32:304-317.

1001 Beck, S., A. Michalski, O. Raether, M. Lubeck, S. Kaspar, N. Goedecke, C. Baessmann,
1002 D. Hornburg, F. Meier, I. Paron, N.A. Kulak, J. Cox, and M. Mann. 2015. The
1003 Impact II, a Very High-Resolution Quadrupole Time-of-Flight Instrument
1004 (QTOF) for Deep Shotgun Proteomics. *Molecular & cellular proteomics : MCP*.
1005 14:2014-2029.

1006 Bockler, S., and B. Westermann. 2014. Mitochondrial ER contacts are crucial for
1007 mitophagy in yeast. *Developmental cell*. 28:450-458.

1008 Boland, B., A. Kumar, S. Lee, F.M. Platt, J. Wegiel, W.H. Yu, and R.A. Nixon. 2008.
1009 Autophagy induction and autophagosome clearance in neurons: relationship to
1010 autophagic pathology in Alzheimer's disease. *The Journal of neuroscience : the*
1011 *official journal of the Society for Neuroscience*. 28:6926-6937.

1012 Brandt, T., L. Cavellini, W. Kuhlbrandt, and M.M. Cohen. 2016. A mitofusin-dependent
1013 docking ring complex triggers mitochondrial fusion in vitro. *eLife*. 5.

1014 Callegari, S., S. Oeljeklaus, B. Warscheid, S. Dennerlein, M. Thumm, P. Rehling, and J.
1015 Dudek. 2016. Phospho-ubiquitin-PARK2 complex as a marker for mitophagy
1016 defects. *Autophagy*:1-11.

1017 Celardo, I., A.C. Costa, S. Lehmann, C. Jones, N. Wood, N.E. Mencacci, G.R. Mallucci,
1018 S.H. Loh, and L.M. Martins. 2016. Mitofusin-mediated ER stress triggers
1019 neurodegeneration in pink1/parkin models of Parkinson's disease. *Cell Death Dis*.
1020 7:e2271.

1021 Chan, N.C., A.M. Salazar, A.H. Pham, M.J. Sweredoski, N.J. Kolawa, R.L. Graham, S.
1022 Hess, and D.C. Chan. 2011. Broad activation of the ubiquitin-proteasome system
1023 by Parkin is critical for mitophagy. *Human molecular genetics*. 20:1726-1737.

1024 Chen, H., S.A. Detmer, A.J. Ewald, E.E. Griffin, S.E. Fraser, and D.C. Chan. 2003.
1025 Mitofusins Mfn1 and Mfn2 coordinately regulate mitochondrial fusion and are
1026 essential for embryonic development. *The Journal of cell biology*. 160:189-200.

1027 Chen, Y., and G.W. Dorn, 2nd. 2013. PINK1-phosphorylated mitofusin 2 is a Parkin
1028 receptor for culling damaged mitochondria. *Science*. 340:471-475.

1029 Chung, S.Y., S. Kishinevsky, J.R. Mazzulli, J. Graziotto, A. Mrejeru, E.V. Mosharov, L.
1030 Puspita, P. Valiulahi, D. Sulzer, T.A. Milner, T. Taldone, D. Krainc, L. Studer,
1031 and J.W. Shim. 2016. Parkin and PINK1 Patient iPSC-Derived Midbrain
1032 Dopamine Neurons Exhibit Mitochondrial Dysfunction and alpha-Synuclein
1033 Accumulation. *Stem Cell Reports*. 7:664-677.

1034 Csordas, G., C. Renken, P. Varnai, L. Walter, D. Weaver, K.F. Buttle, T. Balla, C.A.
1035 Mannella, and G. Hajnoczky. 2006. Structural and functional features and
1036 significance of the physical linkage between ER and mitochondria. *The Journal of*
1037 *cell biology*. 174:915-921.

1038 de Brito, O.M., and L. Scorrano. 2008. Mitofusin 2 tethers endoplasmic reticulum to
1039 mitochondria. *Nature*. 456:605-610.

1040 Denison, S.R., F. Wang, N.A. Becker, B. Schule, N. Kock, L.A. Phillips, C. Klein, and
1041 D.I. Smith. 2003. Alterations in the common fragile site gene Parkin in ovarian
1042 and other cancers. *Oncogene*. 22:8370-8378.

1043 Durcan, T.M., M.Y. Tang, J.R. Perusse, E.A. Dashti, M.A. Aguileta, G.L. McLelland, P.
1044 Gros, T.A. Shaler, D. Faubert, B. Coulombe, and E.A. Fon. 2014. USP8 regulates
1045 mitophagy by removing K6-linked ubiquitin conjugates from parkin. *The EMBO*
1046 *journal*. 33:2473-2491.

1047 Filadi, R., E. Greotti, G. Turacchio, A. Luini, T. Pozzan, and P. Pizzo. 2015. Mitofusin 2
1048 ablation increases endoplasmic reticulum-mitochondria coupling. *Proceedings of*
1049 *the National Academy of Sciences of the United States of America*. 112:E2174-
1050 2181.

1051 Gandhi, S., A. Wood-Kaczmar, Z. Yao, H. Plun-Favreau, E. Deas, K. Klupsch, J.
1052 Downward, D.S. Latchman, S.J. Tabrizi, N.W. Wood, M.R. Duchen, and A.Y.
1053 Abramov. 2009. PINK1-associated Parkinson's disease is caused by neuronal
1054 vulnerability to calcium-induced cell death. *Molecular cell*. 33:627-638.

1055 Gautier, C.A., Z. Erpapazoglou, F. Mouton-Liger, M.P. Muriel, F. Cormier, S. Bigou, S.
1056 Duffaure, M. Girard, B. Foret, A. Iannielli, V. Broccoli, C. Dalle, D. Bohl, P.P.
1057 Michel, J.C. Corvol, A. Brice, and O. Corti. 2016. The endoplasmic reticulum-
1058 mitochondria interface is perturbed in PARK2 knockout mice and patients with
1059 PARK2 mutations. *Human molecular genetics*.

1060 Gelmetti, V., P. De Rosa, L. Torosantucci, E.S. Marini, A. Romagnoli, M. Di Rienzo, G.
1061 Arena, D. Vignone, G.M. Fimia, and E.M. Valente. 2017. PINK1 and BECN1
1062 relocalize at mitochondria-associated membranes during mitophagy and promote
1063 ER-mitochondria tethering and autophagosome formation. *Autophagy*. 13:654-
1064 669.

1065 Gong, G., M. Song, G. Csordas, D.P. Kelly, S.J. Matkovich, and G.W. Dorn, 2nd. 2015.
1066 Parkin-mediated mitophagy directs perinatal cardiac metabolic maturation in
1067 mice. *Science*. 350:aad2459.

1068 Grunewald, A., L. Voges, A. Rakovic, M. Kasten, H. Vandebona, C. Hemmelmann, K.
1069 Lohmann, S. Orolicki, A. Ramirez, A.H. Schapira, P.P. Pramstaller, C.M. Sue,
1070 and C. Klein. 2010. Mutant Parkin impairs mitochondrial function and
1071 morphology in human fibroblasts. *PloS one*. 5:e12962.

1072 Hailey, D.W., A.S. Rambold, P. Satpute-Krishnan, K. Mitra, R. Sougrat, P.K. Kim, and J.
1073 Lippincott-Schwartz. 2010. Mitochondria supply membranes for autophagosome
1074 biogenesis during starvation. *Cell*. 141:656-667.

1075 Halawani, D., A.C. LeBlanc, I. Rouiller, S.W. Michnick, M.J. Servant, and M. Latterich.
1076 2009. Hereditary inclusion body myopathy-linked p97/VCP mutations in the NH2
1077 domain and the D1 ring modulate p97/VCP ATPase activity and D2 ring
1078 conformation. *Molecular and cellular biology*. 29:4484-4494.

1079 Hamasaki, M., N. Furuta, A. Matsuda, A. Nezu, A. Yamamoto, N. Fujita, H. Oomori, T.
1080 Noda, T. Haraguchi, Y. Hiraoka, A. Amano, and T. Yoshimori. 2013.
1081 Autophagosomes form at ER-mitochondria contact sites. *Nature*. 495:389-393.

1082 Hayashi-Nishino, M., N. Fujita, T. Noda, A. Yamaguchi, T. Yoshimori, and A.
1083 Yamamoto. 2009. A subdomain of the endoplasmic reticulum forms a cradle for
1084 autophagosome formation. *Nature cell biology*. 11:1433-1437.

1085 Heo, J.M., A. Ordureau, J.A. Paulo, J. Rinehart, and J.W. Harper. 2015. The PINK1-
1086 PARKIN Mitochondrial Ubiquitylation Pathway Drives a Program of
1087 OPTN/NDP52 Recruitment and TBK1 Activation to Promote Mitophagy.
1088 *Molecular cell*. 60:7-20.

1089 Ishihara, N., Y. Eura, and K. Mihara. 2004. Mitofusin 1 and 2 play distinct roles in
1090 mitochondrial fusion reactions via GTPase activity. *Journal of cell science*.
1091 117:6535-6546.

1092 Itakura, E., C. Kishi-Itakura, I. Koyama-Honda, and N. Mizushima. 2012a. Structures
1093 containing Atg9A and the ULK1 complex independently target depolarized
1094 mitochondria at initial stages of Parkin-mediated mitophagy. *Journal of cell*
1095 *science*. 125:1488-1499.

1096 Itakura, E., C. Kishi-Itakura, and N. Mizushima. 2012b. The hairpin-type tail-anchored
1097 SNARE syntaxin 17 targets to autophagosomes for fusion with
1098 endosomes/lysosomes. *Cell*. 151:1256-1269.

1099 Kane, L.A., M. Lazarou, A.I. Fogel, Y. Li, K. Yamano, S.A. Sarraf, S. Banerjee, and R.J.
1100 Youle. 2014. PINK1 phosphorylates ubiquitin to activate Parkin E3 ubiquitin
1101 ligase activity. *The Journal of cell biology*. 205:143-153.

1102 Karbowski, M., K.L. Norris, M.M. Cleland, S.Y. Jeong, and R.J. Youle. 2006. Role of
1103 Bax and Bak in mitochondrial morphogenesis. *Nature*. 443:658-662.

1104 Katayama, H., T. Kogure, N. Mizushima, T. Yoshimori, and A. Miyawaki. 2011. A
1105 sensitive and quantitative technique for detecting autophagic events based on
1106 lysosomal delivery. *Chemistry & biology*. 18:1042-1052.

1107 Kazlauskaite, A., C. Kondapalli, R. Gourlay, D.G. Campbell, M.S. Ritorto, K. Hofmann,
1108 D.R. Alessi, A. Knebel, M. Trost, and M.M. Muqit. 2014. Parkin is activated by
1109 PINK1-dependent phosphorylation of ubiquitin at Ser65. *The Biochemical*
1110 *journal*. 460:127-139.

1111 Khan, M., G.H. Syed, S.J. Kim, and A. Siddiqui. 2016. Hepatitis B Virus-Induced
1112 Parkin-Dependent Recruitment of Linear Ubiquitin Assembly Complex (LUBAC)
1113 to Mitochondria and Attenuation of Innate Immunity. *PLoS Pathog*. 12:e1005693.

1114 Kimura, Y., J. Fukushi, S. Hori, N. Matsuda, K. Okatsu, Y. Kakiyama, J. Kawawaki, A.
1115 Kakizuka, and K. Tanaka. 2013. Different dynamic movements of wild-type and
1116 pathogenic VCPs and their cofactors to damaged mitochondria in a Parkin-
1117 mediated mitochondrial quality control system. *Genes to cells : devoted to*
1118 *molecular & cellular mechanisms*. 18:1131-1143.

1119 Kishi-Itakura, C., I. Koyama-Honda, E. Itakura, and N. Mizushima. 2014. Ultrastructural
1120 analysis of autophagosome organization using mammalian autophagy-deficient
1121 cells. *Journal of cell science*. 127:4089-4102.

1122 Kitada, T., S. Asakawa, N. Hattori, H. Matsumine, Y. Yamamura, S. Minoshima, M.
1123 Yokochi, Y. Mizuno, and N. Shimizu. 1998. Mutations in the parkin gene cause
1124 autosomal recessive juvenile parkinsonism. *Nature*. 392:605-608.

1125 Klecker, T., S. Bockler, and B. Westermann. 2014. Making connections: interorganelle
1126 contacts orchestrate mitochondrial behavior. *Trends in cell biology*.

1127 Kondapalli, C., A. Kazlauskaite, N. Zhang, H.I. Woodroof, D.G. Campbell, R. Gourlay,
1128 L. Burchell, H. Walden, T.J. Macartney, M. Deak, A. Knebel, D.R. Alessi, and
1129 M.M. Muqit. 2012. PINK1 is activated by mitochondrial membrane potential
1130 depolarization and stimulates Parkin E3 ligase activity by phosphorylating Serine
1131 65. *Open biology*. 2:120080.

1132 Kostic, M., M.H. Ludtmann, H. Bading, M. Hershfinkel, E. Steer, C.T. Chu, A.Y.
1133 Abramov, and I. Sekler. 2015. PKA Phosphorylation of NCLX Reverses
1134 Mitochondrial Calcium Overload and Depolarization, Promoting Survival of
1135 PINK1-Deficient Dopaminergic Neurons. *Cell reports*. 13:376-386.

1136 Koyano, F., K. Okatsu, H. Kosako, Y. Tamura, E. Go, M. Kimura, Y. Kimura, H.
1137 Tsuchiya, H. Yoshihara, T. Hirokawa, T. Endo, E.A. Fon, J.F. Trempe, Y. Saeki,
1138 K. Tanaka, and N. Matsuda. 2014. Ubiquitin is phosphorylated by PINK1 to
1139 activate parkin. *Nature*. 510:162-166.

1140 Lazarou, M., D.P. Narendra, S.M. Jin, E. Tekle, S. Banerjee, and R.J. Youle. 2013.
1141 PINK1 drives Parkin self-association and HECT-like E3 activity upstream of
1142 mitochondrial binding. *The Journal of cell biology*. 200:163-172.

1143 Lazarou, M., D.A. Sliter, L.A. Kane, S.A. Sarraf, C. Wang, J.L. Burman, D.P. Sideris,
1144 A.I. Fogel, and R.J. Youle. 2015. The ubiquitin kinase PINK1 recruits autophagy
1145 receptors to induce mitophagy. *Nature*. 524:309-314.

1146 Lee, S., C. Zhang, and X. Liu. 2015. Role of glucose metabolism and ATP in maintaining
1147 PINK1 levels during Parkin-mediated mitochondrial damage responses. *The*
1148 *Journal of biological chemistry*. 290:904-917.

1149 Magnaghi, P., R. D'Alessio, B. Valsasina, N. Avanzi, S. Rizzi, D. Asa, F. Gasparri, L.
1150 Cozzi, U. Cucchi, C. Orrenius, P. Polucci, D. Ballinari, C. Perrera, A. Leone, G.
1151 Cervi, E. Casale, Y. Xiao, C. Wong, D.J. Anderson, A. Galvani, D. Donati, T.
1152 O'Brien, P.K. Jackson, and A. Isacchi. 2013. Covalent and allosteric inhibitors of
1153 the ATPase VCP/p97 induce cancer cell death. *Nature chemical biology*. 9:548-
1154 556.

1155 Mattie, S., J. Riemer, J.G. Wideman, and H.M. McBride. 2017. A new mitofusin
1156 topology places the redox-regulated C terminus in the mitochondrial
1157 intermembrane space. *The Journal of cell biology*.

1158 McCoy, M.K., A. Kaganovich, I.N. Rudenko, J. Ding, and M.R. Cookson. 2014.
1159 Hexokinase activity is required for recruitment of parkin to depolarized
1160 mitochondria. *Human molecular genetics*. 23:145-156.

1161 McLelland, G.L., S.A. Lee, H.M. McBride, and E.A. Fon. 2016. Syntaxin-17 delivers
1162 PINK1/parkin-dependent mitochondrial vesicles to the endolysosomal system.
1163 *The Journal of cell biology*.

1164 McLelland, G.L., V. Soubannier, C.X. Chen, H.M. McBride, and E.A. Fon. 2014. Parkin
1165 and PINK1 function in a vesicular trafficking pathway regulating mitochondrial
1166 quality control. *The EMBO journal*. 33:282-295.

1167 Naon, D., M. Zaninello, M. Giacomello, T. Varanita, F. Grespi, S. Lakshminaranayan, A.
1168 Serafini, M. Semenzato, S. Herkenne, M.I. Hernandez-Alvarez, A. Zorzano, D.
1169 De Stefani, G.W. Dorn, 2nd, and L. Scorrano. 2016. Critical reappraisal confirms
1170 that Mitofusin 2 is an endoplasmic reticulum-mitochondria tether. *Proceedings of*
1171 *the National Academy of Sciences of the United States of America*.

1172 Narendra, D., A. Tanaka, D.F. Suen, and R.J. Youle. 2008. Parkin is recruited selectively
1173 to impaired mitochondria and promotes their autophagy. *The Journal of cell*
1174 *biology*. 183:795-803.

1175 Neuspiel, M., R. Zunino, S. Gangaraju, P. Rippstein, and H. McBride. 2005. Activated
1176 mitofusin 2 signals mitochondrial fusion, interferes with Bax activation, and

1177 reduces susceptibility to radical induced depolarization. *Journal of Biological*
1178 *Chemistry*. 280:25060-25070.

1179 Nguyen, T.N., B.S. Padman, J. Usher, V. Oorschot, G. Ramm, and M. Lazarou. 2016.
1180 Atg8 family LC3/GABARAP proteins are crucial for autophagosome-lysosome
1181 fusion but not autophagosome formation during PINK1/Parkin mitophagy and
1182 starvation. *The Journal of cell biology*. 215:857-874.

1183 Okatsu, K., F. Koyano, M. Kimura, H. Kosako, Y. Saeki, K. Tanaka, and N. Matsuda.
1184 2015. Phosphorylated ubiquitin chain is the genuine Parkin receptor. *The Journal*
1185 *of cell biology*. 209:111-128.

1186 Ordureau, A., J.M. Heo, D.M. Duda, J.A. Paulo, J.L. Olszewski, D. Yanishevski, J.
1187 Rinehart, B.A. Schulman, and J.W. Harper. 2015. Defining roles of PARKIN and
1188 ubiquitin phosphorylation by PINK1 in mitochondrial quality control using a
1189 ubiquitin replacement strategy. *Proceedings of the National Academy of Sciences*
1190 *of the United States of America*. 112:6637-6642.

1191 Ordureau, A., S.A. Sarraf, D.M. Duda, J.M. Heo, M.P. Jedrychowski, V.O. Sviderskiy,
1192 J.L. Olszewski, J.T. Koerber, T. Xie, S.A. Beausoleil, J.A. Wells, S.P. Gygi, B.A.
1193 Schulman, and J.W. Harper. 2014. Quantitative proteomics reveal a feedforward
1194 mechanism for mitochondrial PARKIN translocation and ubiquitin chain
1195 synthesis. *Molecular cell*. 56:360-375.

1196 Otter-Nilsson, M., R. Hendriks, E.I. Pecheur-Huet, D. Hoekstra, and T. Nilsson. 1999.
1197 Cytosolic ATPases, p97 and NSF, are sufficient to mediate rapid membrane
1198 fusion. *The EMBO journal*. 18:2074-2083.

1199 Qi, Y., L. Yan, C. Yu, X. Guo, X. Zhou, X. Hu, X. Huang, Z. Rao, Z. Lou, and J. Hu.
1200 2016. Structures of human mitofusin 1 provide insight into mitochondrial
1201 tethering. *The Journal of cell biology*. 215:621-629.

1202 Rakovic, A., A. Grunewald, J. Kottwitz, N. Bruggemann, P.P. Pramstaller, K. Lohmann,
1203 and C. Klein. 2011. Mutations in PINK1 and Parkin impair ubiquitination of
1204 Mitofusins in human fibroblasts. *PloS one*. 6:e16746.

1205 Ryan, B.J., S. Hoek, E.A. Fon, and R. Wade-Martins. 2015. Mitochondrial dysfunction
1206 and mitophagy in Parkinson's: from familial to sporadic disease. *Trends in*
1207 *biochemical sciences*. 40:200-210.

1208 Sarraf, S.A., M. Raman, V. Guarani-Pereira, M.E. Sowa, E.L. Huttlin, S.P. Gygi, and
1209 J.W. Harper. 2013. Landscape of the PARKIN-dependent ubiquitylome in
1210 response to mitochondrial depolarization. *Nature*. 496:372-376.

1211 Sauve, V., A. Lilov, M. Seirafi, M. Vranas, S. Rasool, G. Kozlov, T. Sprules, J. Wang,
1212 J.F. Trempe, and K. Gehring. 2015. A Ubl/ubiquitin switch in the activation of
1213 Parkin. *The EMBO journal*. 34:2492-2505.

1214 Shiba-Fukushima, K., Y. Imai, S. Yoshida, Y. Ishihama, T. Kanao, S. Sato, and N.
1215 Hattori. 2012. PINK1-mediated phosphorylation of the Parkin ubiquitin-like
1216 domain primes mitochondrial translocation of Parkin and regulates mitophagy.
1217 *Scientific reports*. 2:1002.

1218 Simmen, T., J.E. Aslan, A.D. Blagoveshchenskaya, L. Thomas, L. Wan, Y. Xiang, S.F.
1219 Feliciangeli, C.H. Hung, C.M. Crump, and G. Thomas. 2005. PACS-2 controls
1220 endoplasmic reticulum-mitochondria communication and Bid-mediated apoptosis.
1221 *The EMBO journal*. 24:717-729.

1222 Soman, S., M. Keatinge, M. Moein, M. Da Costa, H. Mortiboys, A. Skupin, S. Sugunan,
1223 M. Bazala, J. Kuznicki, and O. Bandmann. 2017. Inhibition of the mitochondrial
1224 calcium uniporter rescues dopaminergic neurons in pink1-/- zebrafish. *Eur J*
1225 *Neurosci*. 45:528-535.

1226 Sugiura, A., G.L. McLelland, E.A. Fon, and H.M. McBride. 2014. A new pathway for
1227 mitochondrial quality control: mitochondrial-derived vesicles. *The EMBO*
1228 *journal*. 33:2142-2156.

1229 Sugiura, A., S. Nagashima, T. Tokuyama, T. Amo, Y. Matsuki, S. Ishido, Y. Kudo, H.M.
1230 McBride, T. Fukuda, N. Matsushita, R. Inatome, and S. Yanagi. 2013. MITOL
1231 regulates endoplasmic reticulum-mitochondria contacts via Mitofusin2.
1232 *Molecular cell*. 51:20-34.

1233 Szabadkai, G., K. Bianchi, P. Varnai, D. De Stefani, M.R. Wieckowski, D. Cavagna, A.I.
1234 Nagy, T. Balla, and R. Rizzuto. 2006. Chaperone-mediated coupling of
1235 endoplasmic reticulum and mitochondrial Ca2+ channels. *The Journal of cell*
1236 *biology*. 175:901-911.

1237 Tanaka, A., M.M. Cleland, S. Xu, D.P. Narendra, D.F. Suen, M. Karbowski, and R.J.
1238 Youle. 2010. Proteasome and p97 mediate mitophagy and degradation of
1239 mitofusins induced by Parkin. *The Journal of cell biology*. 191:1367-1380.

1240 Tang, M.Y., M. Vranas, A.I. Krahn, S. Pundlik, J.F. Trempe, and E.A. Fon. 2017.
1241 Structure-guided mutagenesis reveals a hierarchical mechanism of Parkin
1242 activation. *Nature communications*. 8:14697.

1243 Trempe, J.F., V. Sauve, K. Grenier, M. Seirafi, M.Y. Tang, M. Menade, S. Al-Abdul-
1244 Wahid, J. Krett, K. Wong, G. Kozlov, B. Nagar, E.A. Fon, and K. Gehring. 2013.
1245 Structure of parkin reveals mechanisms for ubiquitin ligase activation. *Science*.
1246 340:1451-1455.

1247 Valente, E.M., P.M. Abou-Sleiman, V. Caputo, M.M. Muqit, K. Harvey, S. Gispert, Z.
1248 Ali, D. Del Turco, A.R. Bentivoglio, D.G. Healy, A. Albanese, R. Nussbaum, R.
1249 Gonzalez-Maldonado, T. Deller, S. Salvi, P. Cortelli, W.P. Gilks, D.S. Latchman,
1250 R.J. Harvey, B. Dallapiccola, G. Auburger, and N.W. Wood. 2004. Hereditary
1251 early-onset Parkinson's disease caused by mutations in PINK1. *Science*.
1252 304:1158-1160.

1253 Wang, Z.H., C. Clark, and E.R. Geisbrecht. 2016. Drosophila clueless is involved in
1254 Parkin-dependent mitophagy by promoting VCP-mediated Marf degradation.
1255 *Human molecular genetics*. 25:1946-1964.

1256 Wauer, T., M. Simicek, A. Schubert, and D. Komander. 2015a. Mechanism of phospho-
1257 ubiquitin-induced PARKIN activation. *Nature*. 524:370-374.

1258 Wauer, T., K.N. Swatek, J.L. Wagstaff, C. Gladkova, J.N. Pruneda, M.A. Michel, M.
1259 Gersch, C.M. Johnson, S.M. Freund, and D. Komander. 2015b. Ubiquitin Ser65
1260 phosphorylation affects ubiquitin structure, chain assembly and hydrolysis. *The*
1261 *EMBO journal*. 34:307-325.

1262 Xi, J., Y. Liu, H. Liu, H. Chen, M.E. Emborg, and S.C. Zhang. 2012. Specification of
1263 midbrain dopamine neurons from primate pluripotent stem cells. *Stem Cells*.
1264 30:1655-1663.

1265 Yamano, K., N. Matsuda, and K. Tanaka. 2016. The ubiquitin signal and autophagy: an
1266 orchestrated dance leading to mitochondrial degradation. *EMBO reports*.

1267 Yamano, K., B.B. Queliconi, F. Koyano, Y. Saeki, T. Hirokawa, K. Tanaka, and N.
1268 Matsuda. 2015. Site-specific Interaction Mapping of Phosphorylated Ubiquitin to
1269 Uncover Parkin Activation. *The Journal of biological chemistry*. 290:25199-
1270 25211.

1271 Ye, Y., H.H. Meyer, and T.A. Rapoport. 2003. Function of the p97-Ufd1-Npl4 complex
1272 in retrotranslocation from the ER to the cytosol: dual recognition of
1273 nonubiquitinated polypeptide segments and polyubiquitin chains. *The Journal of*
1274 *cell biology*. 162:71-84.

1275 Yoshii, S.R., C. Kishi, N. Ishihara, and N. Mizushima. 2011. Parkin mediates
1276 proteasome-dependent protein degradation and rupture of the outer mitochondrial
1277 membrane. *The Journal of biological chemistry*. 286:19630-19640.

1278 Yoshii, S.R., and N. Mizushima. 2015. Autophagy machinery in the context of
1279 mammalian mitophagy. *Biochimica et biophysica acta*. 1853:2797-2801.

1280 Yun, J., R. Puri, H. Yang, M.A. Lizzio, C. Wu, Z.H. Sheng, and M. Guo. 2014. MUL1
1281 acts in parallel to the PINK1/parkin pathway in regulating mitofusin and
1282 compensates for loss of PINK1/parkin. *eLife*. 3:e01958.

1283 Zhang, T., P. Mishra, B.A. Hay, D. Chan, and M. Guo. 2017. Valosin-containing protein
1284 (VCP/p97) inhibitors relieve Mitofusin-dependent mitochondrial defects due to
1285 VCP disease mutants. *eLife*. 6.

1286 Zhao, J., J. Zhang, M. Yu, Y. Xie, Y. Huang, D.W. Wolff, P.W. Abel, and Y. Tu. 2013.
1287 Mitochondrial dynamics regulates migration and invasion of breast cancer cells.
1288 *Oncogene*. 32:4814-4824.

1289 Zheng, X., and T. Hunter. 2013. Parkin mitochondrial translocation is achieved through a
1290 novel catalytic activity coupled mechanism. *Cell research*. 23:886-897.

1291 Ziviani, E., R.N. Tao, and A.J. Whitworth. 2010. Drosophila parkin requires PINK1 for
1292 mitochondrial translocation and ubiquitinates mitofusin. *Proceedings of the*
1293 *National Academy of Sciences of the United States of America*. 107:5018-5023.
1294

1295

1296 **FIGURE LEGENDS**

1297 Figure 1. *Ultrastructural analysis of ER-mitochondria contact during mitophagy in*
1298 *U2OS cells and dopaminergic neurons*. (A) Representative TEM images of mitochondria
1299 ("M") in contact with ER (pseudocoloured blue) in untreated and CCCP-treated
1300 U2OS:GFP-parkin cells. Scale bars, 500 nm. (B-E) Quantification of TEM from (A) in
1301 U2OS:GFP and GFP-parkin$^{WT}$ cells, left untreated (red bars) or treated with 20 μM
1302 CCCP for four hours (blue bars). Total apposition length (B), mitochondrial size (C), and
1303 the percent of OMM per mitochondrion (D) and mitochondria per field (E) in contact
1304 with the ER was quantified. Bars represent mean±SEM, n=82 to 152 mitochondria in 15
1305 to 19 fields per condition. n.s., not significant; **, p<.01; ***, p<.001; ****, p<.0001. (F)
1306 TEM image of an isolation membrane ("IM", broken green line) wrapping a
1307 mitochondrion ("mito"). Blue arrowheads indicate the boundaries of OMM rupture, while
1308 red arrowheads indicate ER tubules in contact with the intact portion of the OMM. Scale
1309 bar, 500 nm. (G) Immunoblot analysis of whole-cell lysates from U2OS:GFP-parkin WT
1310 and C431S cells treated with 20 μM CCCP for four hours with or without 10 μM MG132.
1311 In the case of MG132 treatment, cells were first pre-incubated with 10 μM MG132 for 30
1312 minutes prior to addition of CCCP. (H) Representative TEM images of mitochondria in
1313 contact with ER (pseudocoloured blue) in U2OS:GFP-parkin cells transfected with the
1314 indicated siRNA, and treated with 20 μM CCCP ("+CCCP") for four hours, in the
1315 presence or absence of 10 μM MG132 as in (G). Scale bar, 500 nm. (I,J) Quantification
1316 of TEM from (H) in cells treated with (blue bars) or without (red bars) 20 μM CCCP for
1317 four hours. The percent of OMM per mitochondrion (I) and mitochondria per field (J) in
1318 contact with the ER was quantified. Bars represent mean±SEM, n=101 to 203

1319 mitochondria in 14 to 16 fields per condition. n.s., not significant; *, p<.05; ***, p<.001;
1320 ****, p<.0001. (K) Immunoblot analysis of parkin levels in mouse brain cytosol from
1321 parkin$^{+/+}$ and parkin$^{-/-}$ mice, along with whole-cell lysates from iDA neurons derived
1322 from iPSCs isolated from control (ctrl) individuals and a *PRKN* patient (*PRKN*$^{del}$). (L) A
1323 representative wide-field image showing that iDA neurons express TH (green) and β-III
1324 tubulin (red) (Hoechst, blue). Scale bar, 20 microns. (M) Immunoblot analysis of whole-
1325 cell lysates from iDA neurons treated with 20 μM CCCP for one hour. The arrowhead
1326 indicates the unmodified Mfn2 band, while the red asterisk indicates ubiquitinated Mfn2.
1327 (N) Quantification of the percent of the OMM opposed to the ER in iDA neurons treated
1328 with 20 μM CCCP for one hour. Bars represent mean±SEM, n=80 to 131 mitochondria
1329 per condition. n.s., not significant; ****, p<.0001. (O) Representative TEM images of
1330 mitochondria in contact with ER. In the top row, the ER is pseudocoloured blue. In the
1331 second row, the red line denotes an area within 100 nm of the OMM. In the bottom row,
1332 ER tubules within the 100 nm area are psedocoloured red. Scale bars, 200 nm.
1333
1334 Figure 1 – figure supplement 1. *Mitophagy reduces ER-OMM contacts of all*
1335 *intermembrane distances*. (A) Representative TEM image of an untreated U2OS:GFP-
1336 parkin WT cell highlighting ER-OMM distances of less than 100 nm, 50 nm and 25 nm.
1337 Intermembrane distances (d) are indicated. Scale bars, 500 and 100 nm. (B)
1338 Quantification of the relative amount of OMM in contact with the ER (top) and fraction
1339 of mitochondria in contact with the ER per field of view (bottom) for each of the three
1340 ER-OMM distance categories from (A), for cells left untreated or treated with 20 μM
1341 CCCP for four hours. Bars represent mean±SEM, n=83 to 150 mitochondria in 17 to 19

1342 fields per condition. ****, p<0.0001. (C,D) Distribution of ER-OMM contact in CCCP-
1343 treated and untreated U2OS:GFP-parkin WT cells, displayed as the percentage of OMM
1344 corresponding to each intermembrane distance (C) or as a percentage of all ER-OMM
1345 contacts (D).
1346
1347 Figure 2. *Mfn2 is rapidly phosphoubiquitinated upon induction of mitophagy*. (A)
1348 Immunoblot analysis of protein turnover in glucose-maintained U2OS:GFP-parkin WT
1349 and A320R cells treated with 20 μM CCCP for the indicated time. (B) Higher exposures
1350 of Mfn2 and TOM20 immunoblots from (A). Red asterisks indicate ubiquitinated forms
1351 of Mfn2 and TOM20. (C) Co-immunoprecipitation of parkin substrates with GFP-parkin
1352 WT or A320R in U2OS cells treated with 20 μM CCCP for the indicated time, using an
1353 anti-GFP antibody. Immunoprecipitates were separated, along with 4% input, by SDS-
1354 PAGE and immunoblotted for the indicated protein. The arrowhead indicates the
1355 unmodified form of the protein, while the red asterisks denote ubiquitinated forms. (D)
1356 Workflow for the on-bead deubiquitination of Mfn2. U2OS:GFP-parkin WT cells were
1357 treated for one hour with 20 μM CCCP, and GFP-parkin was immunoprecipitated as in
1358 (C). Immunoprecipitates were then treated with Usp2 deubiquitinase and the beads were
1359 re-isolated by centrifugation. (E) Immunoblot detection of Mfn2 after on-bead
1360 deubiquitination, as described in (D). Immunoprecipitates were either incubated at 37°C
1361 in the absence or presence of Usp2 catalytic domain for 30 minutes. Samples were then
1362 centrifuged to separate beads and supernatant ("sup."), which were denatured in sample
1363 buffer prior to separation by SDS-PAGE. Arrowheads indicate unmodified forms of
1364 Mfn2, while the red asterisks denote ubiquitinated forms. (F) Immunoprecipitation of

1365 Mfn2 for LC/MS analysis. Immunoprecipitates were separated, along with 4% input, by
1366 SDS-PAGE and immunoblotted for Ub. (G) Extracted ion chromatogram for the pS65 Ub
1367 peptide (TLSDYNIQKEpSTLHLVLR, a.a. 55-72) from Mfn2 immunoprecipitates from
1368 DMSO- (blue line) and CCCP- (red line) treated U2OS:GFP-parkin$^{WT}$ cells,
1369 immunoprecipitated as in (F). The red arrow indicates the peak corresponding to the
1370 peptide. (H) Immunoprecipitation of Mfn2 under denaturing conditions. Cells were lysed
1371 in buffer containing 1% SDS (see *Materials and Methods*). Immunoprecipitates were
1372 separated, along with 4% input, by SDS-PAGE and immunoblotted for Ub and pS65 Ub.
1373 (I) Crystal structure of parkin complexed with pUb (PDB ID 5N2W, Kumar *et al*., 2017).
1374 The A320 residue at the pUb/parkin interface is highlighted in red, with parkin coloured
1375 blue and ubiquitin in green. (J) GST-R0RBR pulldown of pUb from U2OS:GFP-parkin
1376 WT cells. Pulldowns were performed with WT or A320R GST-R0RBR, with no GST-
1377 R0RBR ("-") as a further negative control. Pulldowns were separated, along with 10%
1378 input, by SDS-PAGE and immunoblotted for the indicated protein. The asterisks
1379 represents a cross-reaction between the pS65 antibody and the GST-R0RBR module.
1380
1381 Figure 2 – figure supplement 1. *LC/MS of immunoprecipitated Mfn2*. (A) Base peak
1382 chromatograms indicating equal loading of both DMSO- and CCCP-treated samples from
1383 Fig. 2F and G. (B) Extracted ion chromatograms of the indicated Ub and Mfn2 peptides
1384 from both DMSO- (blue line) and CCCP- (red line) treated samples.
1385
1386 Figure 3. *Mfn2 antagonizes mitophagy*. (A) Immunoblot analysis of whole-cell lysates
1387 from cells cultured in glucose or galactose transfected with control siRNA or siRNA

1388 targeting Mfn1 (“siMfn1”) or Mfn2 (“siMfn2”). (B) Mitochondrial morphology in
1389 glucose-maintained cells transfected with the indicated siRNA, as revealed by confocal
1390 imaging of TOM20 (red) staining (Hoechst, blue). Scale bar, 30 microns. (C)
1391 Representative confocal images of GFP-parkin recruitment to mitochondria as a function
1392 of time in U2OS:GFP-parkin cells treated with 20 μM CCCP. Red asterisks indicate cells
1393 in which GFP-parkin has fully translocated to mitochondria. Scale bar, 20 microns. (D)
1394 Quantification of parkin recruitment in cells from (C). Data points represent mean±SEM,
1395 n=3 replicates cells per condition, with >100 cells counted per condition for each
1396 replicate. (E) Parkin recruitment at one hour CCCP in cells from (C) arranged as a
1397 histogram. Bars represent mean±SEM. n.s., not significant; **, p<.01; ***, p<.001. (F)
1398 U2OS:mtKeima cells were transfected with the indicated siRNA and GFP-parkin WT or
1399 C431S, and were treated with 20 μM CCCP (or DMSO) for four hours. mtKeima
1400 fluorescence in GFP-positive cells was measured using flow cytometry by excitation at
1401 405 nm (neutral pH) and 561 nm (acidified). The data are represented as scatter plots of
1402 fluorescence emission from excitation at both wavelengths. The gated area encloses cells
1403 undergoing mitophagy (high acidified:neutral Keima ratio), and the percentage of cells
1404 within this gate is indicated in the top-left corner of each plot. (G) Quantification of the
1405 percent of cells undergoing mitophagy in cells from (F) treated with DMSO (red bars) or
1406 CCCP (blue bars) for four hours. Bars represent mean±SEM, n=2 experiments. n.s., not
1407 significant; *, p<.05; **, p<.01; ***, p<.001.
1408
1409 Figure 3 – figure supplement 1. *Mfn2 is a mitochondrion-ER tether.* (A) Representative
1410 TEM images of U2OS:GFP-parkin cells transfected with the indicated siRNA. ER

1411 tubules are pseudocoloured blue. Scale bar, 500 nm. (B-D) Quantification of
1412 mitochondrial length (B), relative percentage of OMM in contact with the ER (C) and
1413 percentage of mitochondria in contact with ER per field of view (D) in cells from (A).
1414 Bars represent mean±SEM, n=66 to 70 mitochondria in 5 to 7 fields per condition. n.s.,
1415 not significant; *, p<.05; ***, p<.001; ****, p<.0001.
1416
1417 Figure 3 – figure supplement 2. *Mitochondrial respiration impedes mitophagy*. (A)
1418 Representative confocal images of U2OS:GFP-parkin (green) cells, grown on either
1419 glucose or galactose, treated with 20 μM CCCP for the indicated times. Cells were then
1420 fixed and stained for TOM20 (red) (Hoechst, blue). Cells marked with asterisks display
1421 parkin fully translocated to mitochondria. Scale bars, 20 microns. (B) Quantification of
1422 parkin recruitment to mitochondria in cells treated in (A). Data points represent
1423 mean±SEM, n=3 replicates cells per condition, with >100 cells counted per condition for
1424 each replicate. ***, p<.001. (C) Representative confocal images of U2OS:GFP-parkin
1425 (cyan) cells expressing the indicated construct, treated with 20 μM CCCP for four hours
1426 and then fixed and stained for TOM20 (yellow) and the indicated tag (magenta) (Hoechst,
1427 blue). In the case of p62 (middle panels), an antibody against endogenous p62 was used.
1428 Scale bars, 30 microns. (D) Immunoblot analysis of whole-cell lysates from U2OS:GFP
1429 and GFP-parkin cells – grown either on glucose ("glu"), converted to galactose
1430 ("glu>gal") or back to glucose ("glu>gal>glu") – treated with 20 μM CCCP for the
1431 indicated times. The asterisk indicates a non-specific band.
1432

1433 Figure 3 – figure supplement 3. *Parkin recruitment kinetics in cells lacking both Mfns*
1434 *and other mitochondria-ER tethering factors*. (A) Immunoblot analysis of whole-cell
1435 lysates from cells cultured in glucose or galactose transfected with control siRNA or
1436 siRNA targeting Mfn1 ("siMfn1"), Mfn2 ("siMfn2") or both ("siMfn1+2"). (B)
1437 Representative confocal images of GFP-parkin recruitment to mitochondria as a function
1438 of time in U2OS:GFP-parkin cells treated with 20 μM CCCP. Red asterisks indicate cells
1439 in which GFP-parkin has fully translocated to mitochondria. Scale bar, 20 microns. (C)
1440 Quantification of parkin recruitment in cells from (B). Data points represent mean±SEM,
1441 n=3 replicates cells per condition, with >100 cells counted per condition for each
1442 replicate. (D) Parkin recruitment at one hour CCCP in cells from (B) arranged as a
1443 histogram. Bars represent mean±SEM. n.s., not significant; *, p<.05; **, p<.01; ***,
1444 p<.001. (E) Immunoblot analysis of whole-cell lysates from glucose-maintained
1445 U2OS:GFP-parkin cells transfected with the indicated siRNA targeting tethering-
1446 promoting proteins. (F) Mitochondrial morphology in cells from (E), as revealed by
1447 confocal imaging of TOM20 (red) staining (Hoechst, blue). Scale bar, 20 microns. (G)
1448 Representative confocal images of GFP-parkin recruitment to mitochondria as a function
1449 of time in U2OS:GFP-parkin cells treated with 20 μM CCCP. Red asterisks indicate cells
1450 in which GFP-parkin has fully translocated to mitochondria. Scale bar, 20 microns. (H)
1451 Quantification of parkin recruitment in cells from (G). Data points represent mean±SEM,
1452 n=3 replicates cells per condition, with >100 cells counted per condition for each
1453 replicate. (I) Parkin recruitment at one hour CCCP in cells from (G) arranged as a
1454 histogram. Bars represent mean±SEM. n.s., not significant; **, p<.01; ***, p<.001.
1455

1456 Figure 3 – figure supplement 4. *Analysis of mitophagy in Mfn2 KO U2OS cells*. (A)
1457 Genomic sequence of human Mfn2 (exon 3) that was mutated in U2OS cells using
1458 CRISPR/Cas9. The arrow indicates the codon corresponding to methionine-1; leucine-29
1459 ("L29"), lysine-30 ("K30") and the introduced stop codon ("*") are also indicated. (B)
1460 Immunoblot analysis of whole-cell lysates from Mfn2 KO clones (A4 and A5). (C)
1461 Mitochondrial morphology in Mfn2 KO cells, as revealed by confocal imaging of
1462 TOM20 (green) staining. The asterisks indicate nuclei. Scale bar, 20 microns. (D)
1463 Representative wide-field images of mitochondrial polarization in live WT and Mfn2 KO
1464 (clone A4) cells as indicated by TMRM staining. (E) Representative confocal images of
1465 GFP-parkin recruitment to mitochondria as a function of time in WT or Mfn2 KO (clone
1466 A4) U2OS cells, transfected with GFP-parkin and treated with 20 μM CCCP. Red
1467 asterisks indicate cells in which GFP-parkin has fully translocated to mitochondria. Scale
1468 bar, 20 microns. (F) Quantification of parkin recruitment in cells from (E). Data points
1469 represent mean±SEM, n=3 replicates per condition, with >100 cells counted per
1470 condition for each replicate. n.s., not significant; *, p<.05; **, p<.01. Significance (or
1471 lack thereof) is colour-coded according to genotype. (G) Representative images of
1472 glucose-cultured WT and Mfn KO cells transfected with GFP-parkin (green) treated with
1473 20 μM CCCP for 24 hours analyzed for their mitochondrial content (represented by
1474 SDHA, red). Green lines delineate the boarders of parkin-expressing cells, and red
1475 asterisks indicate cells devoid of SDHA signal. "Untransfected" refers to cells in the
1476 experiment lacking parkin expression. Scale bar, 20 microns. (H) Quantification of
1477 complete mitochondrial turnover in cells from (G). Bars represent mean±SEM, n=3

1478 replicates cells per condition, with 38 to 63 cells counted per condition for each replicate.
1479 n.s., not significant; ****, p<.0001.
1480
1481 Figure 3 – figure supplement 5. *Parkin recruitment in Mfn2-depleted cells requires*
1482 *PINK1 and phosphoubiquitin binding*. (A) Immunoblot analysis of PINK1 depletion in
1483 WT and Mfn2 KO (clone A4) U2OS cells treated with 20 μM CCCP for four hours. The
1484 arrowhead indicates the PINK1 band, while the asterisk indicates a non-specific band. (B)
1485 U2OS cells from (A) were transfected with GFP-parkin and treated with 20 μM CCCP
1486 for four hours prior to fixation. Blue asterisks mark cells in which parkin has been
1487 recruited to mitochondria. Scale bar, 10 microns. (C) Quantification of parkin-expressing
1488 cells from (A), left untreated (red bars) or treated with 20 μM CCCP for four hours (blue
1489 bars). Bars represent mean±SEM, n=3 replicates cells per condition, with >100 GFP-
1490 positive cells counted per condition for each replicate. n.s., not significant; ****,
1491 p<.0001. (D) Quantification of parkin recruitment in U2OS:GFP-parkin cells, grown on
1492 glucose or galactose, treated with 20 μM CCCP for one hour prior to fixation. Cells were
1493 transfected with control siRNA ("ctrl siRNA") or siMfn2, and either additional ctrl
1494 siRNA (red bars) or siPINK1 (blue bars). Bars represent mean±SEM, n=3 replicates cells
1495 per condition, with >100 cells counted per condition for each replicate. n.s., not
1496 significant; ****, p<.0001. (E) Crystal structure of parkin complexed with pUb (PDB ID
1497 5N2W, Kumar *et al*., 2017). Sites of Ub phosphorylation (S65 in Ub), pUb binding
1498 (A320 in parkin) and catalysis (C431 in parkin) are highlighted in red, with relevant
1499 domains of parkin coloured different shades of blue, and ubiquitin in green. (F)
1500 Representative confocal images of U2OS cells stably expressing WT or A320R mutant

1501 parkin. Cells were treated with 20 μM CCCP for the indicated time prior to fixation. Blue
1502 asterisks indicate cells in which GFP-parkin has been recruited to mitochondria. Scale
1503 bar, 20 microns. (G) Quantification of parkin recruitment in cells from (F). Data points
1504 represent mean±SEM, n=3 replicates cells per condition, with >100 cells counted per
1505 condition for each replicate. n.s., not significant; ****, p<.0001.
1506
1507 Figure 4. *Parkin ubiquitinates Mfn2 in the HR1 domain to derepress mitophagy*. (A)
1508 Mnf2 KO:YFP-parkin$^{WT}$ cells were transfected with the indicated plasmid and CFP in a
1509 3:1 ratio, then fixed and immunostained for TOM20 (red) and counterstained with
1510 Hoechst 33342 (blue). Scale bars, 20 and 1 microns. (B) Mfn2 KO:YFP-parkin WT and
1511 C431S cells, transfected as in (A), were treated with 20 μM CCCP for four hours prior to
1512 fixation, then scored for YFP-parkin recruitment. Green and red asterisks indicated CFP-
1513 positive cells with mitochondrial and cytosolic YFP-parkin, respectively. Scale bar, 20
1514 microns. (C) Quantification of recruitment in (B). Bars represent mean±SEM, n=3
1515 replicates cells per condition, with >50 cells counted per condition for each replicate.
1516 ****, p<.0001. (D) Immunoblot analysis of Mfn2 KO:YFP-parkin cells (WT and C431S)
1517 transfected with Mfn2 and treated with 20 μM CCCP for the indicated time. An untreated
1518 U2OS cell lysate is included as a control for endogenous Mfn2 levels. (E) Representative
1519 mmunoblot analysis of Mnf2 KO:YFP-parkin$^{WT}$ cells transfected with the indicated Mfn2
1520 mutant and treated with 20 μM CCCP for four hours. (F) Quantification of Mfn2
1521 modification in immunoblot analyses from (E), given as the percent of Mfn2 reduction
1522 after CCCP relative to actin. Bars represent mean±SEM, n=4 replicates. **, p<.01; ***,
1523 p<.001. (G) Quantification of steady-state ("- CCCP") levels of Mfn2 in immunoblot

1524 analyses from (E), relative to actin. Bars represent mean±SEM, n=4 replicates. n.s., not
1525 significant. (H) Mnf2 KO:YFP-parkin$^{WT}$ cells were transfected with the indicated
1526 plasmid and CFP in a 3:1 ratio, then fixed and immunostained for TOM20 (red) and
1527 counterstained with Hoechst 33342 (blue). Scale bars, 20 and 1 microns. (I) Immunoblot
1528 analysis of BN- and SDS-PAGE gels of solubilized mitochondria from cells from (H).
1529 Arrows indicated two Mfn2-containing complexes in the native condition. (J)
1530 Representatitve widefiled images of Mfn2 KO:YFP-parkinWT cells transfected with the
1531 indicated Mfn2 construct. Cells were treated with 20 μM CCCP for 24 hours prior to
1532 fixation, then stained with CIV-COX1 (red) and Hoechst (blue). Scale bar, 20 microns.
1533 (K) Quantification of mitophagy in (J). Bars represent mean±SEM, n=4 replicates per
1534 condition, with >50 cells counted per condition for each replicate. ****, p<0.0001; n.s.,
1535 not significant.
1536
1537 Figure 4 – figure supplement 1. *Location and conservation of ubiquitination and*
1538 *phosphorylation sites in Mfn2*. (A) Sequence alignment of sites of Mfn2 modification
1539 across species. Ubiquitinated lysines and phosphorylated serines and threonines are
1540 indicated by arrowheads. Residue numbering is according to the human sequence. HR,
1541 heptad repeat domain. (B) Diagram of Mfn2 post-translational modification by parkin-
1542 mediated ubiquitination (Sarraf *et al*., 2013) and PINK1-mediated phosphorylation (Chen
1543 & Dorn, 2012) for both double- (top) and single- (bottom) pass topologies. Phosphosites
1544 are denoted in red, while sites of ubiquitination are marked in grey. HR, heptad repeat
1545 domain; OMM, outer mitochondrial membrane.
1546

1547 Figure 5. *p97 governs ER-OMM contact via the extraction of Mfn2 complexes*. (A)
1548 Immunoblot analysis of NP-40-solubilized mitochondria, isolated from U2OS:GFP-
1549 parkin$^{WT}$ cells treated with 20 μM CCCP for the indicated time, separated by blue
1550 native- (BN-) and SDS-PAGE. (B, C) Immunoblot analysis of Mfn1- (B) and Mfn2- (C)
1551 containing complexes in NP-40-solubilized mitochondria, isolated from U2OS:GFP-
1552 parkin WT and C431S cells treated with 20 μM CCCP for four hours, separated by BN-
1553 and SDS-PAGE. (D) Mitochondria isolated from U2OS:GFP-parkin$^{WT}$ cells treated with
1554 20 μM CCCP for one hour were, after solubilization in NP-40, incubated with 1 μM Usp2
1555 for 30 minutes at 37°C prior to separation by SDS-PAGE. Red asterisks indicate
1556 ubiquitinated species of Mfn1 and Mfn2. Densitometry calculations for the Mfn1 and
1557 Mfn2 bands (shorter exposure) relative to CIII-core2 are shown under the respective
1558 immunoblots. (E) Immunoblot analysis of NP-40-solubilized mitochondria, isolated from
1559 U2OS:GFP-parkin$^{WT}$ cells treated with 20 μM CCCP in the presence or absence of 25
1560 μM NMS-873 for the indicated time, separated by blue native- (BN-) and SDS-PAGE.
1561 Red asterisks indicate ubiquinated Mfn species visible by SDS-PAGE, while the
1562 arrowhead denotes the unmodified band. (F) Representative TEM images of
1563 mitochondria in contact with ER (pseudocoloured blue) in U2OS:GFP-parkin cells
1564 treated with 20 μM CCCP ("+CCCP") for four hours in the presence or absence of 25 μM
1565 NMS-873. Scale bar, 500 nm. (G,H) Quantification of TEM from (F) in cells treated with
1566 (blue bars) or without (red bars) 20 μM CCCP for four hours. The percent of OMM per
1567 mitochondrion (G) and mitochondria per field (H) in contact with the ER was quantified.
1568 Bars represent mean±SEM, n=99 to 187 mitochondria in 12 to 14 fields per condition.
1569 n.s., not significant; *, p<.05; ***, p<.001; ****, p<.0001.

1570

1571 Figure 6. *Degradation of ubiquitinated Mfn2 involves p97 translocation to mitochondria*
1572 *and is controlled by p97-ubiquitin interactions*. (A) Representative confocal images of
1573 p97 recruitment to mitochondria in cells treated with 20 μM CCCP and/or 25 μM NMS-
1574 873 for the indicated time. Blue asterisks denote cells with mitochondrial p97, and p97
1575 signal intensity is represented as a heat map. Scale bar, 20 microns. (B) Quantification of
1576 cells with p97 translocation to mitochondria in cells treated with either 25 μM NMS-873
1577 (red line), 20 μM CCCP (blue line) or both simultaneously (magenta line). Bars represent
1578 mean±SEM, n=3 replicates per condition, with >100 cells counted per condition for each
1579 replicate. ****, p<.0001. (C) Immunoblot analysis of whole-cell lysates from
1580 U2OS:GFP-parkin cells treated with 20 μM CCCP and the specified concentration of
1581 NMS-873 for the indicated time, separated by SDS-PAGE. For each Mfn, longer (upper
1582 panel) and shorter (lower panel) exposures are shown. Red asterisks indicate
1583 ubiquitinated Mfn species, while the arrowheads denote the unmodified band. (D)
1584 U2OS:GFP-parkin cells were treated with 20 μM CCCP in the presence or absence of 25
1585 μM NMS-873 for four hours, then fixed and immunostained for Mfn2 (yellow) and
1586 cytochrome c (magenta). Scale bar, 10 microns. (E) Immunoblot analysis of Mfn2
1587 ubiquitination in U2OS:GFP-parkin$^{WT}$ cells transfected with siRNA targeting p97 (sip97)
1588 or control (ctrl siRNA) and treated with 20 μM CCCP for two hours. Arrowheads
1589 indicate the unmodified Mfn2 band (two exposures), while the red asterisk denotes
1590 ubiquitinated Mfn2. (F) Immunoblot analysis of exogenous Mfn2 in Mfn2 KO:YFP-
1591 parkin$^{WT}$ cells reconstituted with the indicated Mfn2 construct. Cells were treated with 25
1592 μM NMS-873 and/or 20 μM CCCP for four hours prior to lysis. The arrowhead indicates

1593 the unmodified Mfn2 band and the red asterisk denotes ubiquitinated Mfn2 conjugates.
1594 (G) Immunoprecipitation of Mfn2 under denaturing conditions from Mfn2 KO:YFP-
1595 parkin WT cells reconstituted with the indicated Mfn2 construct. Cells were lysed in
1596 buffer containing 1% SDS (see *Materials and Methods*). Immunoprecipitates were
1597 separated by SDS-PAGE and immunoblotted for Ub. (H) Representative wide-field
1598 images of p97 translocation to mitochondria (pseudocoloured as in [A]) in Mfn2
1599 KO:YFP-parkin WT or C431S cells, reconstituted with the indicated plasmid, treated
1600 with 20 μM CCCP (or DMSO) for four hours. CFP (blue) is included as a marker of
1601 Mfn2 transfection, and blue asterisks indicate cells where p97 has translocated to
1602 mitochondria. Scale bar, 20 microns. (I) Quantification of mitochondrial recruitment of
1603 p97 in Mfn2 KO:YFP-parkin cells from (H). Bars represent mean±SEM, n=3 replicates
1604 per condition, with >50 cells counted per condition for each replicate. *, p<.05; **,
1605 p<.01; ****, p<.0001. (J) Co-immunoprecipitation of mitofusins with GFP-parkin
1606 U2OS:GFP-parkin cells treat with 20 μM CCCP in the presence or absence of 25 μM
1607 NMS-873 for the indicated time, using an anti-GFP antibody. Immunoprecipitates were
1608 separated, along with 4% input, by SDS-PAGE and immunoblotted for the indicated
1609 protein. The arrowhead indicates the unmodified form of the protein, while the asterisks
1610 denote ubiquitinated forms. (K) Quantification of the relative amount of ubiquitinated
1611 Mfn2 co-immunoprecipitated with GFP-parkin in cells from (J). Bars represent
1612 mean±SEM, n=3 replicates. *, p<.05.
1613
1614 Figure 6 – figure supplement 1. *Analysis of pUb interactors from mouse brain*. (A)
1615 Workflow of protein purification, phosphorylation, pull-down and LC/MS. GST-

1616 4xUb$^{G76V}$, which cannot be cleaved by the cellular Ub processing machinery, was
1617 phosphorylated on S65 by *Tribolium castaneum* PINK1 (*Tc*PINK1) to form GST-
1618 4xpUb$^{G76V}$. Both GST-4xUb and -4xpUb were incubated with mouse brain lysate, and
1619 binding partners were analyzed by LC/MS. See *Materials and Methods* for more detail.
1620 (B) Ub phosphorylation was determined by separation by SDS-PAGE over Phos-tag gel,
1621 which slows the migration of phosphorylated proteins. (C) Quantification of the number
1622 of peptides corresponding to p97-related factors identified by LC/MS in GST (black
1623 dots), GST-4xUb (red dots) and GST-4xpUb (blue dots) pull-downs from mouse brain
1624 lysate. Bars represent the mean, n=3 independent experiments. See Supplementary File 1
1625 for complete lists of identified interactors.
1626
1627 Figure 7. *p97 and Mfn2 effect mitophagy through parkin substrate availability*. (A)
1628 U2OS:mtKeima cells were transfected with the indicated siRNA and GFP-parkin$^{WT}$, and
1629 were treated with 20 μM CCCP (or DMSO) for five hours in the presence (dark grey box)
1630 or absence (light grey box) of 25 μM NMS-873. mtKeima fluorescence in GFP-positive
1631 cells was measured using flow cytometry by excitation at 405 nm (neutral pH) and 561
1632 nm (acidified). The data are represented as scatter plots of fluorescence emission from
1633 excitation at both wavelengths. The gated area encloses cells undergoing mitophagy and
1634 the percentage of cells within this gate is indicated in the top-left corner of each plot. (B)
1635 Quantification of the percent of cells undergoing mitophagy in cells from (A), expressed
1636 as a ratio of CCCP-treated cells to those treated with DMSO. Bars represent mean±SEM,
1637 n=2 experiments. n.s., not significant; ****, p<.0001. (C) Immunoblot analysis of
1638 U2OS:GFP-parkin cells, transfected with siRNA targeting Mfn2 (siMfn2) or control (ctrl

1639 siRNA), treated with 20 μM CCCP in the presence or absence of 25 μM NMS-873 over a
1640 period of six hours. (D) Immunoblot quantification of VDAC1 levels (relative to actin)
1641 from cells from (C). Bars represent mean±SEM, n=5 experiments. (E) The 6 hour time-
1642 point data from (D) is represented as a fold change in VDAC1 remaining when NMS-873
1643 is added. Data points are represented on the graph, n=5 experiments. *, $p<0.05$. (F)
1644 Quantification of VDAC1 half-lives ($t_{1/2}$) in cells from (C) over 6 hours. Half-lives were
1645 obtained from decay curves generated with the time-points in (C). Bars represent
1646 mean±SEM, n=5 experiments. (G) Immunoblot analysis of U2OS:GFP-parkin cells,
1647 transfected with the indicated siRNA, treated with 20 μM CCCP in the presence or
1648 absence of 25 μM NMS-873 for six hours. (H) Immunoblot quantification of VDAC1
1649 levels (relative to actin) in cells from (G), represented as a fold change in VDAC1
1650 remaining when NMS-873 is added. Data points are represented on the graph, n=3
1651 experiments. Factors promoting ER-OMM contact are contained within the blue box.
1652
1653 Figure 8. *Cell-free reconstitution of* in organello *ubiquitination of Mfn2 and VDAC1*. (A)
1654 Workflow for the *in organello* ubiquitination assay, where HeLa cells are depolarized
1655 with 20 μM CCCP for four hours and mitochondria are isolated ("mito$^{CCCP}$", with control
1656 "mito$^{DMSO}$"). These are combined with ubiquitination assay components (blue box) and
1657 incubated at 37°C (see *Materials and Methods* for full details). (B) Immunoblot analysis
1658 of PINK1 levels in mitochondria isolated from depolarized ("mito$^{CCCP}$") or control
1659 ("mito$^{DMSO}$") cells. (C) *In organello* ubiquitination assays, using the depolarized or
1660 control mitochondria and 100 nM of the indicated parkin construct, were incubated at
1661 37°C for the indicated time, and reactions were quenched with SDS-PAGE samples

1662 buffer. Mfn2 ubiquitination was analyzed by immunoblot. Ubiquitinated species are
1663 indicated by red asterisks, while unmodified bands are denoted by arrowheads. (D)
1664 Immunoblot analysis of PINK1 levels in mitochondria isolated from depolarized cells
1665 transfected with control siRNA (ctrl siRNA) or siRNA targeting PINK1 (siPINK1). (E)
1666 Mitochondria from (D) were used for 30 minute *in organello* ubiquitination assays using
1667 100 nM WT or C431A parkin, and Mfn2 ubiquitination was analyzed by immunoblot.
1668 Ubiquitinated species are indicated by red asterisks, while unmodified bands are denoted
1669 by arrowheads. (F) Depolarized mitochondria were used for 30 minute *in organello*
1670 ubiquitination assays with the indicated concentration of WT parkin, or 100 nM
1671 parkin$^{C431A}$ as a negative control. Ubiquitinated species are indicated by red asterisks,
1672 while unmodified bands are denoted by arrowheads. (G) Immunoblot analysis of mouse
1673 brain fractionation. Mouse brain homogenate was separated into heavy membrane (P7k),
1674 cytosolic (S200k) and light membrane (P200k) fractions. Distribution of mitochondrial
1675 (Mfn2, VDAC1, PDH E2), ER (Grp78), soluble (parkin) and endosomal (Rab11A)
1676 markers are shown. (H) CCCP-uncoupled ("mito$^{CCCP}$") or control ("mito$^{DMSO}$")
1677 mitochondria were incubated for 60 minutes with 2 mg/ml cytosol from WT mouse brain
1678 ("WT cytosol") or from the brain of parkin-/- mice ("KO cytosol"). As a positive control,
1679 mitochondria were incubated with 100 nM uncleaved GST-parkin$^{WT}$ (without cytosol).
1680 Ubiquitinated species are indicated by red asterisks, while unmodified bands are denoted
1681 by arrowheads. (I) CCCP-uncoupled ("mito$^{CCCP}$") or control ("mito$^{DMSO}$") mitochondria
1682 were incubated for 60 minutes with 100 nM parkin WT or C431A and in the presence or
1683 absence of 2 mg/ml cytosol from parkin$^{-/-}$ mouse brain ("KO cytosol"). Mfn2 and
1684 VDAC1 ubiquitination were assayed by immunoblot. Ubiquitinated species are indicated

1685 by red asterisks, while unmodified bands are denoted by arrowheads. (J) *In organello*
1686 ubiquitination reactions were performed with parkin$^{-/-}$ mouse brain ("KO cytosol") in the
1687 presence of absence of 25 μM NMS-873. Reactions were incubated on ice for 30 minutes
1688 prior to a 60-minute 37°C incubation. In the immunoblot analysis, ubiquitinated species
1689 are indicated by red asterisks, while unmodified bands are denoted by arrowheads. (K)
1690 Quantification of the level of ubiquitinated VDAC1 as compared to control, relative to
1691 mitochondrial loading control (TIM23 or CIII-core2). Data points are represented on the
1692 graph, n=3 experiments. *, $p<0.05$; n.s., not significant. (L) Recombinant, hexameric His-
1693 p97 runs as a ~700 kDa complex as assayed by BN-PAGE. Prior to separation on the gel,
1694 samples were incubated at the indicated temperature for 10 minutes. (M) Immunoblot
1695 analysis of 60 minute *in organello* ubiquitination assays using depolarized mitochondria,
1696 100 nM parkin, 200 nM His-p97 hexamer, and 2 mg/ml parkin KO brain cytosol.
1697 Ubiquitinated species are indicated by red asterisks, while unmodified bands are denoted
1698 by arrow heads. Recombinant His-p97 is additionally indicated on the Ponceau. (N) *In*
1699 *organello* retrotranslocation of Mfn2. *In organello* ubiquitination reactions with or
1700 without recombinant p97 were centrifuged at 10,000 g to separate mitochondria (pellet)
1701 from soluble factors (supernatant). As a control, reactions were lysed in 1% TX-100 prior
1702 to centrifugation. The inset on the supernatant Mfn2 blot shows ubiquitination (red
1703 asterisks) of the protein.
1704
1705 Figure 8 – figure supplement 1. *Effect of NMS-873 on cytosol-free ubiquitination. In*
1706 *organello* ubiquitination reactions were performed in the presence of absence of 25 μM
1707 NMS-873. Reactions were incubated on ice for 30 minutes prior to a 60-minute 37°C

1708 incubation. In the immunoblot analysis, ubiquitinated species are indicated by red
1709 asterisks, while unmodified bands are denoted by arrowheads.
1710
1711 Figure 9. *Dismantling of Mfn2 interorganellar bridges by PINK1, parkin and p97 during*
1712 *mitophagy*. (A) PINK1-phosphorylated Ub on Mfn2 initially recruits parkin to Mfn2
1713 complexes, where it is phosphorylated and activated by PINK1. (B) Parkin and PINK1
1714 cooperate to catalyze a pUb burst on Mfn2. (C) Ubiquitinated Mfn2 HMW complexes are
1715 recognized by p97, which translocates to mitochondria. (D) Ubiquitinated Mfn2 is
1716 retrotranslocated from the OMM and degraded by the proteasome. (E) VDACs and
1717 possibly other substrates become available to the parkin/PINK1 system, and their
1718 phosphoubiquitination stabilizes parkin on mitochondria to drive mitophagy.
1719
1720 Supplementary File 1. *MS identification of selective Ub and pUb interactors*. Table
1721 depicting GST-4xUb interactors that are selective for S65-phosphorylated (top) or
1722 unphosphorylated (bottom) Ub. p97-related data (shaded in yellow) are also depicted in
1723 Fig. 6–figure supplement 1C.
1724
1725 **SOURCE DATA**
1726 Figure 1–source data 1. *Numerical source data for Fig. 1B to 1D, 1E, 1I, 1J, 1N and*
1727 *Figure 1-figure supplement 1B to D.*
1728
1729 Figure 3–source data 1. *Numerical source data for Fig. 3D, 3E and 3G, Figure 3-figure*
1730 *supplements 1B to D, 2B, 3C, 3D, 3H, 3I, 4F, 4H and 5C.*

Figure 4–source data 1. *Numerical source data for Fig. 4C, 4F, 4G and 4K.*

Figure 5–source data 1. *Numerical source data for Fig. 5G and 5H.*

Figure 6–source data 1. *Numerical source data for Fig 6I, 6K and Figure 6-figure supplement 1C.*

Figure 7–source data 1. *Numerical source data for Fig. 7B, 7D to 7F, and 7H.*

Figure 8–source data 1. *Numerical source data for Fig. 8K.*

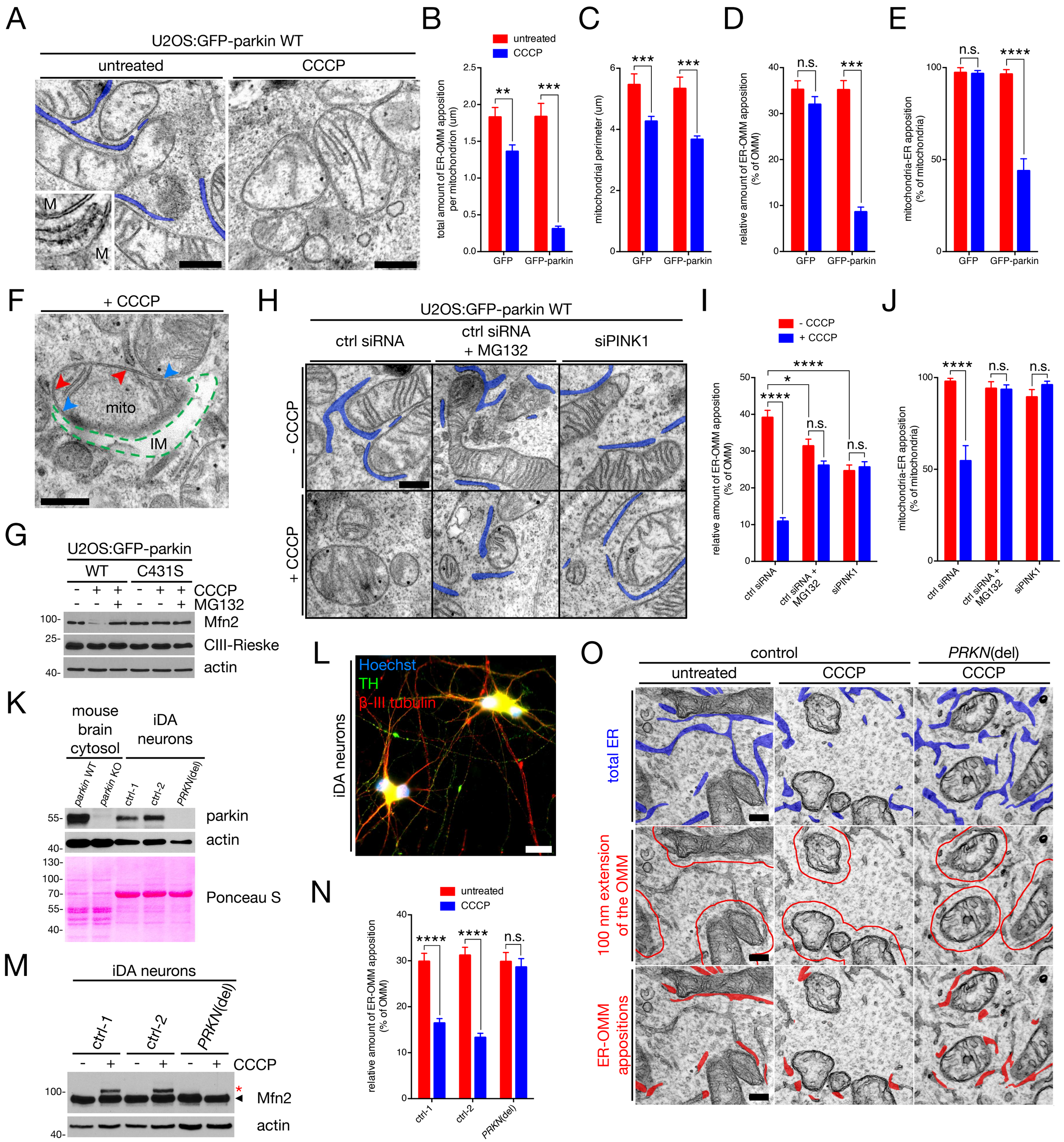


McLelland et al., Figure 1

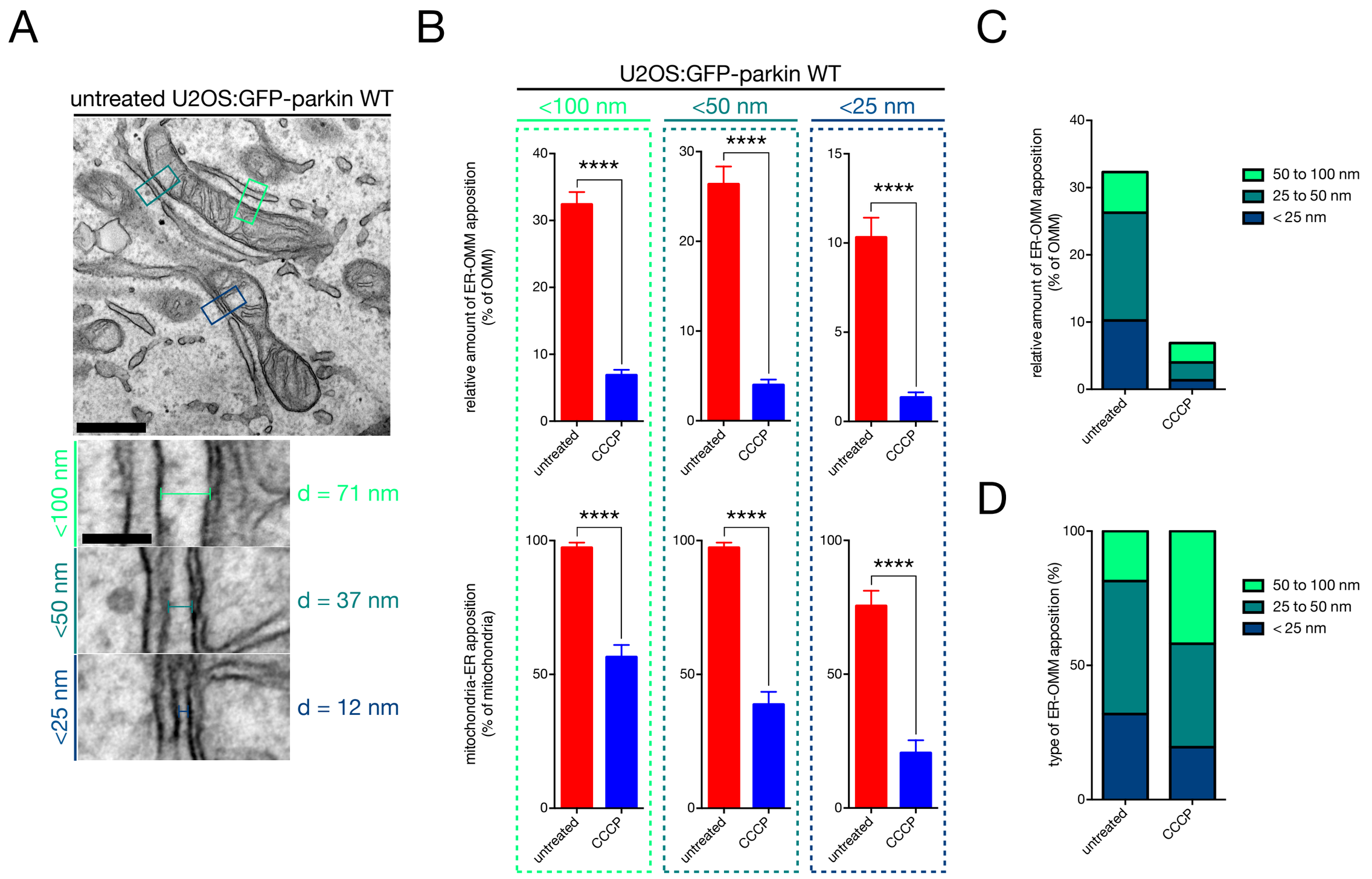


McLelland et al., Figure 1-S1

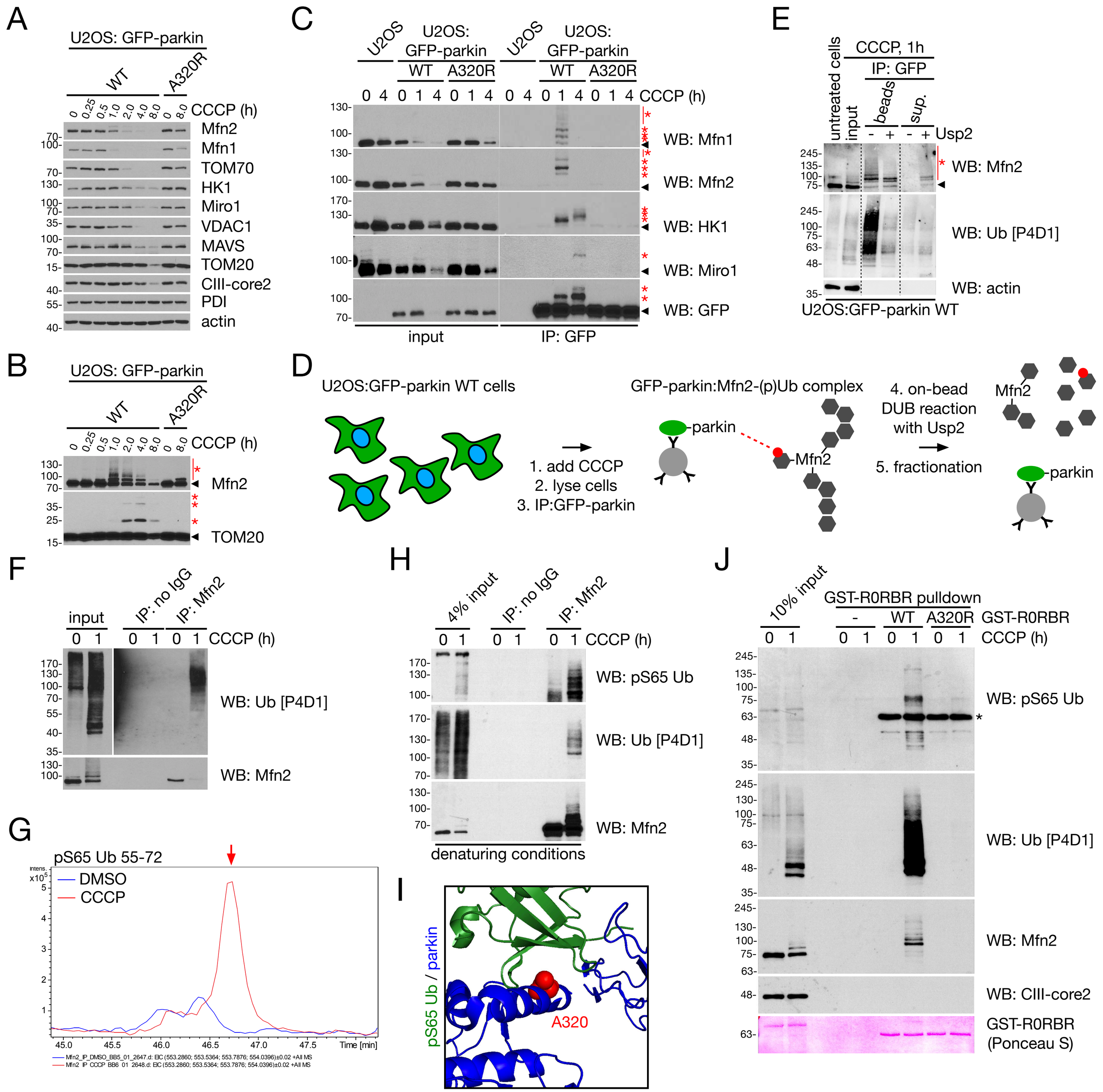


McLelland et al., Figure 2

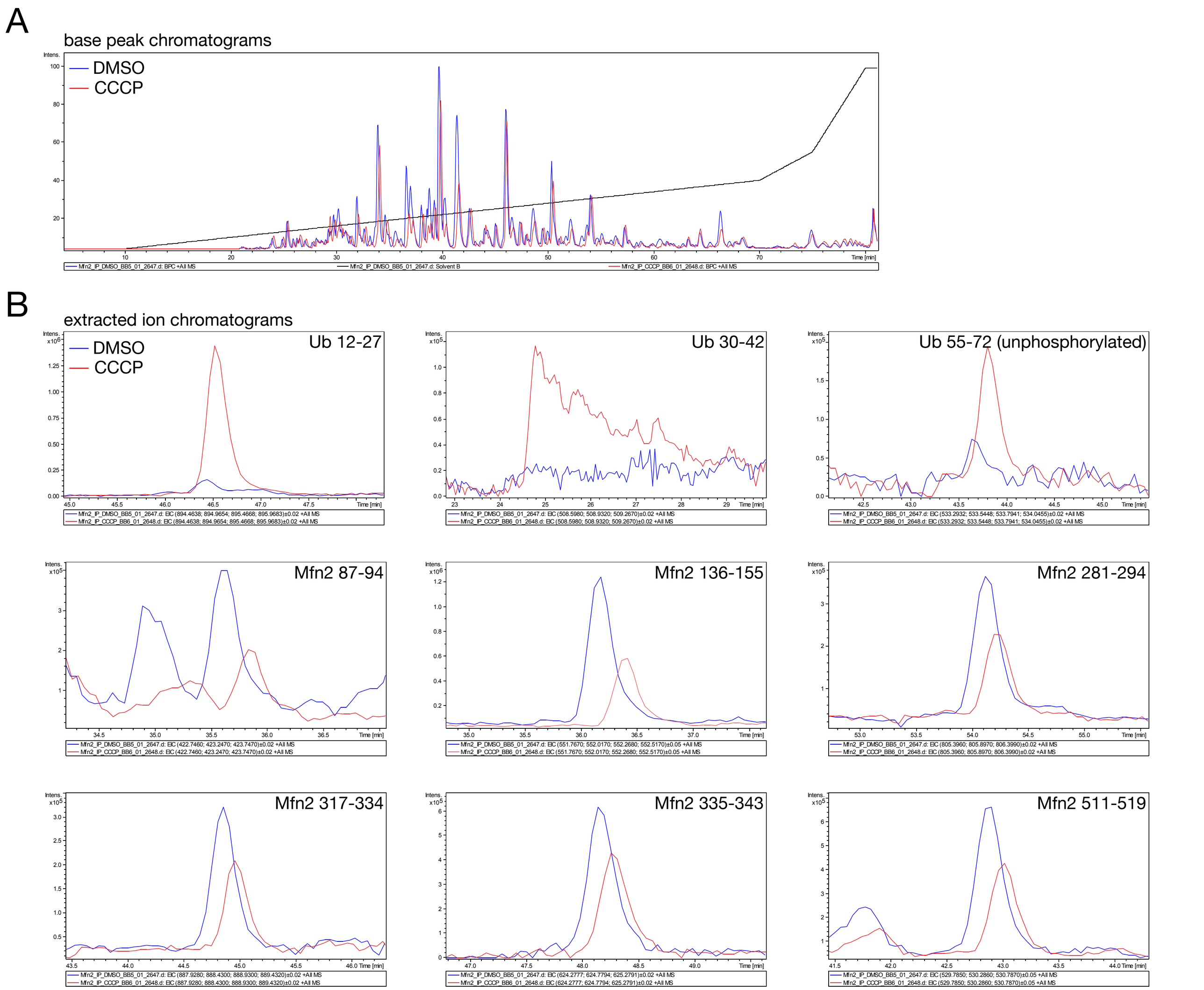


McLelland et al., Figure 2-S1

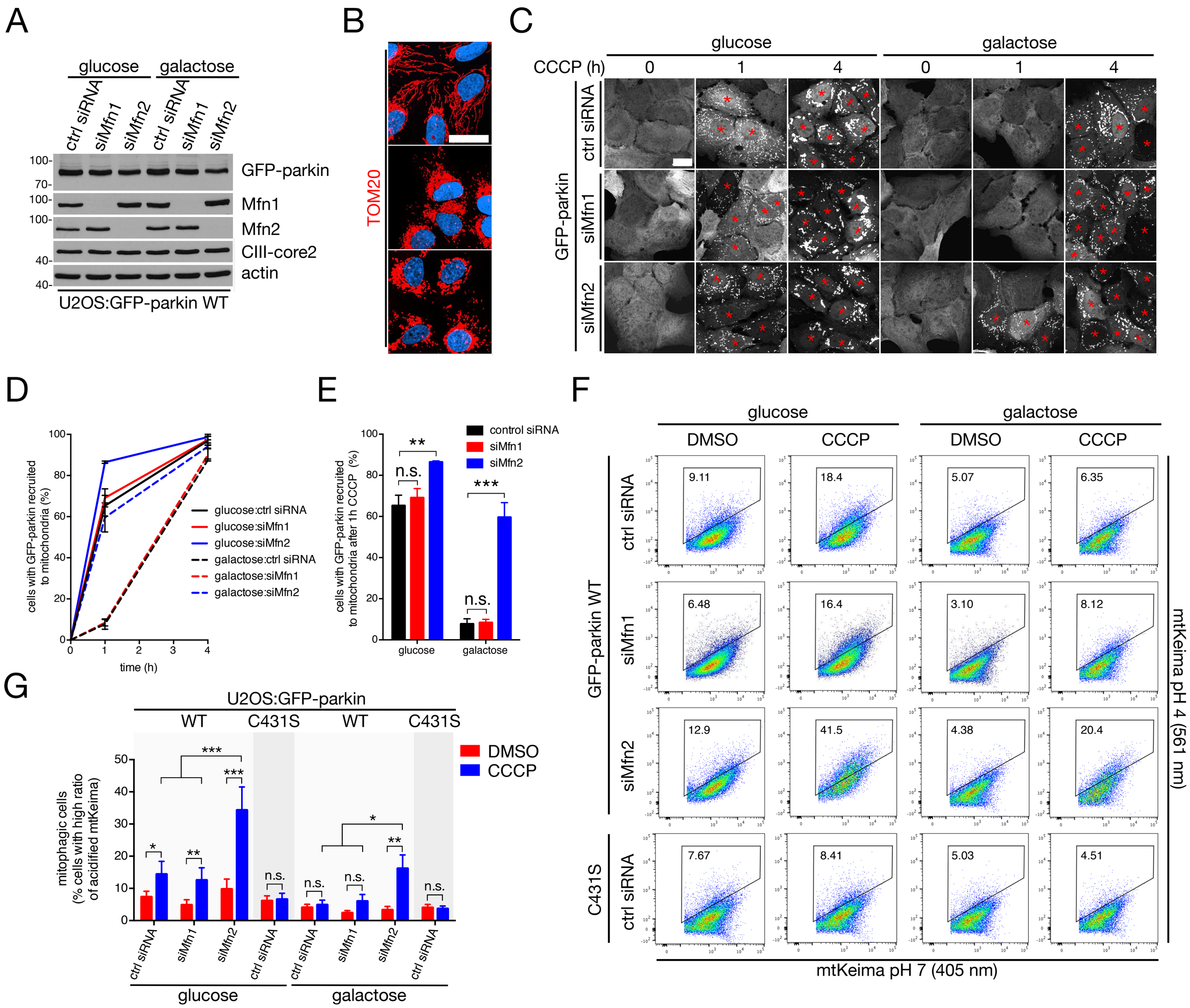


McLelland et al., Figure 3

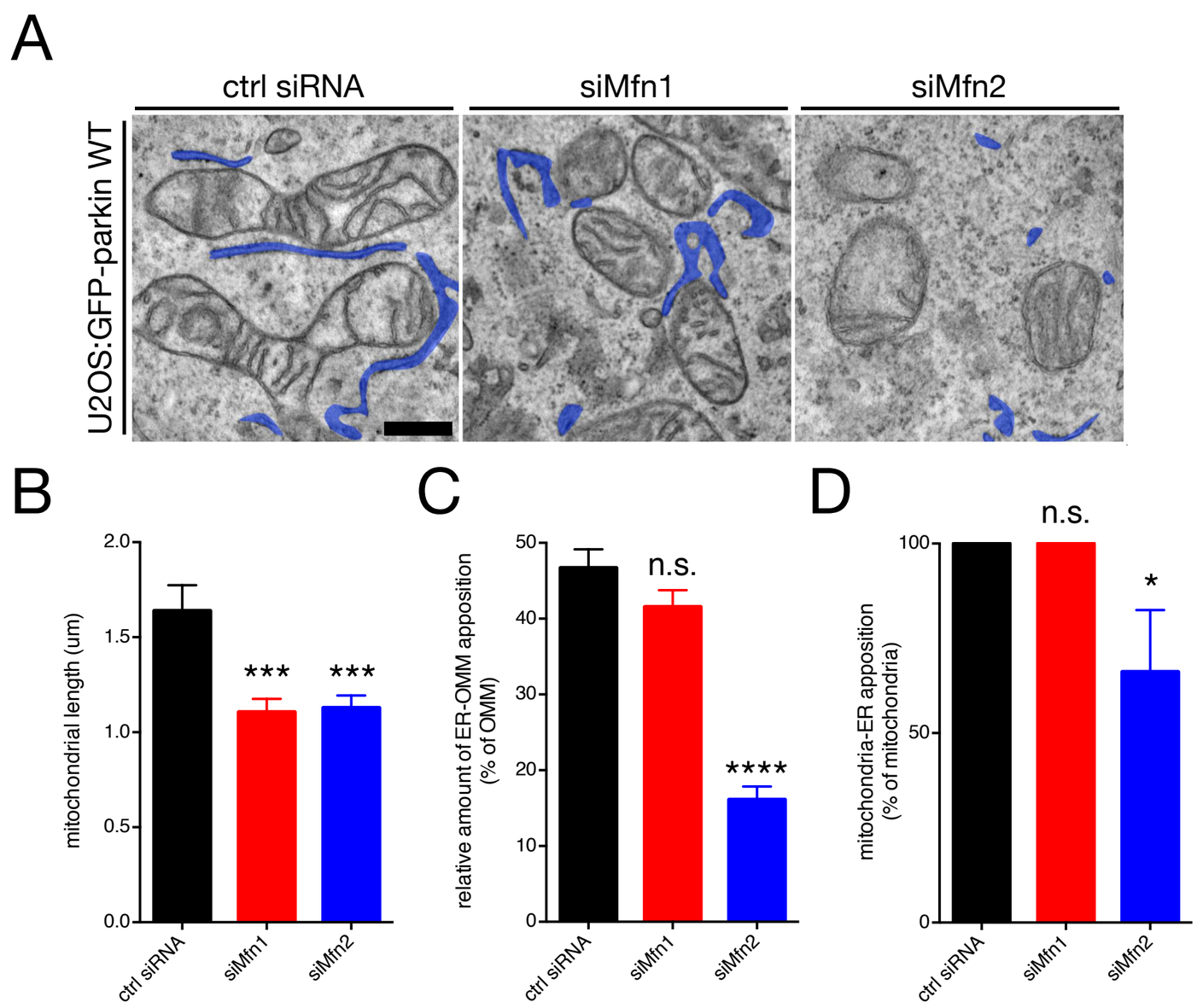


McLelland et al., Figure 3-S1

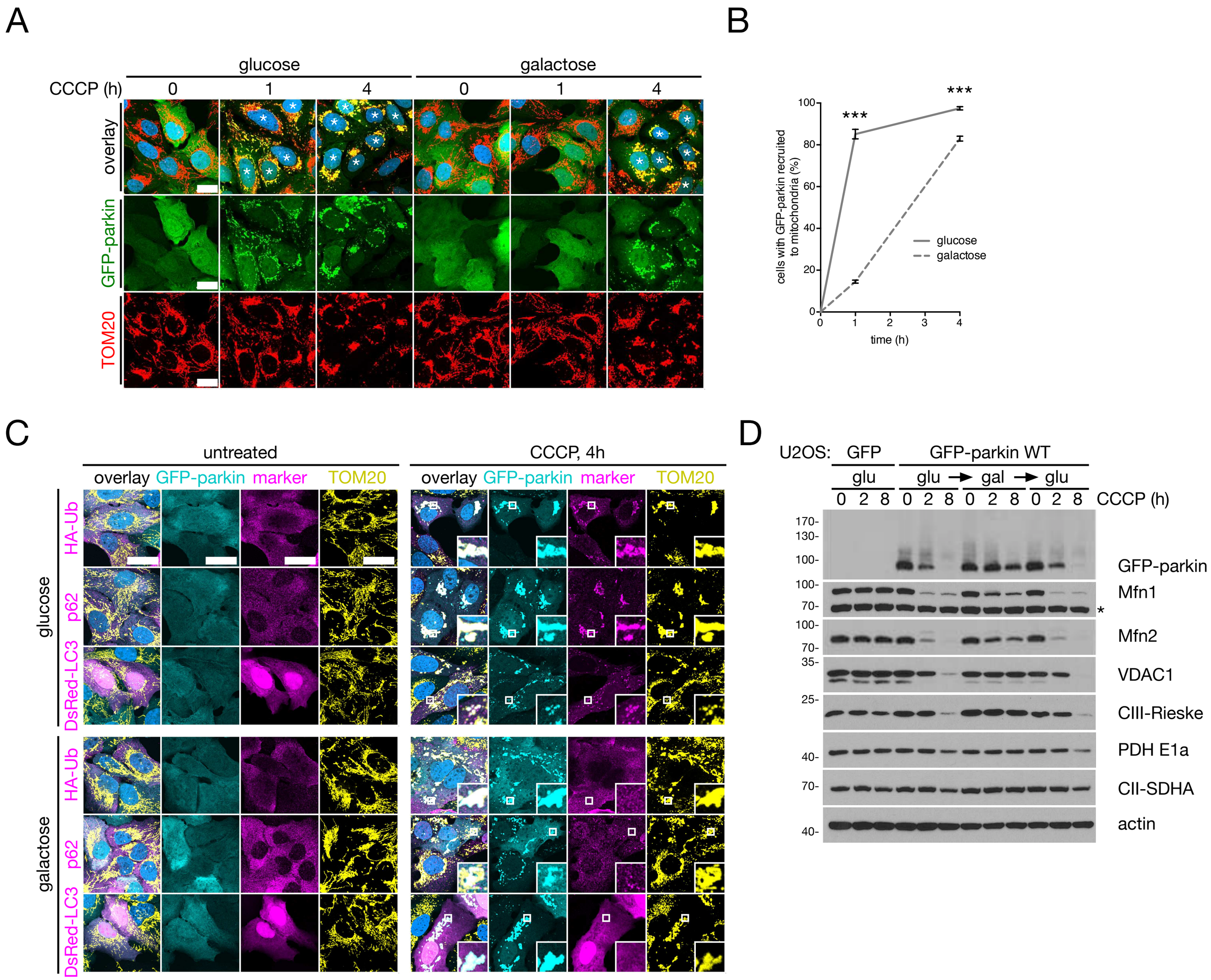


McLelland et al., Figure 3-S2

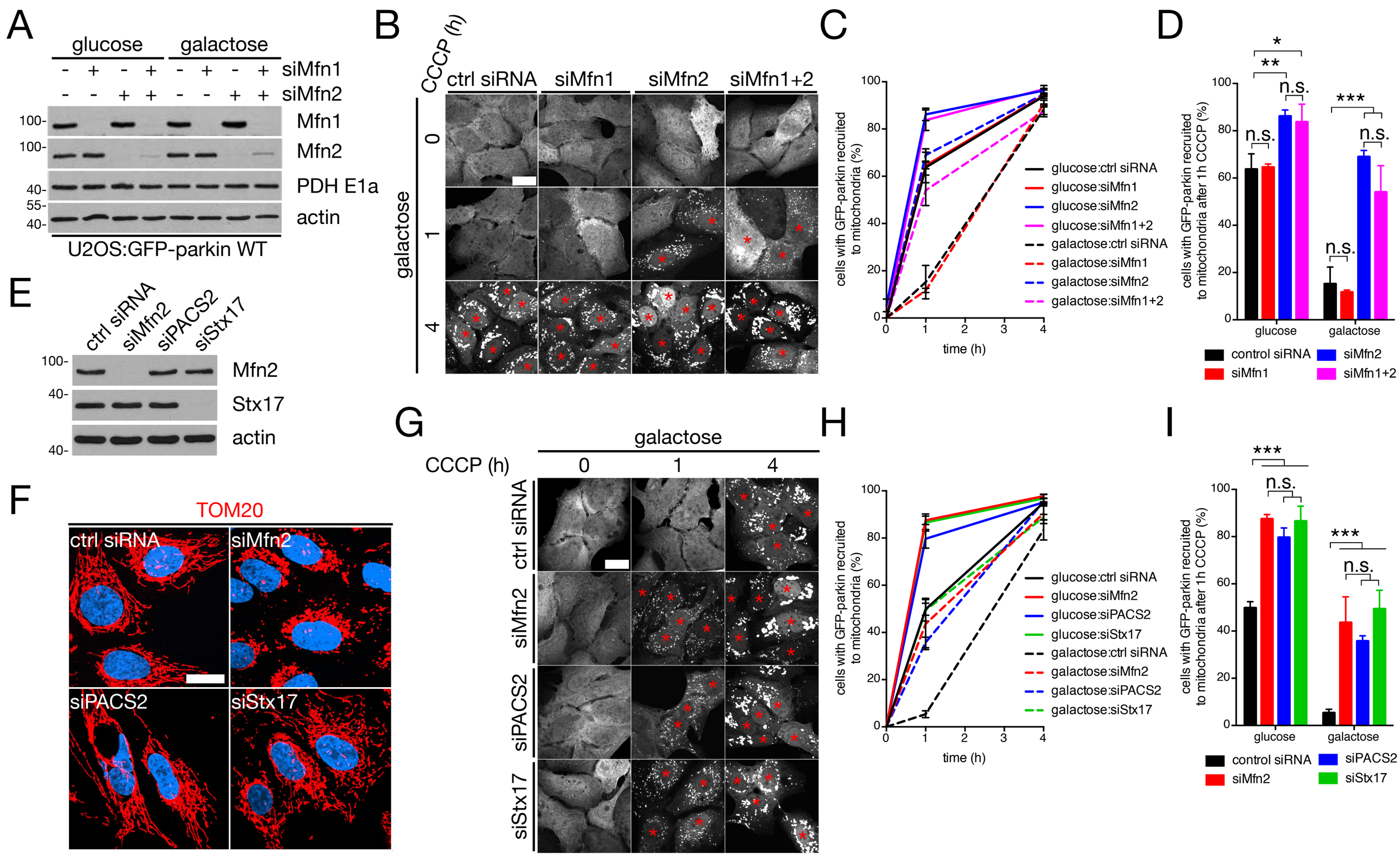


McLelland et al., Figure 3-S3

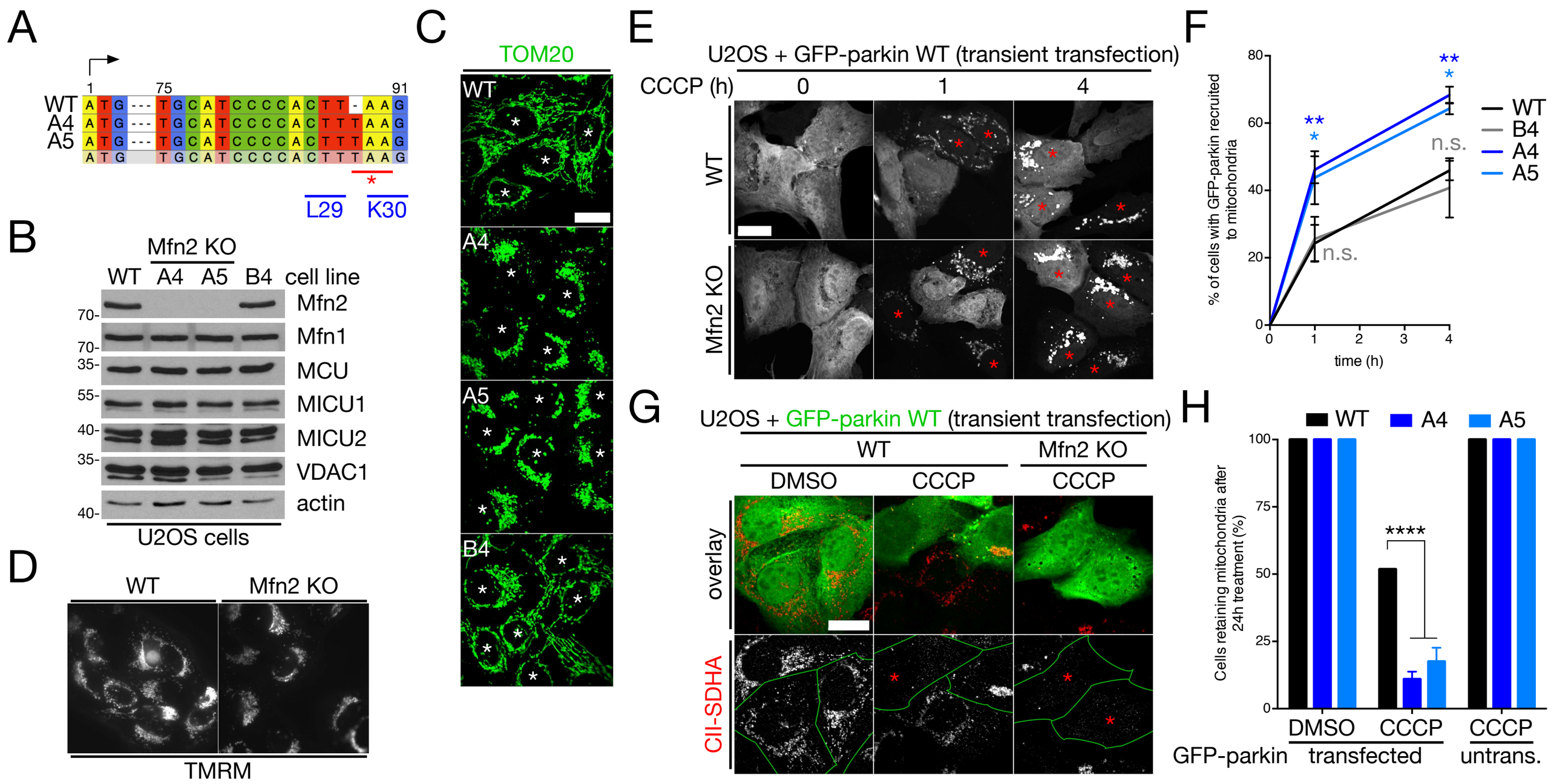


McLelland et al., Figure 3-S4

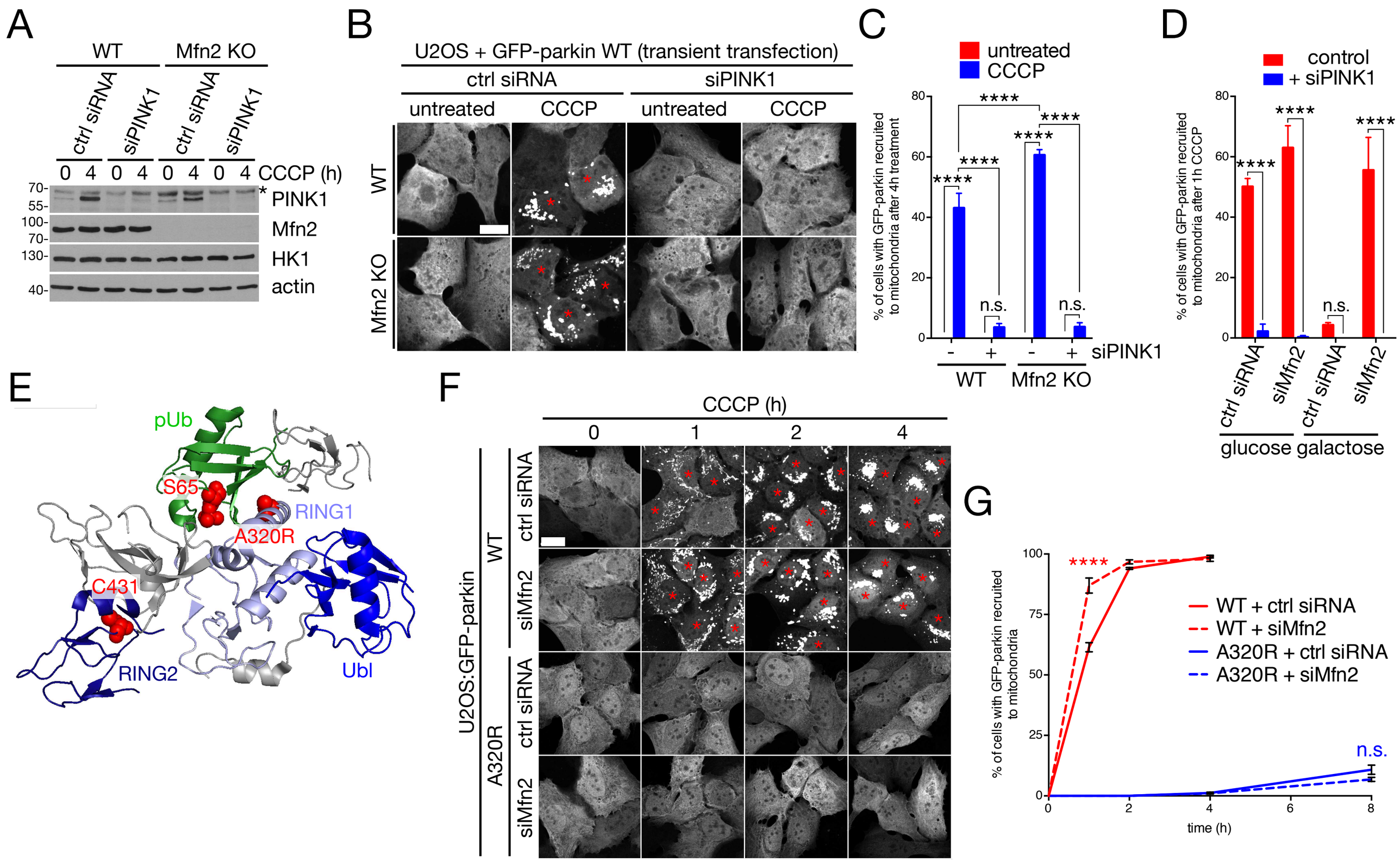


McLelland et al., Figure 3-S5

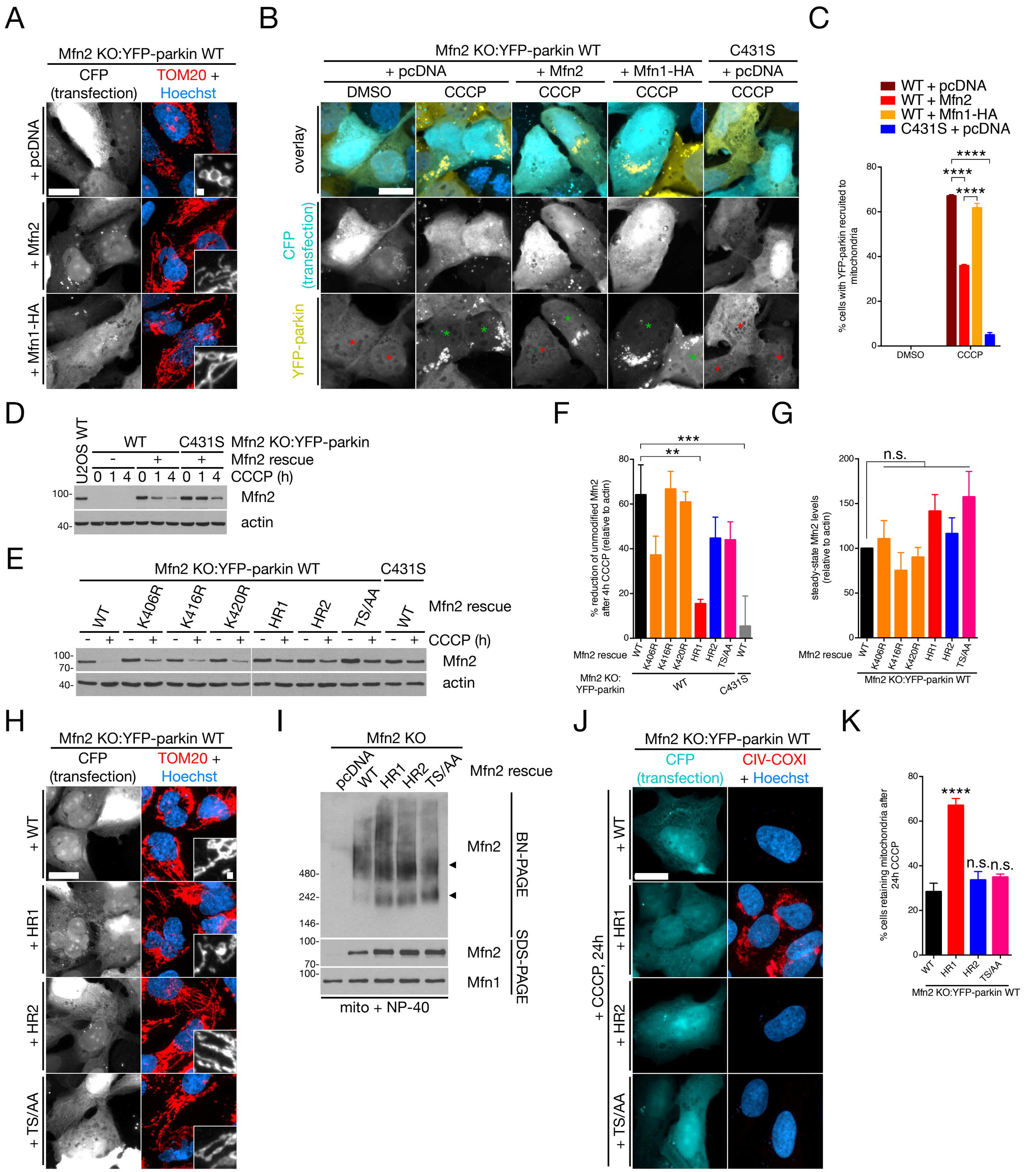


McLelland et al., Figure 4

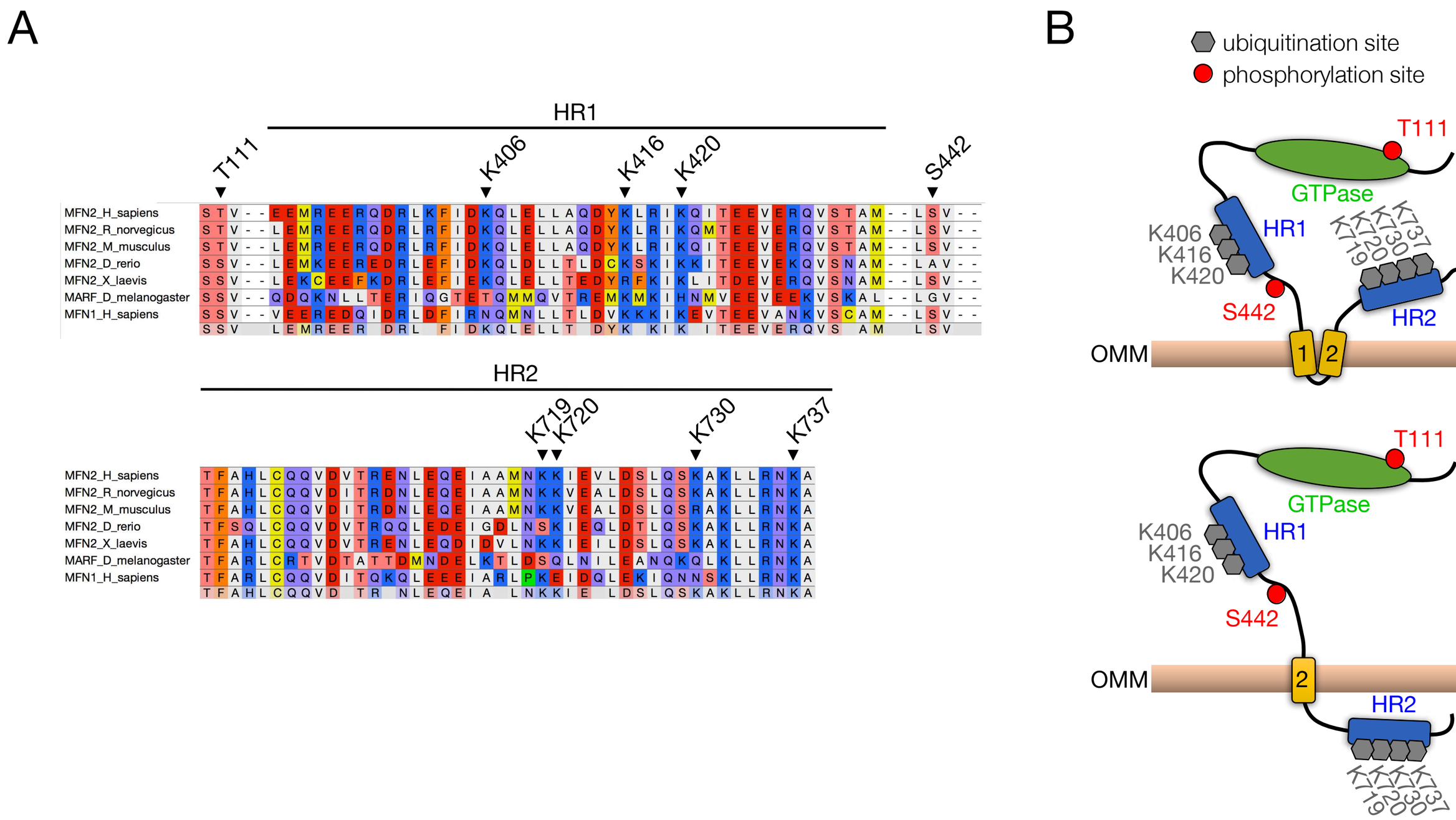


McLelland et al., Figure 4-S1

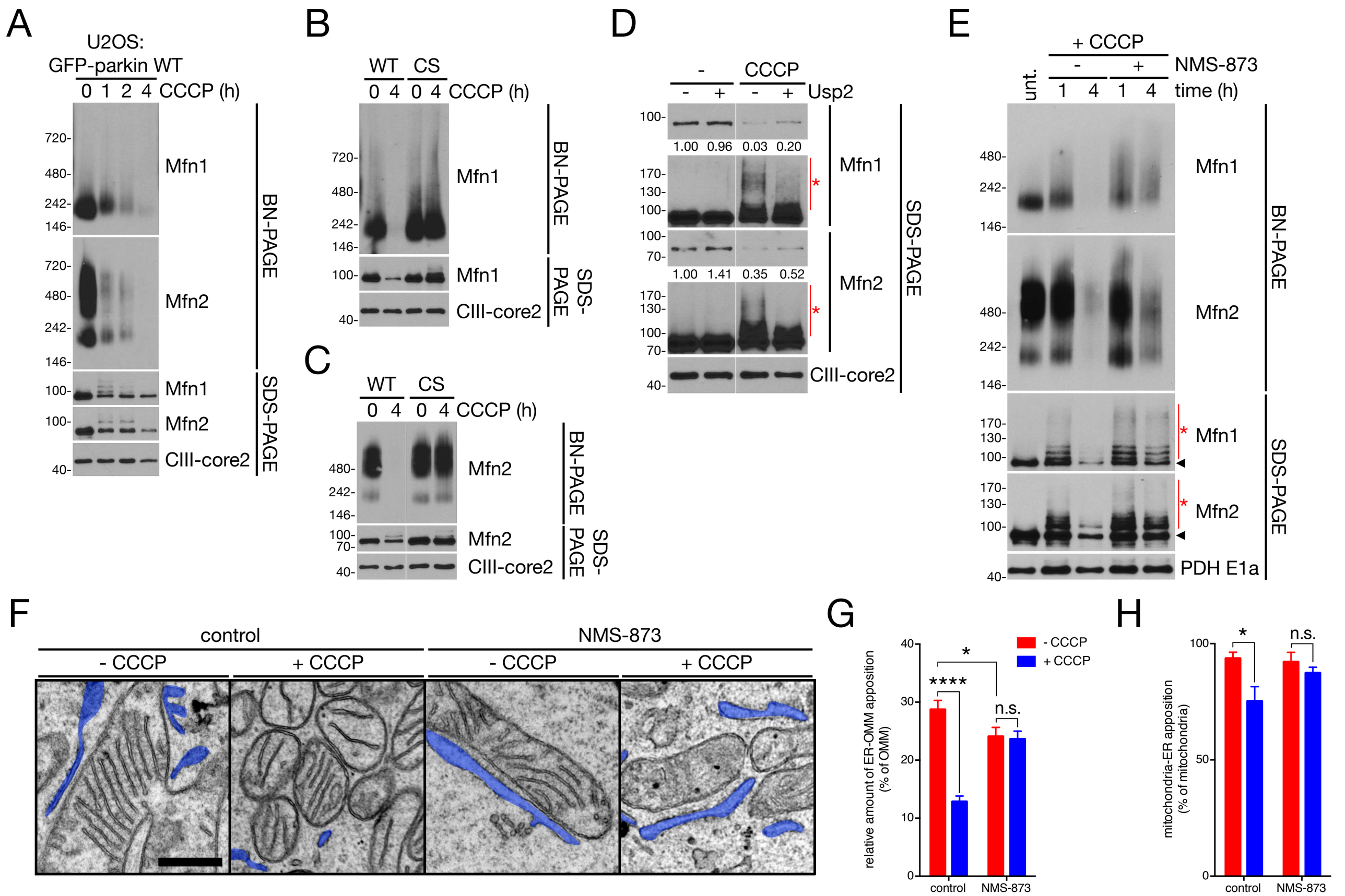


McLelland et al., Figure 5

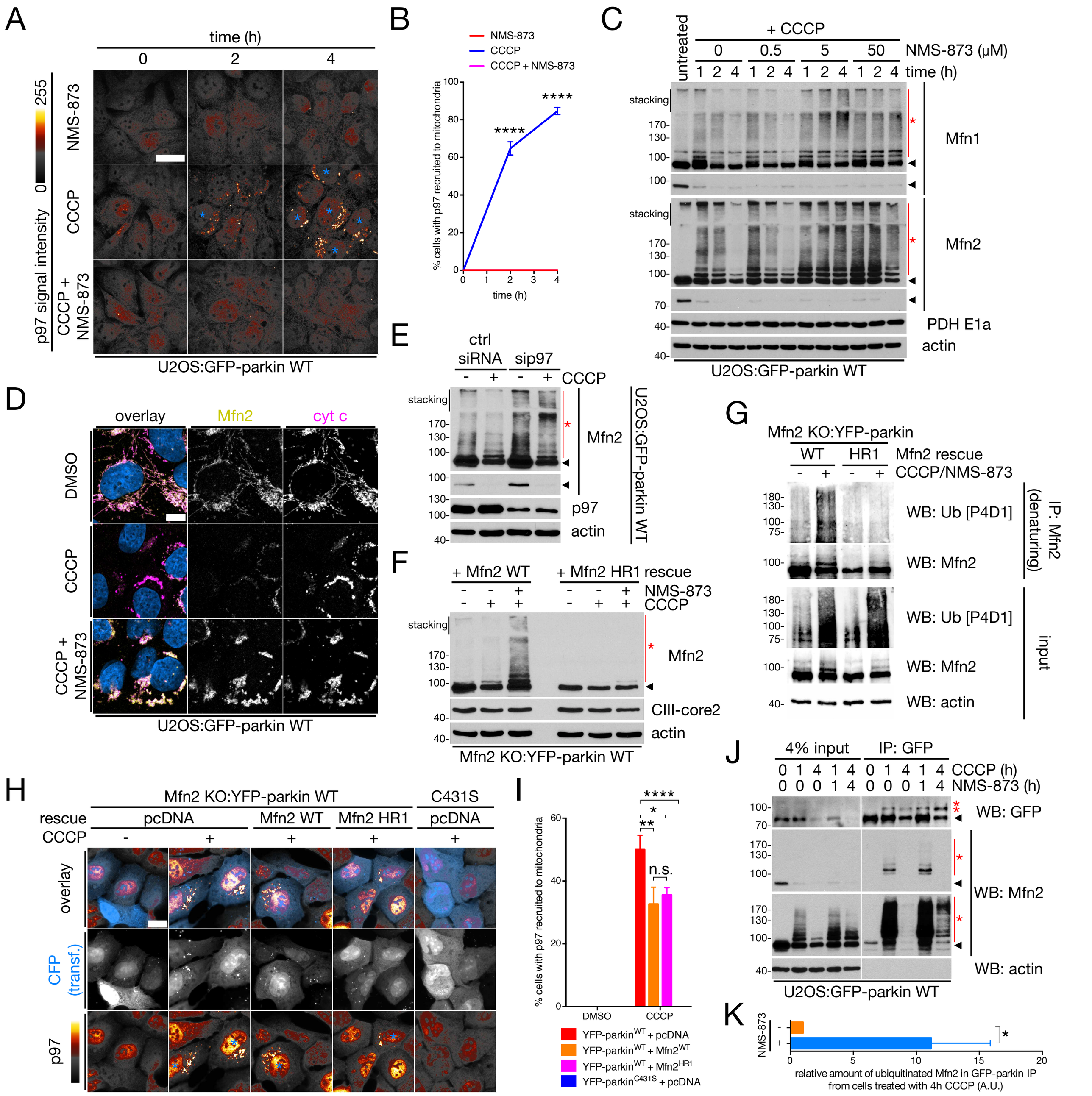


McLelland et al., Figure 6

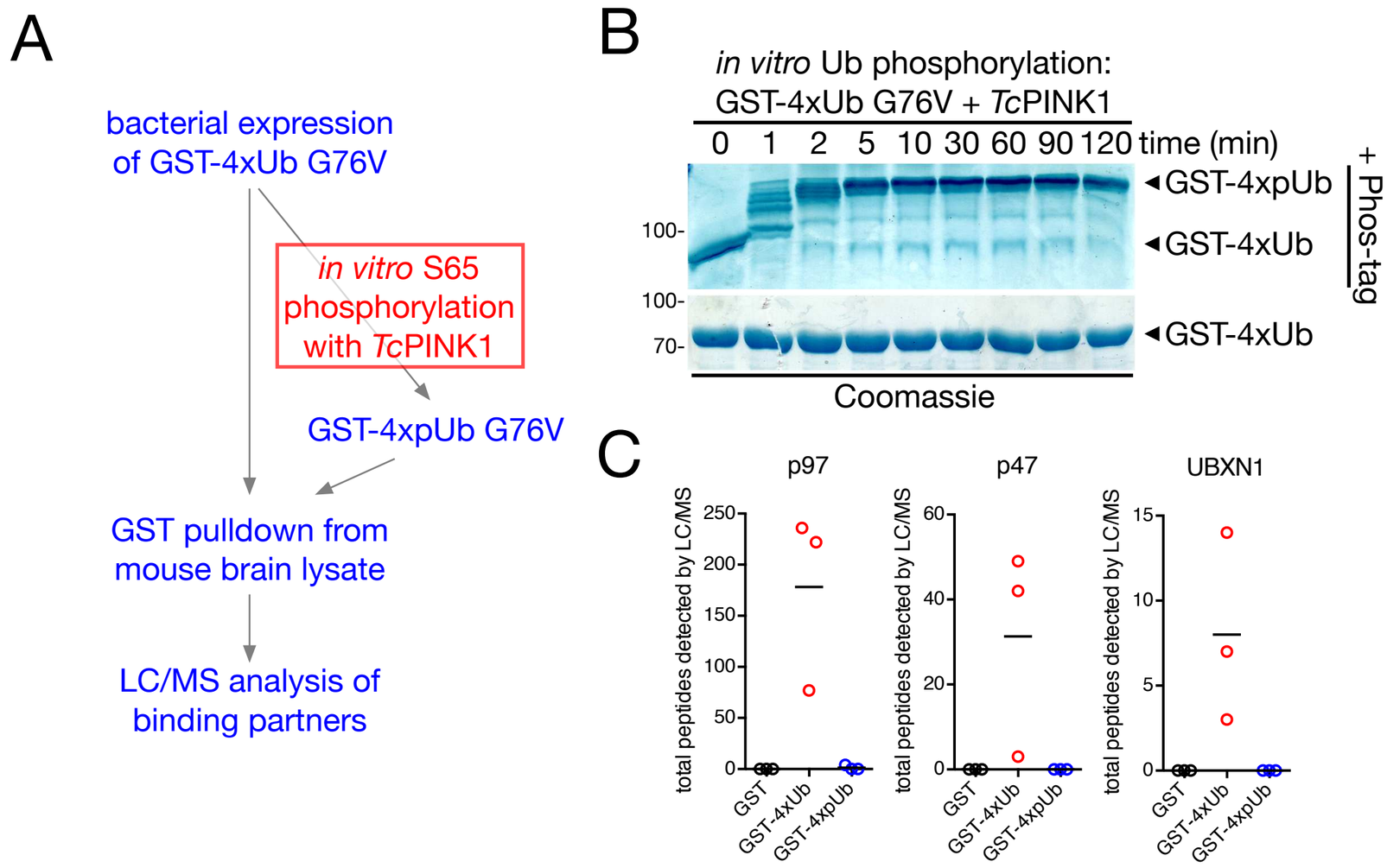


McLelland et al., Figure 6-S1

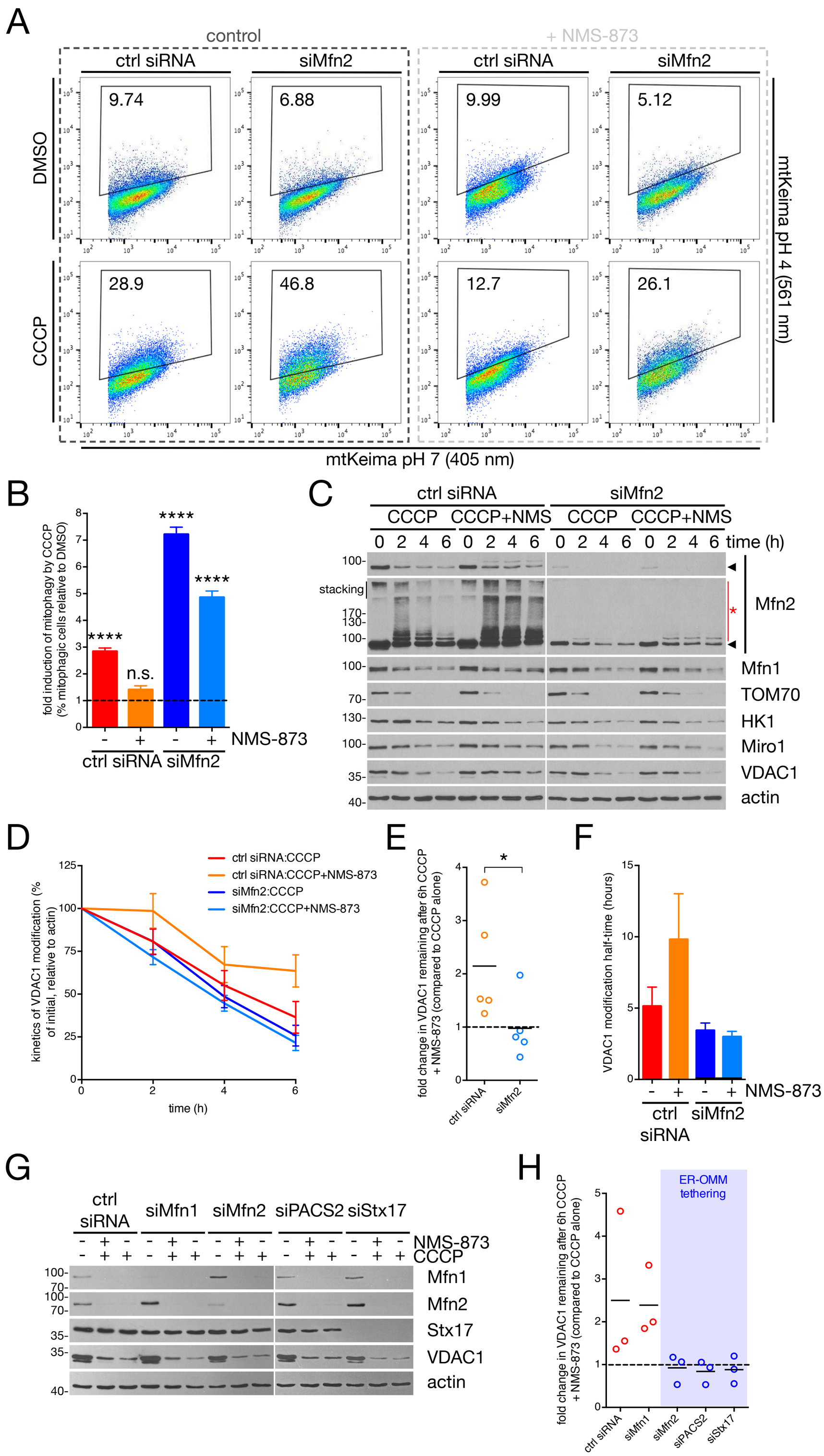


McLelland et al., Figure 7

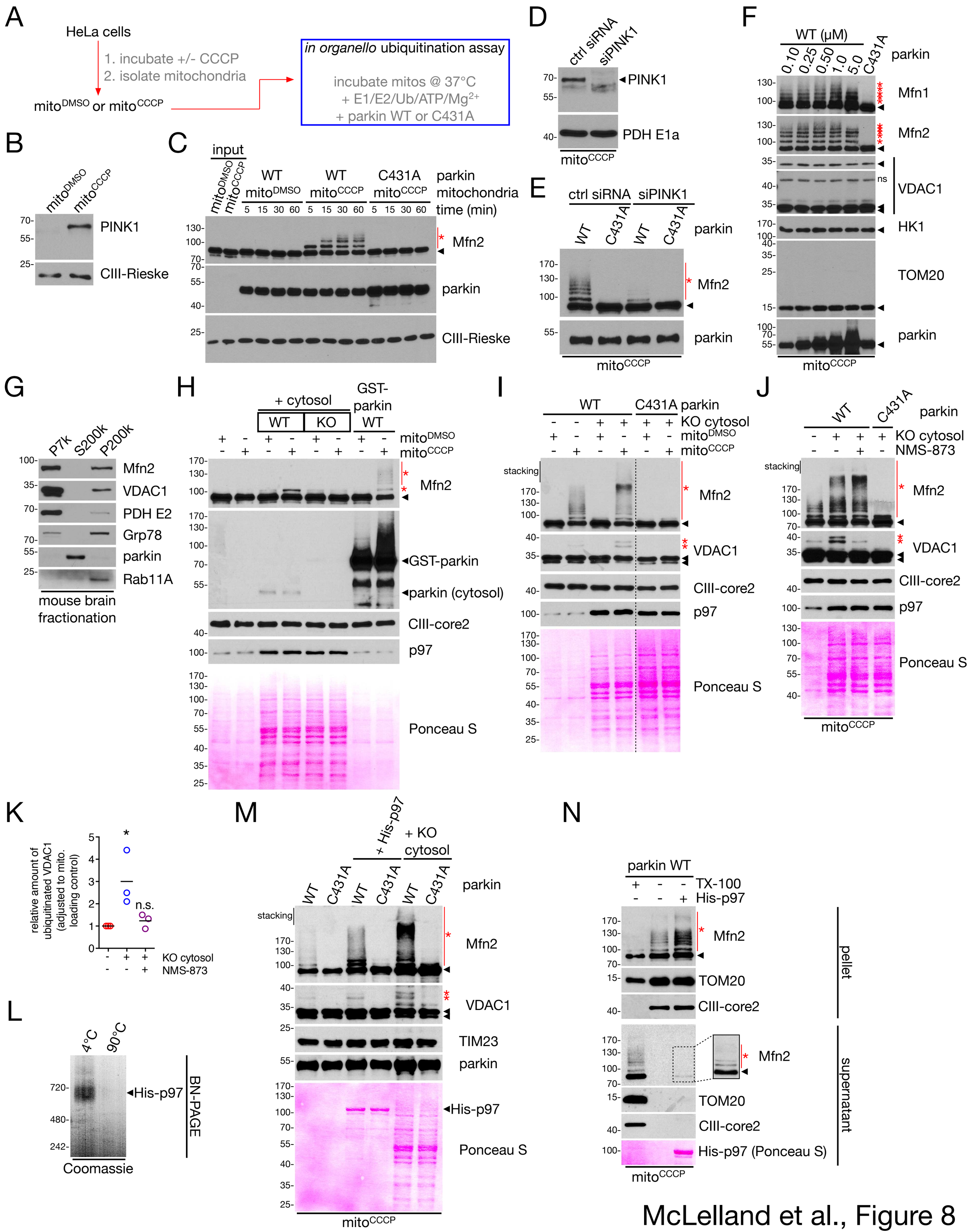


McLelland et al., Figure 8

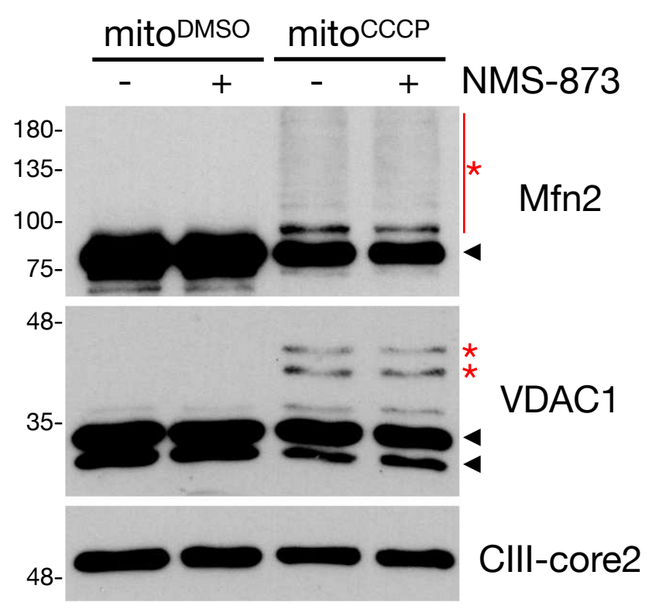


McLelland et al., Figure 8-S1

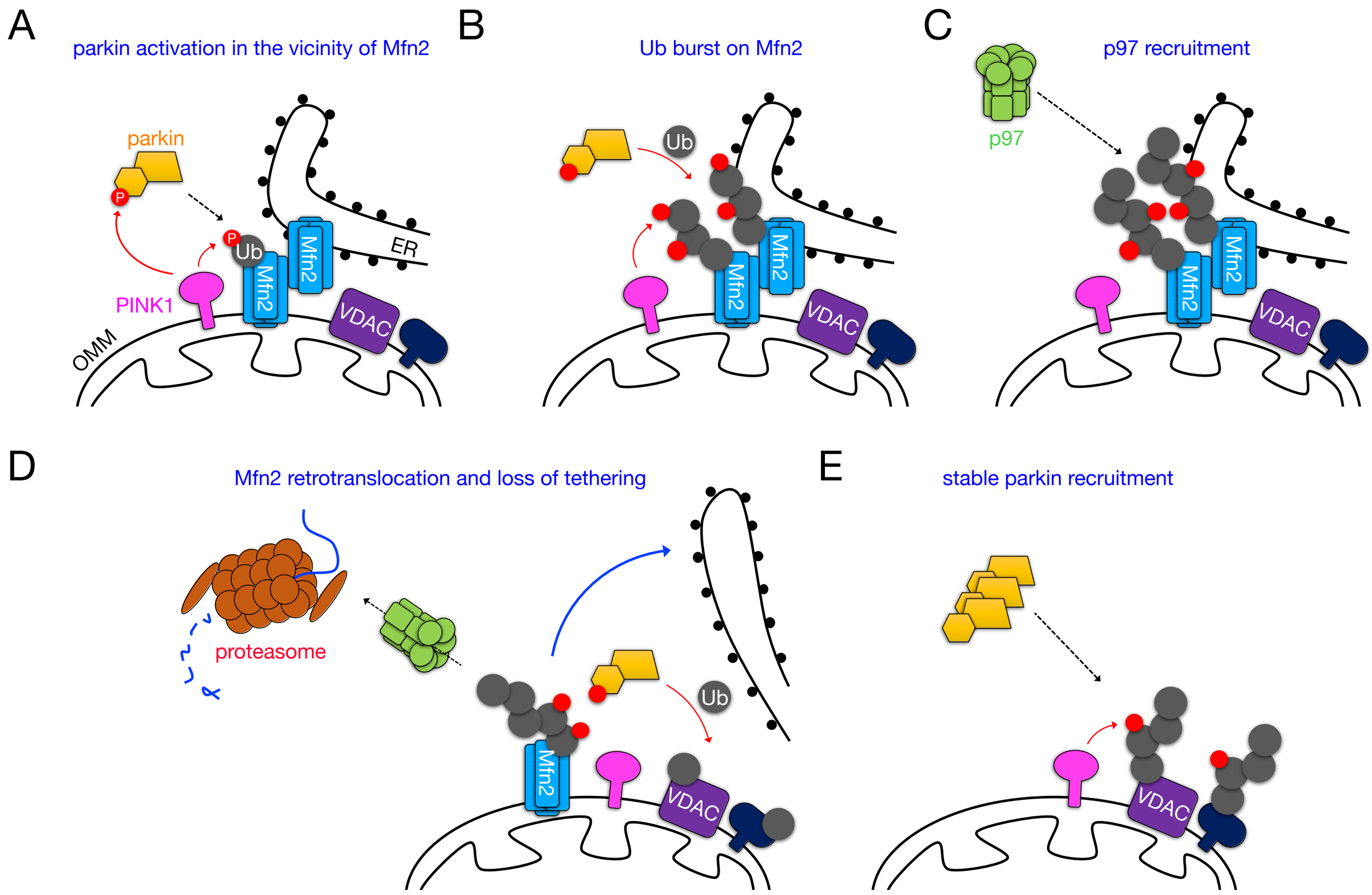


McLelland et al., Figure 9